

# Synthesis of New Analogs of 2-Methoxyestradiol

*Dissertation for the Degree of Master of Pharmacy*

Samuel Kwame Opoku Nsowah



The Department of Pharmaceutical Chemistry  
School of Pharmacy  
The Faculty of Mathematics and Natural Sciences  
45 credits

UNIVERSITY OF OSLO

May 2023

*The stone which the builders rejected*

*Has become the chief cornerstone*

*This is the LORD's doing;*

*It is marvellous in our eyes and*

*This is the day that the LORD has made,*

*Let us rejoice and be glad in it!*

*- Psalm 118:22-24*

# Synthesis of New Analogs of 2-Methoxyestradiol

*Dissertation for the Degree of Master of Pharmacy*

Samuel Kwame Opoku Nsowah



The Department of Pharmaceutical Chemistry  
School of Pharmacy  
The Faculty of Mathematics and Natural Sciences  
45 credits

UNIVERSITY OF OSLO

May 2023

© Samuel Kwame Opoku Nsowah

2023

Synthesis of New Analogs of 2-Methoxyestradiol

Samuel Kwame Opoku Nsowah

<http://www.duo.uio.no/>

Printed in Norway: Graphic centre, University of Oslo

# Acknowledgement

This master project was performed at the Department of Medicinal Chemistry at the School of Pharmacy affiliated with the Faculty of Mathematics and Natural sciences, University of Oslo, between August 2022 and June 2023.

To begin with, I would like to express my outmost gratitude to the Almighty God for His grace upon my life that has led me and brought me this far.

I would also like to thank my supervisors professor Trond Vidar Hansen and associate professor Anders Vik whose unique guidance and supervision over the project have been the cause of success today. You will always remain in my memory forever.

Special thanks to all my fellow master students Cecilia, Naol, Victoria, Åsmund and Emma. Your moral and academic support as well as your outstanding cooperation is very much appreciated. The efforts of Mathias Ryslett Lepsøe and Åshild Moi Sørskår cannot be underestimated as they assisted me with every technical aspect of my lab work. Thanks very much Mathias and Åshild.

I would also like to thank all other members of the Medicinal Chemistry Department; Åsmund Kaupang, Osman Gani, Amalie Reinertsen, Marcus De Bourg, Karina Ervik and Mina Bathen for their wonderful cooperation with academic and non-academic activities. You all made me feel a sense of belonging and will always remain in my memory.

It will almost be criminal if I forget to thank my dear friends in my study group and fellow students at the School of Pharmacy; Sasha Shabani, Ole Henrik Holt, Zakariya Abdirab and Daniel Rahmati whose efforts and friendship kept me going throughout my five-year spell at the School of Pharmacy. I am very grateful for all the moments we shared together. You made me stronger and better every day. A warm appreciation to Alfreda Serwaah Antobreh and Joseph Azumah, my fellow Ghanaian colleagues at the School of Pharmacy. Your unflinching support and exemplary lives gave me so much motivation to complete this work.

Finally, I would like to thank my parents Felicia Gyasi and Joseph Kwame Nsowah for giving me the opportunity to develop my intellect and always believing in me. God bless you. My greatest respect and gratitude goes to all my former teachers, school mates, pastors, church friends and all other family members. We certainly made it together. Thank you very much.

May 2023

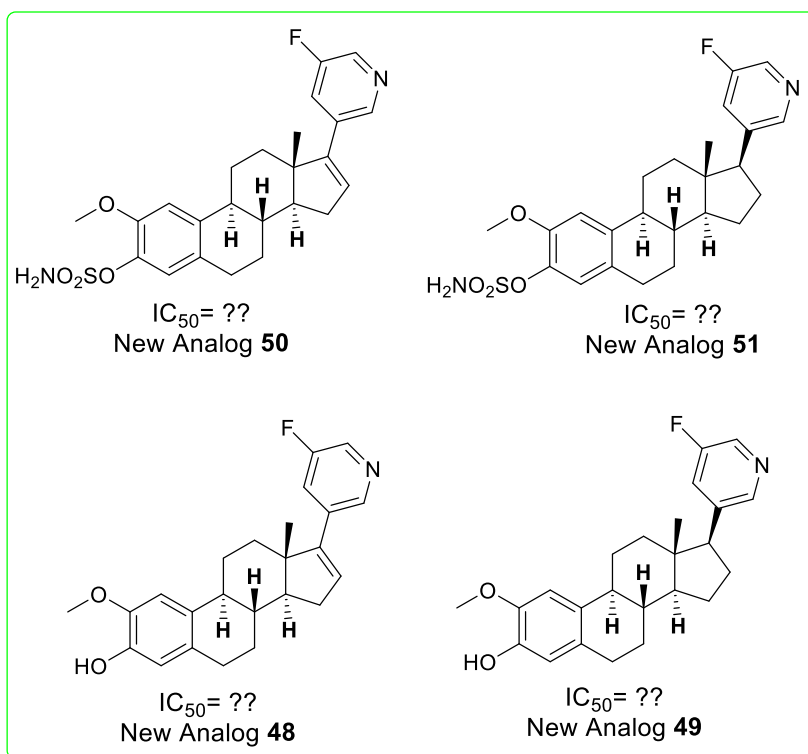
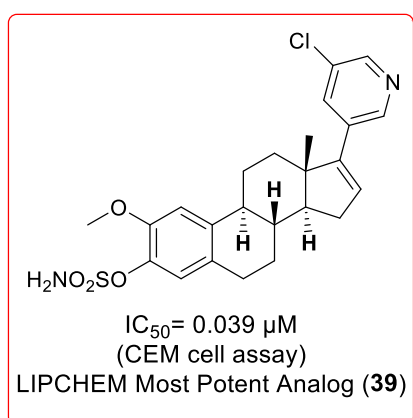
Oslo

Samuel Kwame Opoku Nsowah

# Abstract

2-Methoxyestradiol (2-ME), an endogenous metabolite of  $17\beta$ -estradiol was initially regarded as inactive metabolite devoid of any interesting biological activities but has in recent years attracted much attention due to its significant anti-cancer activities. 2-ME has been subjected to phase I and II clinical trials for the treatment of several different cancers alongside many different analogs with the most prominent one being ENMD-1198 developed by Entremed. 2-ME does not act as an agonist on the estrogen-receptor binding sites, making it a suitable anti-cancer agent. Unfortunately, 2-ME exhibit a very short in vivo half-life due to its rapid metabolism.

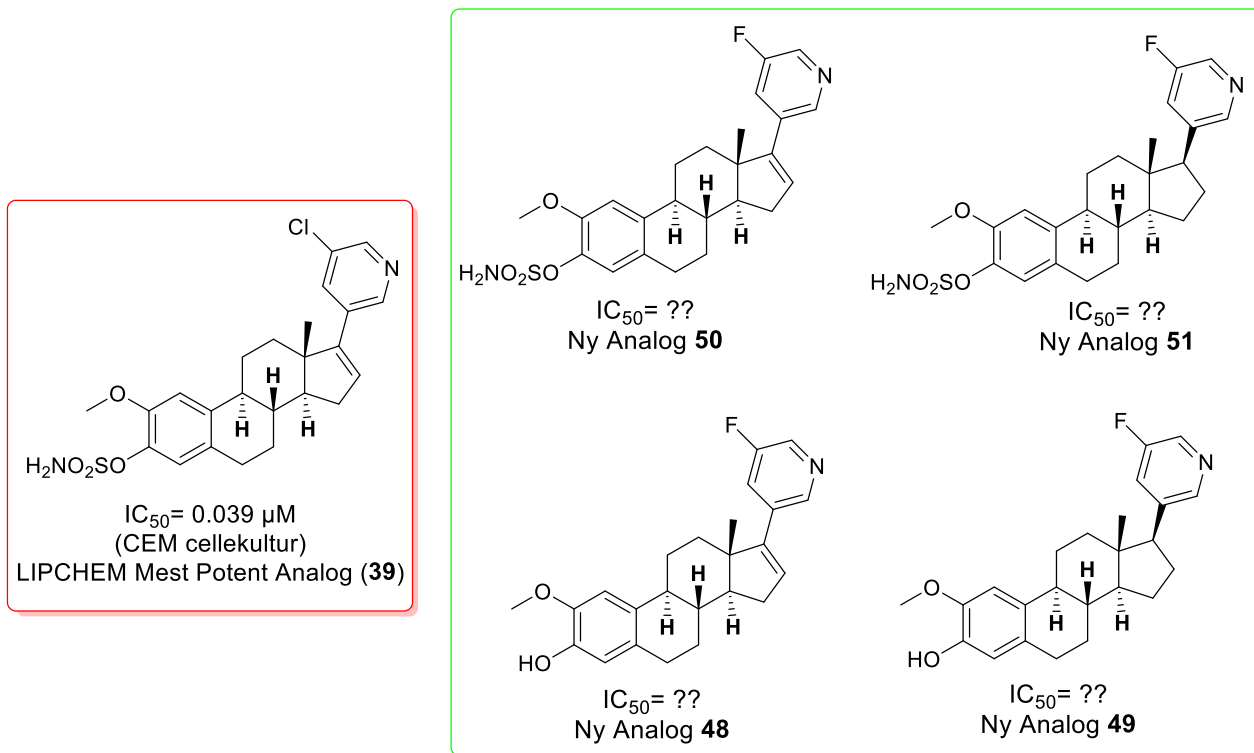
In the past 10 years, professor Hansen and co-workers at the Department of Medicinal Chemistry, University of Oslo have synthesized several analogs of 2-ME with improved potency and metabolism. As a continuation of this progressive research, four new analogs of 2-ME have been prepared with modifications at C-3, C-16 and C-17 where metabolism occurs most. All new analogs are currently under biological testing in collaboration with the Norwegian Centre for Molecular Medicine, Oslo, Norway.



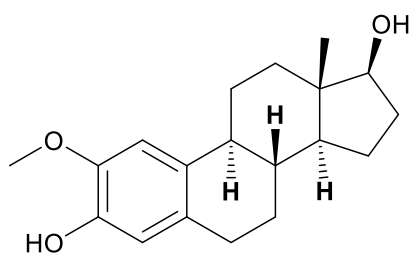
# Sammendrag

2-Metoksyøstradiol (2-ME), en endogen metabolitt av 17 $\beta$ -østradiol var tidligere kjent som inaktiv metabolitt uten noen interessante biologiske aktiviteter, men i senere tid har den fått mye oppmerksomhet som følge av dets viktige anti-kreft aktiviteter. 2-ME har vært i fase I og II kliniske studier til behandling av flere ulike kreftformer sammen med flere ulike analoger der det meste potente har vært ENMD-1198 utviklet av Entremed. 2-ME virker ikke som agonist på de østrogen-reseptor bindingssetene hvilken som gjør den til en egnet anti-kreft medisin. Dessverre har 2-ME veldig kort halveringstid in vivo som følge av dets raske metabolisme.

I de siste 10 årene har professor Hansen og sine medarbeidere ved avdeling for legemiddelkemi, Universitetet i Oslo syntetisert flere analoger av 2-ME med forbedret virkning og metabolisme. Som en fortsettelse av denne videregående forskningen har det blitt syntetisert fire nye analoger av 2-ME med modifikasjoner ved C-3, C-16 og C-17 der det ofte skjer metabolisme. Alle nye analoger er foreløpig under biologisk testing i samarbeid med Norsk senter for molekulærmedisin i Oslo, Norge.



# Graphical Abstract



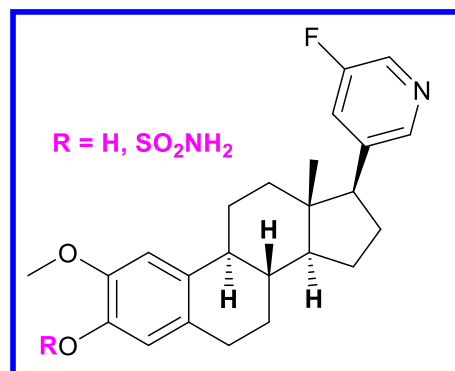
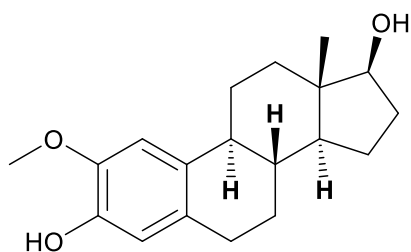
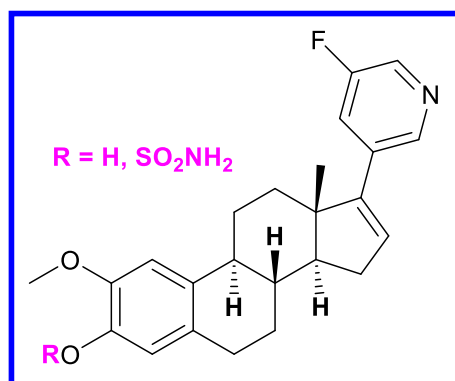
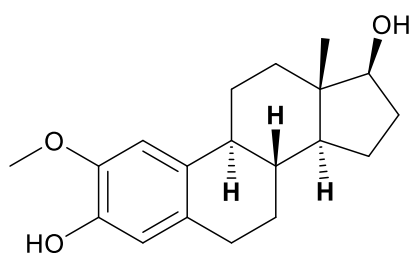
2-Methoxyestradiol

-Potent anti-cancer agent

-Short in vivo half life due to rapid metabolism at C-3, C-16 and C-17

-Subjected to phase I and II clinical trials for treatment of several cancers

-Poor solubility and oral bioavailability



# List of Abbreviations

2-ME	2-Methoxyestradiol
VEGF	Vascular endothelial growth factor
VEGFR	Vascular endothelial growth factor receptors
FDA	Food and Drug Administration in the United States of America
PDGF	Platelet derived growth factor
PDGFR	Platelet derived growth factor receptors
TK	Tyrosine kinase
RAF	Rapid accelerated fibrosarcoma kinase
EPC	Endothelial progenitor cells
CA4P	Combretastatin A4 phosphate
SAR	Structure activity relationship
DEPBG	4'-O-dimethyl-epipodophyllotoxin benzylidene $\beta$ -d-glucoside
HMGCR	3-hydroxy-3-methylglutaryl coenzyme A reductase (HMGCR)
SREBP2	Sterol regulatory element-binding protein 2
P450 <sub>SSC</sub>	Cholesterol side chain cleavage enzyme
17 $\beta$ -HSD	17 $\beta$ -Hydroxysteroid dehydrogenase
SERMS	Selective estrogen receptor modulators
COMT	Catechol-O-methyl transferase
2-HDE	2-hydroxyestradiol
NO	Nitric oxide
JNK	c-Jun N-terminal kinase
Bcl-2	$\beta$ -cell lymphoma 2
p38 <sup>MAPK</sup>	mitogen-activated protein kinase
HIF-1 $\alpha$	Hypoxia-induced factor-1 $\alpha$
HUVECs	Human umbilical vein endothelial cells

# Table of contents

Acknowledgement.....	V
Abstract.....	VII
Sammendrag.....	VIII
Graphical Abstract.....	IX
List of abbreviations.....	XI
1 Introduction.....	1
1.1 Cancer.....	1
1.2 Anti-cancer agents.....	1
1.2.1 Chemotherapeutic agents.....	2
1.2.2 Tumour angiogenesis.....	2
1.2.3 Anti-angiogenetic agents.....	3
1.2.4 Natural products as anti-cancer agents.....	6
1.3 Steroids.....	9
1.3.1 Biosynthesis of steroids.....	10
1.3.2 Steroids as anti-cancer agents.....	12
1.3.3 2-Methoxyestradiol.....	15
1.3.4 Anti-cancer activities of 2-methoxyestradiol.....	16
1.3.5 SAR studies of 2-methoxyestradiol for anti-cancer effect.....	18
1.3.6 Clinical studies of 2-methoxyestradiol and its analogs.....	22
1.4 Synthetic Methods.....	24
1.4.1 Oppenauer oxidation.....	24
1.4.2 Suzuki-Miyaura coupling reaction.....	25
1.5 Aim of study.....	26
2 Results and discussion.....	27
2.1 Synthesis and characterization of new analogs of 2-methoxyestradiol ( <b>28</b> ).....	28
2.1.1 Synthesis of 2-methoxyestrone ( <b>31</b> ).....	28
2.1.2 NMR characterization of 2-methoxyestrone ( <b>31</b> ).....	29
2.1.3 Synthesis of 3- <i>tert</i> -butyldimethylsiloxy-2-methoxyestrone ( <b>45</b> ).....	29
2.1.4 NMR characterization of 3- <i>tert</i> -butyldimethylsiloxy-2-methoxyestrone ( <b>45</b> )...30	
2.1.5 Synthesis of 3- <i>tert</i> -butyldimethylsiloxy-2-methoxy-steroid-triflate ( <b>46</b> ).....	31

2.1.6	NMR characterization of 3- <i>tert</i> -butyldimethylsiloxy-2-methoxy-steroid-triflate (46).....	31
2.1.7	Synthesis of 3- <i>tert</i> -butyldimethylsiloxy-2-methoxy-steroid-analog (47).....	32
2.1.8	NMR characterization of 3- <i>tert</i> -butyldimethylsiloxy-2-methoxy-steroid-analog (47).....	33
2.1.9	Synthesis of 2-methoxy-steroid-analog (48).....	34
2.1.10	NMR & HRMS characterization of 2-methoxy-steroid-analog (48).....	34
2.1.11	Synthesis of 2-methoxy-steroid-analog (49).....	35
2.1.12	NMR and HRMS characterization of 2-methoxy-steroid-analog (49).....	36
2.1.13	Synthesis of 2-methoxy-steroid-analog (50).....	37
2.1.14	NMR and HRMS characterization of 2-methoxy-steroid-analog (50).....	37
2.1.15	Synthesis of 2-methoxy-steroid-analog (51).....	38
2.1.16	NMR and HRMS characterization of 2-methoxy-steroid-analog (51).....	39
2.1.17	Attempted synthesis of 3- <i>tert</i> -butyldimethylsiloxy-2-methoxy-steroid-analog (52).....	40
2.2	Biological testing of new analogs of 2-methoxyestradiol (28).....	41
3	Future prospective.....	42
4	Conclusion.....	44
5	Methods and Procedures.....	45
5.1	General Methods.....	45
5.2	Synthetic and Experimental Procedures.....	46
5.2.1	Synthesis of 2-methoxyestrone (31).....	46
5.2.2	Synthesis of 3- <i>tert</i> -butyldimethylsiloxy-2-methoxyestrone (45).....	47
5.2.3	Synthesis of 3- <i>tert</i> -butyldimethylsiloxy-2-methoxy-steroid-triflate (46).....	48
5.2.4	Synthesis of 3- <i>tert</i> -butyldimethylsiloxy-2-methoxy-steroid-analog (47).....	49
5.2.5	Synthesis of 2-methoxy-steroid-analog (48).....	50
5.2.6	Synthesis of 2-methoxy-steroid-analog (49).....	51
5.2.7	Synthesis of 2-methoxy-steroid-analog (50).....	52
5.2.8	Synthesis of 2-methoxy-steroid-analog (51).....	53
6	References.....	54
7	Appendix.....	59
7.1	<sup>1</sup> H NMR and <sup>13</sup> C NMR of the synthesized compounds.....	59
7.2	HRMS of the synthesized compounds.....	76

# **1 Introduction**

## **1.1 Cancer**

Cancer is a group of diseases characterized by abnormal and uncontrollable growth of cells in a tissue or an organ [1]. It is a general term for multiple types of diseases which differs in nature and has the ability to affect every part of the body. In a normal cell, cell division, differentiation and apoptosis are deeply regulated by the body's own mechanisms [2]. In a rare situation, these regulatory mechanisms may fail, thereby leading to a physiological imbalance between cell proliferation and cell death [2]. When this occurs, it paves way for the development of tumours. A tumour can be malignant or benign. Malignant tumour tends to grow slowly and lacks the ability to spread to other tissues [2]. Benign tumour on the other hand can grow rapidly and have the ability to invade and destroy adjoining parts of the body, spreading to other organs through the blood and lymphatic system [1, 2]. The latter process is termed as metastasis and is the main cause of death from cancer [1]. In 2018, 9.6 million people were estimated to have died from cancer, accounting for one in six deaths worldwide [3]. Today, about 18.1 million people are diagnosed with cancer every year including 400 000 children [3]. An estimated amount of US\$ 1.16 trillion was the total annual economic cost of cancer in 2010 [3]. The most common types of cancers among women are colorectal, cervical, thyroid, lung and breast cancer [1]. In men, prostate, stomach, lung, liver and colorectal cancers occur more often [1]. Cancer could be prevented in 30-50 % cases worldwide by avoiding the main risk factors such as tobacco use, alcohol consumption, physical inactivity and unhealthy diet [3].

## **1.2 Anti-cancer agents**

In recent years, there have been promising improvement in treatment and patient outcomes on certain types of cancers, while for others, there have been nearly no change in survival rates for many years [4]. There are many factors that contribute to these developments, but the most defining factor has always been the ability of the cytotoxic agent to selectively affect cancer cells, leaving the normal cells unaffected [4]. Many anti-cancer agents exhibit significant cytotoxic effect towards cancer cells. However, side effects resulting from toxicity towards normal cells, coupled with the development of drug-resistance and pharmacokinetic challenges curtail the potency of these agents [4, 5].

## 1.2.1 Chemotherapeutic agents

Conventional chemotherapeutic agents are often used to treat many cancers, but due to issues with selectivity and dose limiting toxicity on normal cells, their potency is severely restricted [5]. The diverse response of cancer patients to chemotherapy is as a result of variation in the proliferation rate of the tumours as well as composition of the tumour microenvironment and different cellular mechanisms [5]. Historically, chemotherapy has contributed immensely to cancer treatment, but the effects of other treatment forms such as radiotherapy, surgery and biological therapy cannot be underestimated [3]. The latter alternatives are often used in combination with chemotherapy for cancer treatment [3].

## 1.2.2 Tumour angiogenesis

Tumour angiogenesis is a process by which blood vessels penetrate and grow in the tumour microenvironment [6]. It is a very important factor considering the tumour's survival as it plays a vital role in supplying oxygen and nutrients to the cells as well as eliminating metabolic waste from the cells [6] (see figure 1).

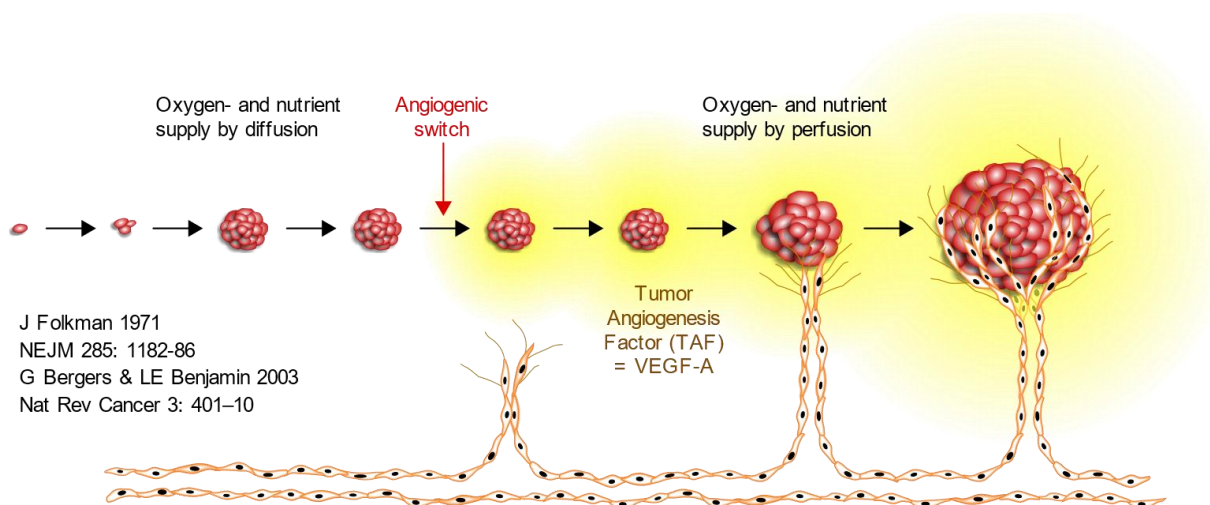


**Figure 1:** Illustration of tumour angiogenesis as a requirement for tumour growth and survival [7]. Accessed: April 27, 2023. from: [[https://commons.wikimedia.org/wiki/File:Tumor\\_angiogenesis.svg](https://commons.wikimedia.org/wiki/File:Tumor_angiogenesis.svg)].

In 1971, Dr. Folkman introduced the term “anti-angiogenesis” to mean prevention of new vessel sprouts from penetrating into an early tumour implant [8]. It was established that blocking the formation of new vessels in a tumour may prevent metastasis and increase the vulnerability of the tumour to chemotherapy alongside exposing it to full force of cell mediated attack without protection of blocking antibody [6, 8]. Meaning that, “anti-angiogenesis” synergizes chemotherapy and immunotherapy [8].

### 1.2.3 Anti-angiogenic agents

Anti-angiogenic agents are very important for cancer treatment considering their many comparative advantages to chemotherapy. It has been established that, when tumours acquire a size of 1-2 mm, they initiate angiogenesis in order to continue growing because inadequate nutrient and oxygen supply may lead to cell death [6]. Inhibition of angiogenesis therefore retards the growth of tumours and initiates apoptosis. There are many factors that affects angiogenesis and therefore inhibition can occur at different levels. The most important factor is the vascular endothelial growth factor (VEGF) which is produced by tumour and stroma cells and acts on its tyrosine kinase receptors, VEGF receptors (VEGFR) to activate endothelial cells, thereby leading to proliferation, migration and invasion of the cells into the tumour to form new blood vessels [6] (see figure 2).

#### Blood Vessel Overgrowth on Cell

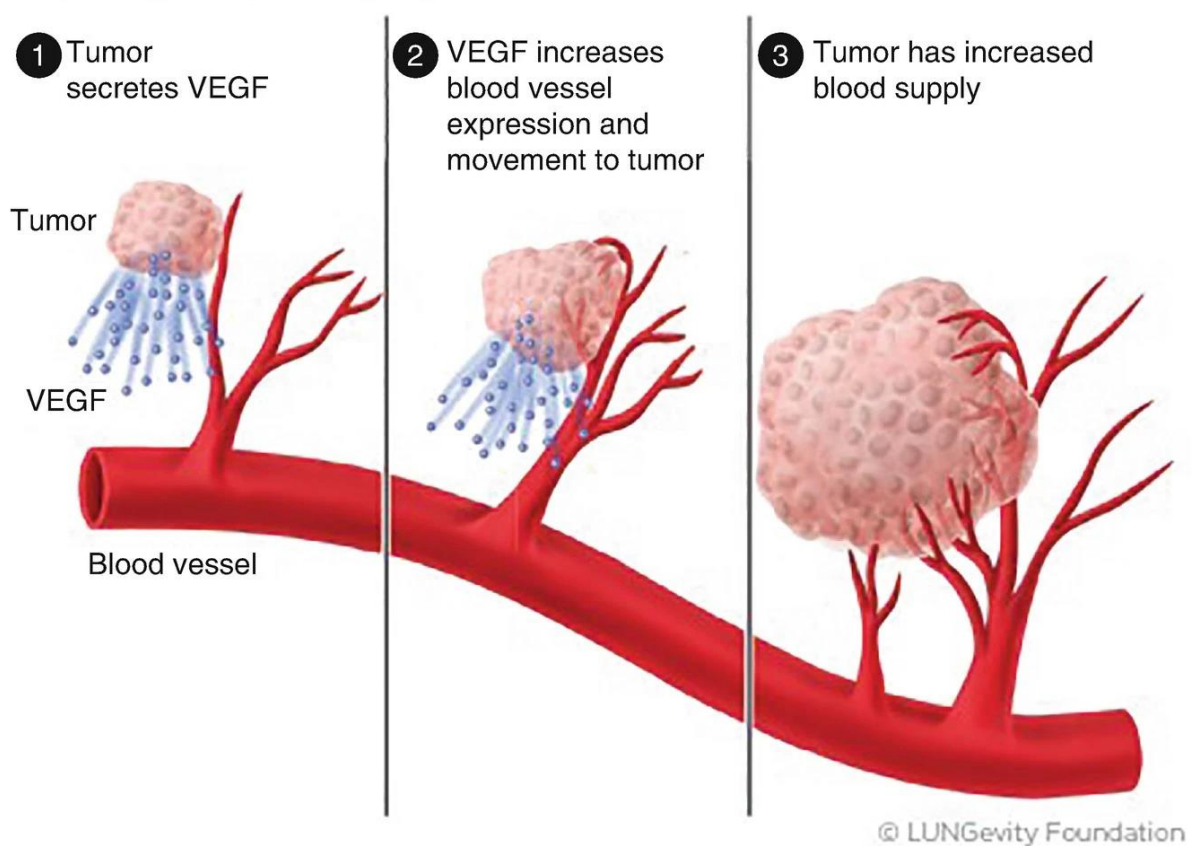


**Figure 2:** *The role of VEGF in tumour angiogenesis [9]. Accessed: March 8, 2023. from: [https://www.lungevity.org/for-patients-caregivers/navigating-your-diagnosis/treatment-options/angiogenesis-inhibitors].*

Inhibition of VEGF pathway has therefore become an interesting target for anti-angiogenesis. Bevacizumab (see figure 3) is a recombinant humanized monoclonal antibody which binds to

VEGF and prevents it from binding to VEGFR [6]. It was approved by the Food and Drug Administration in the United States of America (FDA) in 2004, as the first clinically available anti-angiogenic agent for treatment against colon cancer and subsequently approved for treatment of kidney, brain and breast cancers [10].

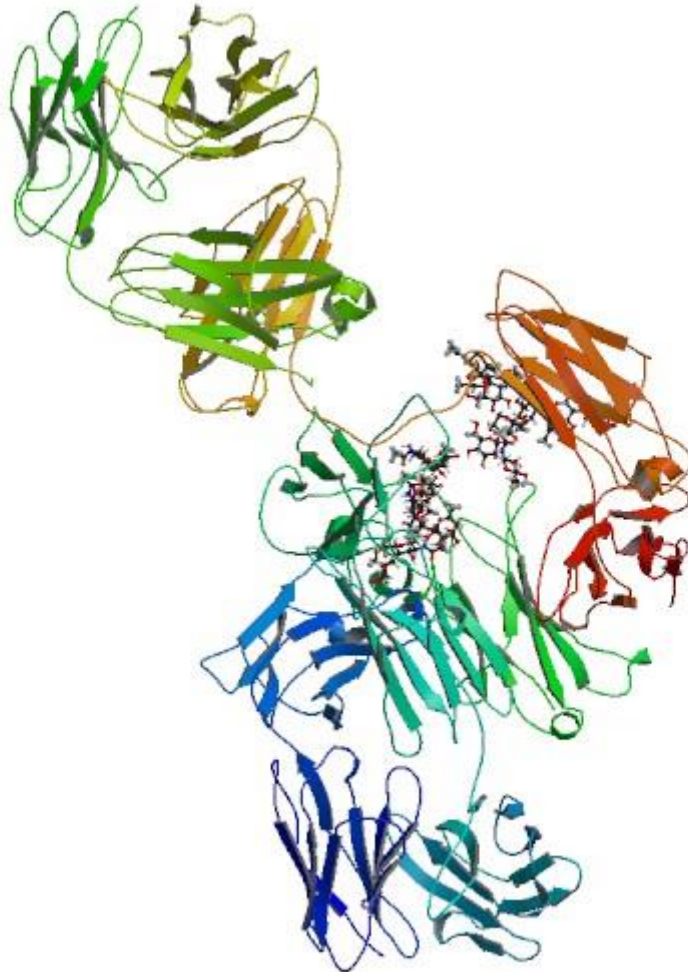


**Figure 3:** Protein structure of Bevacizumab. Accessed: March 8, 2023. from [[https://s3-us-west-2.amazonaws.com/drugbank/protein\\_structures/full/DB00112.png?1266600377](https://s3-us-west-2.amazonaws.com/drugbank/protein_structures/full/DB00112.png?1266600377)].

Endothelial cell proliferation can also be activated by platelet derived growth factor (PDGF) which binds to its tyrosine kinase receptors, PDGF receptors (PDGFR) on endothelial cells and tumour cells to promote tumour cell proliferation and angiogenesis [11]. Inhibition of PDGF receptors is therefore another useful target in cancer treatment. In addition to their anti-angiogenic activity, PDGF inhibitors also prevent tumour cell proliferation by directly blocking PDGF receptors on tumour cells [6, 11].

Both PDGF and VEGF receptors are classified as tyrosine kinase (TK) receptors and there are several FDA approved drugs which act on both receptors to inhibit angiogenesis and tumour

growth [6]. Examples of such drug molecules are sorafenib (1), pazopanib (2) and sunitinib (3) which are all synthetic compounds [6] (see figure 4). Sorafenib (1) binds to VEGFR and PDGFR to prevent their signalling molecules VEGF and PDGF from binding to them, thus inhibiting angiogenesis [6]. In addition, it also inhibits rapid accelerated fibrosarcoma kinase (RAF), a critical component that controls cell division and proliferation, thus inhibiting tumour growth [6]. It was approved by the FDA for treatment against several different cancers such as kidney and liver cancers [6]. Pazopanib (2) and sunitinib (3) acts in similar ways to prevent angiogenesis and tumour growth [6]. Pazopanib (2) is indicated against kidney cancer and soft tissue sarcoma, while sunitinib (3) is approved for treatment against kidney cancer and gastrointestinal stromal tumour [6].

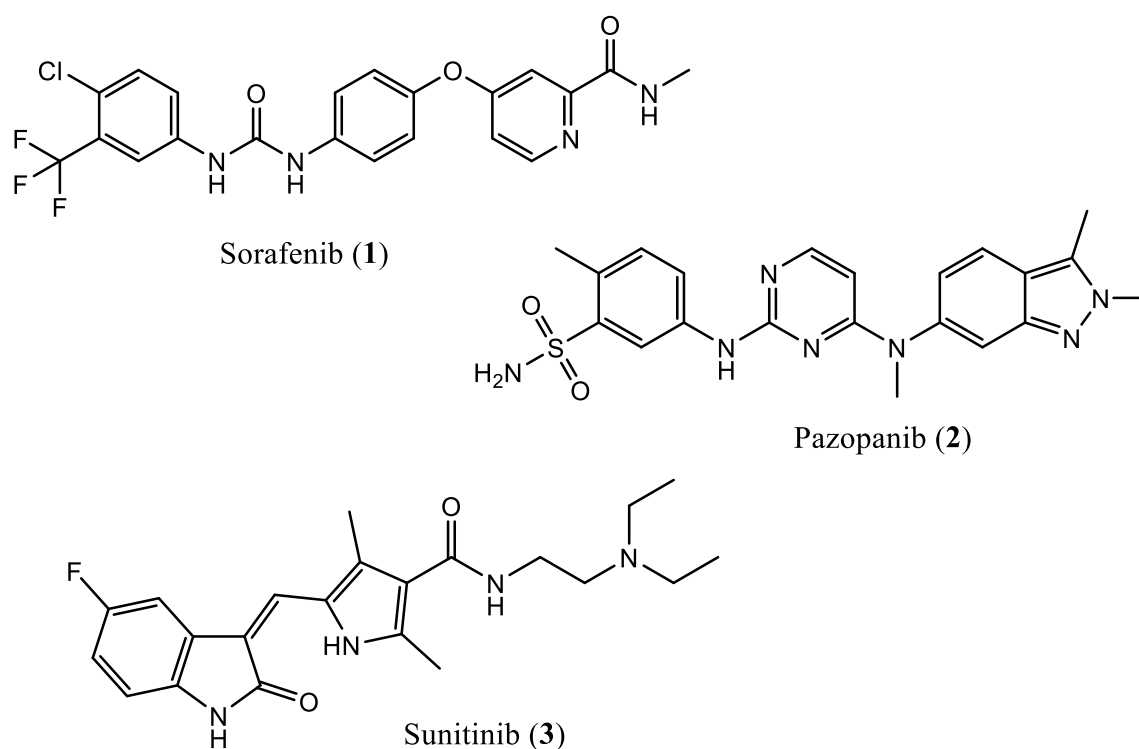


**Figure 4:** Examples of VEGF and PDGF inhibitors. Created with ChemDraw 21.0.0 as inspired by; (Solum et al., 2014, al-Kazaale et al., 2017).

Another interesting target for anti-angiogenesis is inhibition of endothelial progenitor cells (EPCs) proliferation. EPCs are pro-endothelial cells that stems from the bone marrow and differentiate into endothelial cells to form new blood vessels [12]. They participate in many key physiological processes such as angiogenesis and wound healing [6]. Examples of EPCs are CD34 and CD 309, basically identified by the expression of their co-markers. Production and release of EPCs is a fundamental step in tumour angiogenesis. Several studies have revealed that EPCs levels are higher in the blood of cancer patients than in healthy individuals

[6]. Consequently, concentration of EPCs in the blood has been used as biomarkers for certain types of cancers. Inhibition of EPCs proliferation is therefore a critical approach in tumour anti-angiogenesis [6, 12].

#### **1.2.4 Natural products as anti-cancer agents**

Historically, natural products derived from plants and algae have played a significant role in the discovery of several anti-cancer agents, as well as the treatment of cancer [13]. In 2009, Cragg and his co-workers revealed that more than 3000 plant species have been used in cancer treatment [13]. Natural products exhibit a unique form for cytotoxic activity in that they are very potent and highly selective. Additionally, their structural activity relationship (SAR) studies have been the basis for the discovery and development of many anti-cancer agents today. There are many mechanisms by which natural products exhibit their cytotoxic activity, but the most prominent one is the inhibition of tubulin polymerization [13, 14]. Tubulin is a protein nanoelement that polymerizes to build up microtubules [15]. Microtubules are protein structures that form the skeleton of the cell, together with actin and intermediate filaments [15]. In addition to providing mechanical support to the cell, microtubules also play a vital role in cell division, transport of organelles in the cell and mobility of the cell [14]. Inhibition or interference with tubulin polymerization is therefore a key target in cancer therapy as the cell cannot function or exist without microtubules [14, 15].

Taxol (**4**) (see figure 5) is a diterpenoid that promotes tubulin polymerization [14]. This effect leads to suppression of dynamic changes in microtubules which causes mitotic arrest, meaning that during mitosis the duplicated chromosomes cannot segregate, thus inhibiting cell division [14]. It belongs to the family of taxanes and was first discovered in 1971 as a cytotoxic sample constituent from the bark of *Taxus brevifolia* where its structure was first published [14]. It entered clinical trials in 1984 and by 1994, it was approved by the FDA for treatment against refractory ovarian cancer and refractory breast cancer [14]. The discovery and development of Taxol (**4**) is regarded as one of the most spectacular research projects in cancer therapy. Other natural products that act similarly to Taxol (**4**) include epothilones and discodermolide which are all FDA approved drugs [14, 15].

Combretastatin is another natural compound that inhibits tubulin polymerization [14]. Its mechanism of action is the opposite of that of Taxol (**4**) [14]. However, both of them leads to suppression of microtubule dynamism, thereby disrupting cell division [14]. It was first isolated in 1982 as a cytotoxic constituent of a sample from *Combretum caffrum* [14]. Based

on structural activity relationship studies conducted on combretastatin, several other analogs have been developed and some more analogs have also been isolated from *C. caffrum*. One of the most potent analogs that evolved from clinical studies through to FDA approval is combretastatin A4 phosphate (CA4P) (**8**) [14] (see figure 5). Several studies have revealed that CA4P (**8**) is very effective when combined with other therapies such as hyperthermia, antibody-based approaches and chemotherapy [14, 15]. CA4P (**8**) is indicated against thyroid cancer as a single therapy but used in combinatorial therapy against several different types of cancers [14].

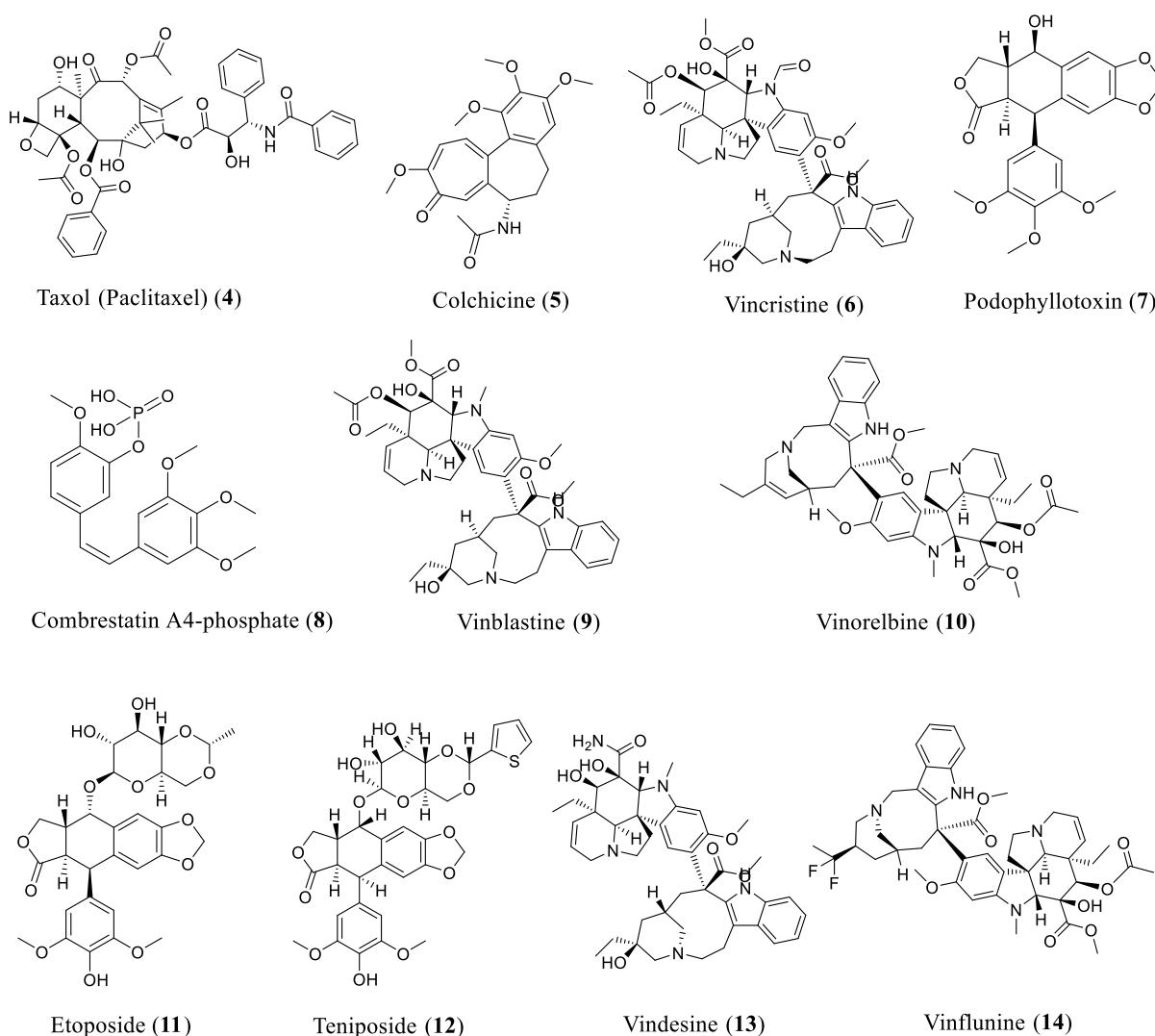


**Figure 5:** Examples of natural products used as anti-cancer agents. Created with ChemDraw 21.0.0 as inspired by; (Solum et al., 2014, al-Kazaale et al., 2017).

Other natural compounds that act similarly to combretastatin include colchicine (**5**), vinblastine (**9**), vincristine (**6**) and podophyllotoxin (**7**) which all have distinct binding sites on the tubulin-microtubule protein system [15] (see figure 5). They all exert their cytotoxic

effect by binding to tubulin heterodimers and blocking their assembly into microtubules, thereby inhibiting cell division [14, 15].

Basically, there are three identified binding sites on the tubulin-microtubule protein system which include the colchicine site, the vinca-alkaloid site and the taxoid site [14]. All natural products that bind to these sites either leads to assembling or disassembling of tubulin heterodimers [14]. However, they all interrupt cell division by causing suppression in dynamic changes of the microtubules [14].

Podophyllotoxins belongs to the class of podophyllins and was first isolated in 1880 from an alcoholic extract of *Podophyllum* rhizome [14]. It was later revealed that podophyllotoxins, which is the major constituent of podophyllins exhibit cytotoxic activity by binding to the colchicine site [14]. However, during preclinical studies, it was reported that the cytotoxic potency of podophyllotoxin incurred unacceptable side effects such as gastrointestinal toxicity and this led to a halt in its development [14]. In the early 1950s, interest in podophyllotoxins was revived again and there was an assumption that podophyllotoxin glycosides in similarity to cardiac glycosides might show greater pharmacological profiles compared to their aglycones [14]. This assumption coupled with subsequent collaborative efforts by chemist and biologists led to the discovery and isolation of 4'-O-dimethyl-epipodophyllotoxin benzylidene  $\beta$ -d-glucoside (DEPBG) in 1963 [14]. Subsequently, etoposide (**11**) and teniposide (**12**) were later discovered as analogs of podophyllotoxin as a result of efforts to condense DEPBG with various ketones and aldehydes [14] (see figure 5). Etoposide (**11**) was approved by the FDA in 1983 for treatment against testicular cancer, while teniposide (**12**) as a single therapy or in combination with other chemotherapeutic agents was approved by the FDA in 1992 for treatment against refractory childhood acute lymphoblastic leukemia [14, 15]. It has been established that both drugs exert their cytotoxic effects by three mechanisms which include; inhibition of tubulin polymerization, inhibition of DNA topoisomerase II and induction of apoptosis [14].

Vinca alkaloids represent another important subgroup of natural products used in cancer chemotherapy. They are classified as indol-indoline dimeric compounds and belong to the plant family *Apocynaceae* [14]. The two most important anti-cancer agents belonging to vinca alkaloids are vinblastine (**9**) and vincristine (**6**) which were isolated from the leaves of *Catharanthus roseus* in the 1950s [14] (see figure 5). Both vinblastine (**9**) and vincristine (**6**) possess the indole moiety and the vindoline dihydroindole nucleus, where vinblastine (**9**) bears an N-methyl group and vincristine (**6**) has an N-formyl group, accounting for their

structural differences [14]. In spite of this, it has been established that both of them binds to the vinca domain of the tubulin-microtubule system to exert their cytotoxic activities [14]. However, their affinities and anti-tumour activities, as well as clinical toxicities strongly differ [14]. Based on SAR studies conducted on vincristine (**6**) and vinblastine (**9**), other analogs of vinca alkaloids such as vindesine (**13**), vinorelbine (**10**) and vinflunine (**14**) have been developed [14] (see figure 5). Vinblastine (**9**) is commonly used in combination with other chemotherapeutic agents in the treatment of breast and bladder cancers as well as Hodgkin's disease [14]. Vincristine (**6**) is indicated as combinatorial therapy against acute lymphoblastic leukemia and neuroblastoma [14]. Vinorelbine (**10**) has been approved worldwide for treatment against lung cancer and in Europe for treatment against breast cancer [14]. Finally, vinflunine (**14**) has also been approved as monotherapy in Europe for treatment against metastatic bladder cancer [14].

### 1.3 Steroids

Steroids comprise a group of lipophilic compounds containing carbon atoms conjoined in a four-member ring system [16]. Based on the number of carbon atoms in the molecule, steroids are classified into three groups consisting of the pregnane (21 carbon atoms), androstane (19 carbon atoms) and estrane (18 carbon atoms) [17].

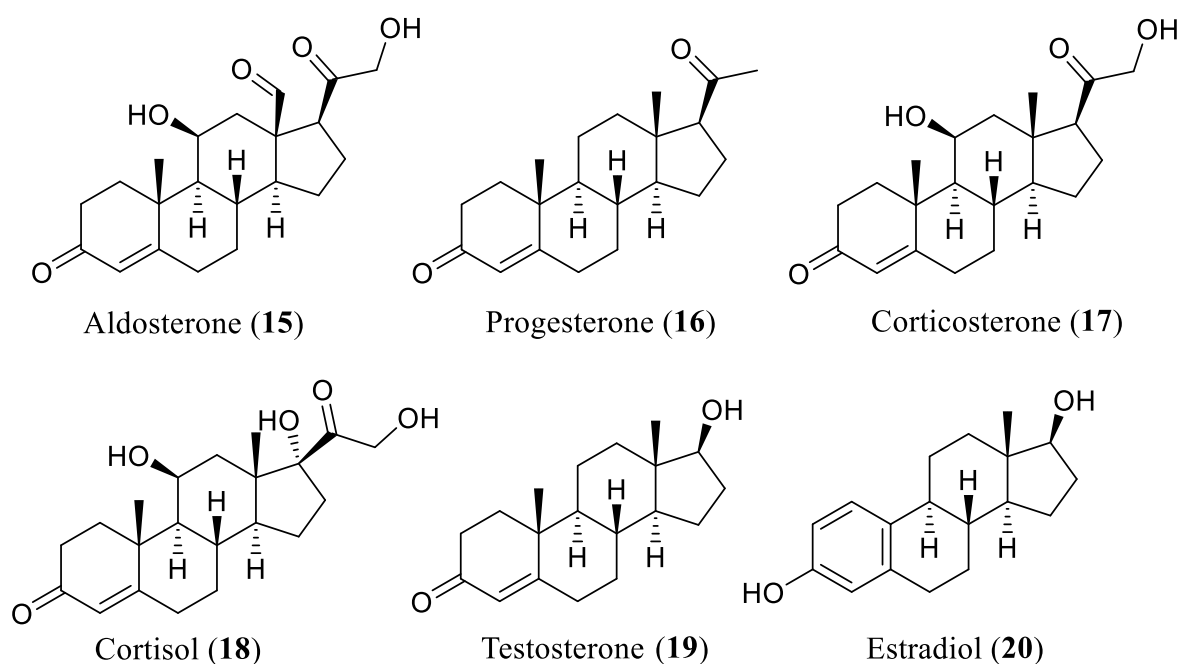


**Figure 6:** Examples of steroid compounds. Created with ChemDraw 21.0.0 as inspired by; (Solum et al., 2014, al-Kazaale et al., 2017).

Examples of steroids containing the pregnane nucleus (C-21) include aldosterone (**15**), progesterone (**16**), corticosterone (**17**) and cortisol (**18**) [17] (see figure 6). Testosterone (**19**), dihydrotestosterone and androstenedione contains the androstane nucleus (C-19), while estrone, estradiol (**20**) and estriol possesses the estrane (C-18) nucleus [17] (see figure 6).

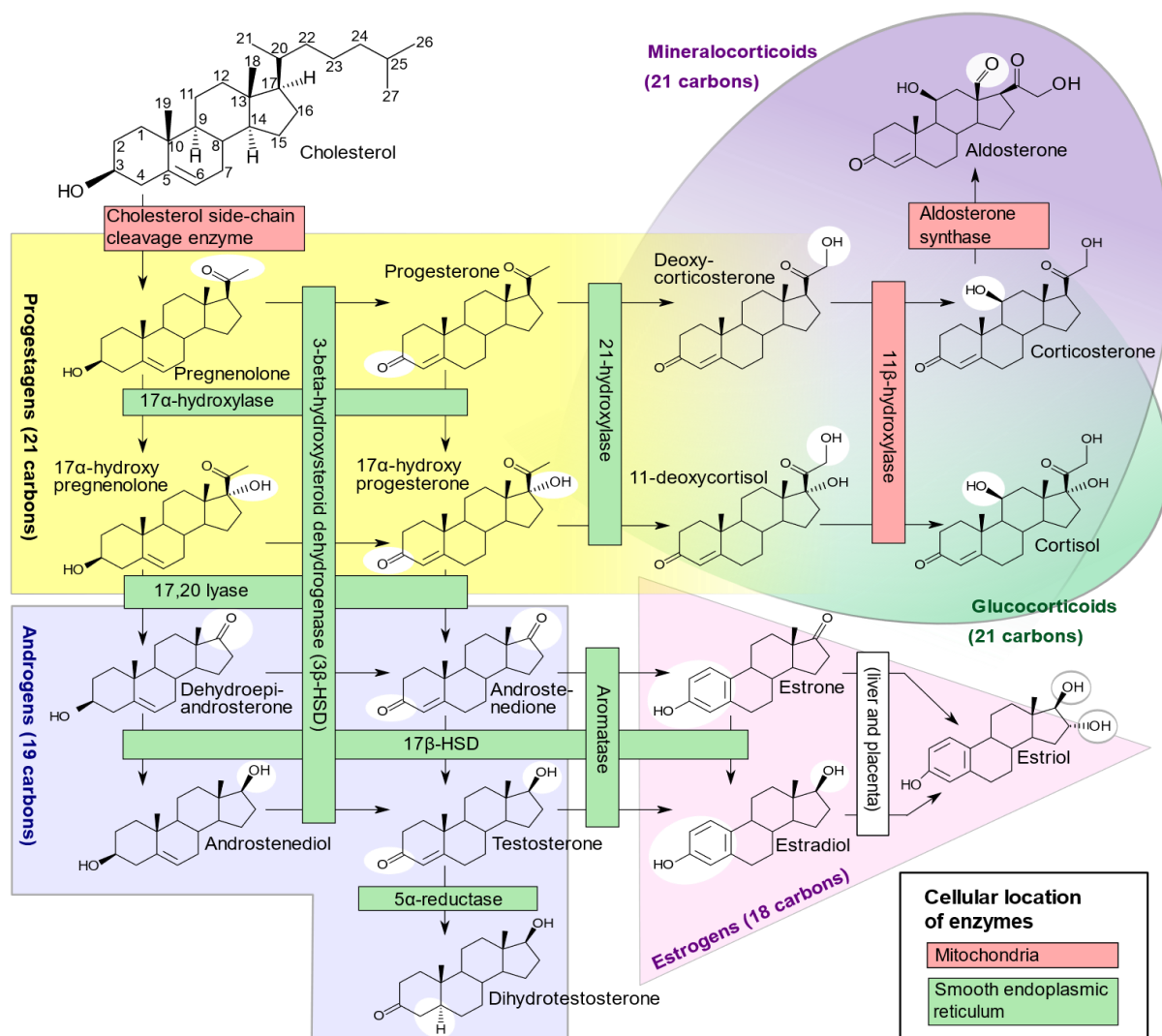
Principally, steroids are well known for their functions which include regulation of important physiological processes such as glucose metabolism, inflammation, menstruation and fetal development [16]. Based on their functions, steroids are also classified into estrogens (estradiol (**20**), estrone and estriol), mineralocorticoids (aldosterone (**15**) and deoxycorticosterone), glucocorticoids (cortisol (**18**) and corticosterone), androgens (testosterone (**19**) and dihydrotestosterone) and progestins (progesterone (**16**)) [17]. All steroids in the body are derived from cholesterol (see scheme 1) through a series of biosynthetic pathways operating primarily in distinct organs including the adrenal gland, ovary and testis [16]. Subsequent modifications of the steroid structure to perform other vital roles in the body can also occur in the skin, liver and prostate [16].

### **1.3.1 Biosynthesis of steroids**

Cholesterol (see scheme 1), the precursor for the synthesis of all steroids in the body was isolated from human gallstones about two hundred years ago and since then, has been of keen interest to the scientific society considering its vital role in physiological processes [18]. It is predominantly synthesized in the endoplasmic reticulum of hepatic cells, but synthesis can also take place almost in all other cells [18]. It is synthesized from acetyl coenzyme A through a series of biochemical reactions where the enzymes 3-hydroxy-3-methylglutaryl coenzyme A reductase (HMGCR) and squalene monooxygenase regulate the rate-determining steps respectively [18]. The protein sterol regulatory element-binding protein 2 (SREBP2) functions as the major regulator of cholesterol biosynthesis affecting the expression of the rate-determining enzymes as well as other important enzymes directly and indirectly involved in the biosynthetic pathway [18].

In the adrenal gland, testis and ovary cholesterol is transported to the mitochondria of their steroidogenic cells and converted to pregnenolone which is then transported to the smooth endoplasmic reticulum [16] (scheme 1). Conversion of cholesterol to pregnenolone is regarded as a pivotal step in the regulation of steroid synthesis and is catalysed by the cytochrome P450 enzyme, cholesterol side chain cleavage enzyme (P450<sub>SSC</sub>) [16, 17] (see scheme 1). Pregnenolone is then modified to produce specific steroids depending on the

expression of specific biosynthetic enzymes in the outer cortex of the adrenal gland, where there are three divisions; the outer zona glomerulosa, the inner zona reticularis and the centrally located zona fasciculata [16].



**Scheme 1:** Illustration of steroid biosynthesis in humans [19]. Accessed: April 27, 2023. from [https://en.wikiversity.org/wiki/WikiJournal\_of\_Medicine/Diagram\_of\_the\_pathways\_of\_human\_steroidogenesis].

For example, adrenal androgens such as testosterone, dihydroepiandrosterone and androstenedione are synthesized in the inner zona reticularis by the enzymes sulfotransferase 2A1, aldo-keto reductase 1C3 and 3-beta-hydroxysteroid dehydrogenase 3 [16] (see scheme 1). After synthesis, the steroids are then transported to the cell membrane and released into the blood to peripheral tissues where they act as precursors for the synthesis of more biologically active hormones [17]. In the testis, cholesterol is also converted into androstenedione and testosterone by Leydig cells in a five-step enzymatic pathway [16] (see scheme 1).

Surprisingly, production of dihydrotestosterone which is more potent than testosterone occurs less in the testis, but more in peripheral tissues such as liver and prostate where there is higher enzymatic activity of 5 $\alpha$ -reductase, the enzyme responsible for the conversion of testosterone to dihydrotestosterone [16] (see scheme 1). Testosterone and androstenedione can also be synthesized from cholesterol in the ovary theca cells, providing a precursor to aromatase in the granulosa cells where testosterone is converted into estradiol by aromatase, a cytochrome P450 enzyme [16] (see scheme 1). The estrogenic and androgenic steroids accounts for the male and female secondary sexual characteristics in adolescents including regulation of reproduction [17].

### 1.3.2 Steroids as anti-cancer agents

Steroids play an important role in cell proliferation and are therefore of key interest when it comes to cancer therapy. Generally, the overexpression of steroid hormones in various tissues stimulate cell proliferation leading to various types of hormone dependent cancers such as breast, prostate and ovarian cancers [20].

Aromatase inhibitors constitute one key area of steroid compounds capable of inhibiting tumour growth. The enzyme aromatase is responsible for converting androgens to estrogens (see scheme 1) and is found in the bone, gonads, placenta, adipose tissues, brain, breast and skin [17]. In breast cancer tissues, aromatase is overexpressed and inhibition of the enzyme is therefore an important target for breast cancer treatment [20]. Currently, three drug molecules acting as aromatase inhibitors have been approved by the FDA for breast cancer treatment. These include; exemestane (**21**), letrozole (**22**) and anastrozole (**23**) [20] (see figure 7).

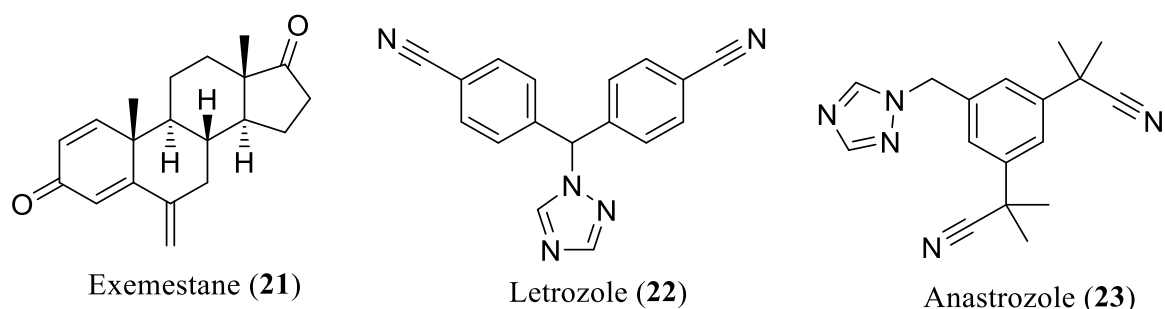


**Figure 7:** Examples of aromatase inhibitors. Created with ChemDraw 21.0.0 as inspired by; (Solum et al., 2014, al-Kazaale et al., 2017).

Exemestane (**21**) inhibits aromatase irreversibly and is steroidal in nature, whereas letrozole (**22**) and anastrozole (**23**) possesses non-steroidal structures, inhibiting aromatase reversibly

[20]. Aromatase inhibitors are very potent against estrogen dependent cancers, but often incur side effects such as vaginal dryness, hot flashes and headache [20].

Sulfatase inhibitors is another important group of steroid compounds used in cancer treatment. The enzyme sulfatase belongs to the mammalian sulfatase family and is responsible for the synthesis of free hydroxysteroids from their ester sulfates by hydrolysis [21]. The ester sulfates of steroids are inactive and conversion by hydrolysis into their free hydroxy forms is very crucial for activity [16]. Inhibition of the enzyme sulfatase therefore reduces the activity of various androgenic and estrogenic steroids, thereby limiting cell proliferation in their corresponding tissues or organs [21]. Under normal conditions, there is an equilibrium between the ester sulfates and their free hydroxysteroids where sulfatase catalyses the forward reaction and another enzyme called steroid sulfotransferase reversibly converts the free hydroxysteroids back to their ester sulfates [21]. However, when there is an overexpression of sulfatase in an organ, for example in the breast, it disturbs the equilibrium leading to higher amounts of the free hydroxysteroids, higher estrogenic and androgenic activities and higher rate of cell proliferation [16, 21]. Inhibition of steroid sulfatase is therefore an important target for breast cancer treatment as well as other types of cancers where overexpression of estrogenic and androgenic steroids is the leading cause [21]. Nomegestrol (**24**) and irosustat (**25**) are examples of lead compounds that inhibit steroid sulfatase (see figure 8). Both compounds are currently in clinical trials [21].

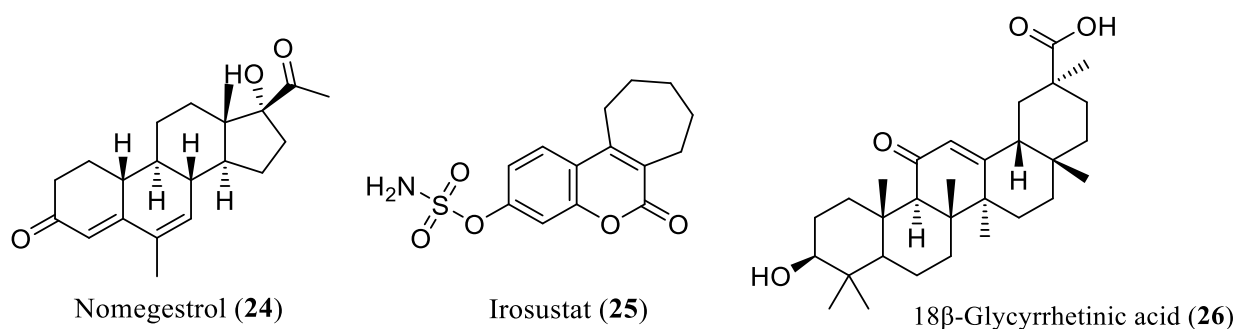


**Figure 8:** Examples of steroid sulfatase- and 17 $\beta$ -Hydroxysteroid dehydrogenase inhibitors. Created with ChemDraw 21.0.0 as inspired by; (Solum et al., 2014, al-Kazaale et al., 2017).

17 $\beta$ -Hydroxysteroid dehydrogenase (17 $\beta$ -HSD) inhibitors are another interesting group of steroid compounds used in cancer treatment. Their mechanism of action is quite similar to that of sulfatase inhibitors in that they catalyze the hydrogenation of 17 $\beta$ -hydroxysteroids to more biologically active forms [16]. Examples of such actions include conversion of estrone to estradiol, conversion of dehydroepiandrosterone to androstenediol and conversion of

androstenedione to testosterone [16] (see scheme 1). Inhibition of this enzyme therefore leads to reduction in estrogenic and androgenic activities in their host tissues, thereby reducing the rate of cell proliferation [16]. The enzyme is mostly expressed in breast and ovary tissues as well as prostate and kidney tissues, especially in tumour development [16]. Cancer treatment in these tissues therefore features the use of 17-HSD inhibitors [16]. However, it is necessary to emphasize that 17-HSD inhibitors are categorized into several subgroups, some of which on the contrary are responsible for the inactivation of specific biologically active steroid hormones such as estradiol [16]. Inhibition of the enzyme can therefore incur several adverse effects [16]. Examples 17-HSD inhibitors include: 18 $\beta$ -Glycyrrhetic acid (**26**) (see figure 8) as well as other analogs of estradiol (**20**) with modifications at C-3, C-5, C-11 and C-20 of the steroid core structure [16].

All three categories of steroid compounds described above are enzyme inhibitors. However, there are other categories of steroid compounds used in cancer treatment, namely anti-estrogens and anti-progestins which selectively bind to estrogen and progestin receptors and modulate their activities by changing the cofactors with which the receptors are connected to, thereby preventing estrogen and progestin from binding to these receptors and thus limiting their activities [20]. One interesting group of steroids in this category is the selective estrogen receptor modulators (SERMS), compounds that act as antagonists on estrogen receptors [22]. They exert their effect by causing conformational changes on distinct sites in the receptor and thus blocking its' activation [20]. Based on their chemical structures, SERMs can be classified into four subgroups consisting of benzothiophenes, triphenylethylenes, phenylindoles and tetrahydronaphthalenes [22]. Tamoxifen (**27**) (see figure 9) belongs to the triphenylethylenes and is the most commonly used SERM in breast cancer treatment worldwide [22].

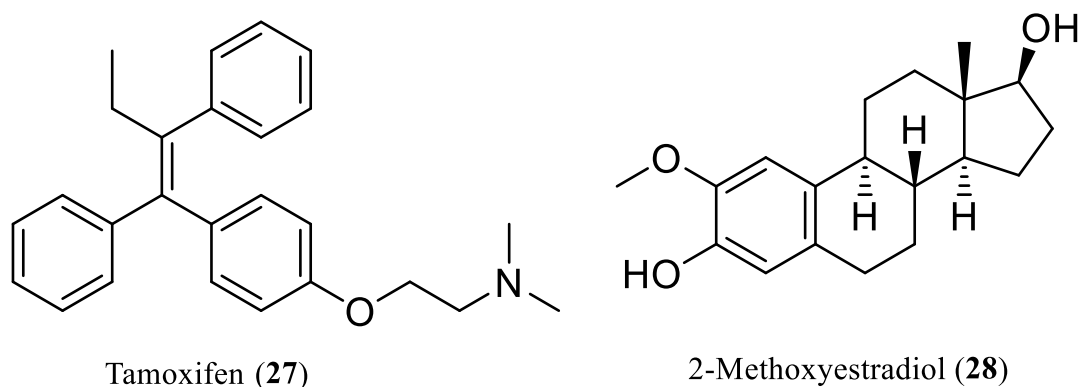
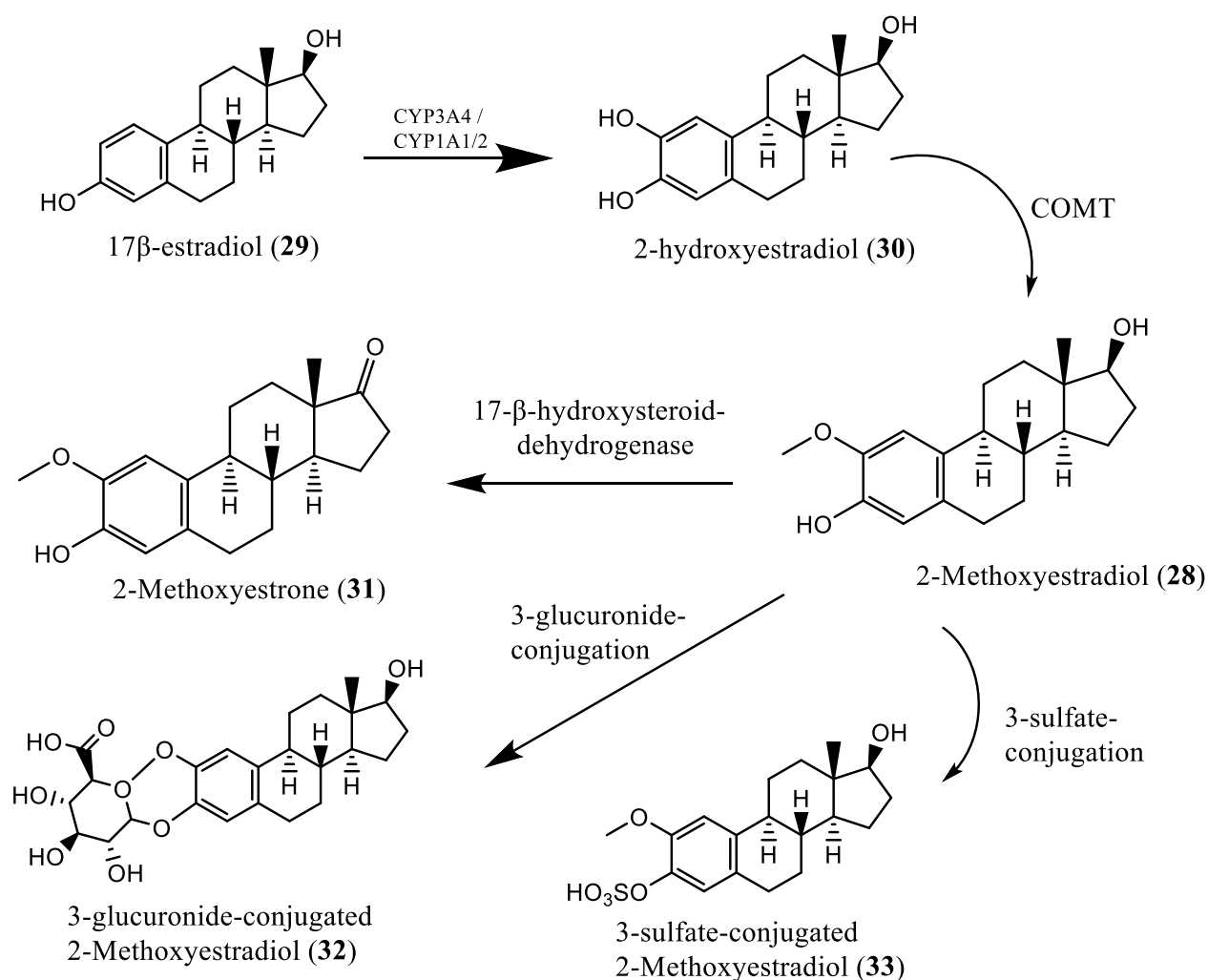


**Figure 9:** Chemical structure of tamoxifen (**27**) and 2-methoxyestradiol (**28**). Created with ChemDraw 21.0.0 as inspired by; (Solum et al., 2014, al-Kazaale et al., 2017).

### 1.3.3 2-Methoxyestradiol

2-Methoxyestradiol (2-ME) (**28**) (see figure 9) is an endogenous metabolite of estrogen which was previously regarded as inactive but has now become a wide of area of interest to the scientific society due to its cytotoxic, anti-angiogenic and anti-proliferative activities [23, 24]. 2-ME is formed by the conversion of the estrogenic steroids 17 $\beta$ -estradiol (**29**) and estrone (see scheme 1) to 2-hydroxyestradiol (2-HDE) (**30**) through a cytochrome P450 dependent enzymatic reaction [23] (see scheme 2). 2-HDE (**30**) is then methylated by catechol-O-methyl transferase (COMT) to form 2-ME (**28**) [23] (see scheme 2).



**Scheme 2:** Biosynthesis and metabolism of 2-ME (**28**). Created with ChemDraw 21.0.0 as inspired by; (Solum et al., 2014, al-Kazaale et al., 2017).

Two main metabolic pathways that lead to rapid deactivation and excretion of 2-ME (**28**) are oxidation by 17- $\beta$ -hydroxysteroid dehydrogenase of the D-ring (C-17-OH) to form 2-methoxyestrone (**31**), and conjugation with glucuronide or sulfate on the A-ring forming the

compounds **32** and **33** respectively (see scheme 2). In spite of its biosynthetic pathway, 2-ME (**28**) does not produce any undesirable estrogenic activities [24].

### **1.3.4 Anti-cancer activities of 2-methoxyestradiol**

Recent advances in the biology and pharmacology of 2-ME (**28**) have indicated that it does not only exhibit anti-cancer activities, but also cardioprotective activities [25]. However, its anti-cancer activities which is generally attributed to anti-proliferative, anti-angiogenic, pro-apoptotic, anti-tubulin and anti-metastatic activities are the most extensively studied [23, 25].

#### **Anti-proliferative activity**

In vitro studies conducted on several human cancer cell lines have revealed that 2-ME (**28**) inhibits cell proliferation and cell growth at a concentration within the nanomolar to micromolar range [23]. Surprisingly, inhibition is not dependent on estrogen receptor binding as 2-ME (**28**) has a very low affinity for estrogen receptors [25]. However, it was reported in other studies that 2-ME (**28**) exhibits anti-proliferative activities by inhibiting the production of endogenous estrogens through a feedback mechanism [25]. In some animal models, it was also reported that 2-ME (**28**) stimulated tumour development at low doses (1 mg/kg), while at high doses (5 mg/kg), tumour development was inhibited [25]. It is therefore important to emphasize that, the anti-proliferative effects of 2-ME (**28**) are dose-dependent and very likely independent of estrogen receptor binding [23-25]. The latter assumption is strengthened by the fact that endogenous estrogen does not share the anti-proliferative activities of 2-ME (**28**) [25]. Studies have revealed that 2-ME (**28**) inhibits cell proliferation through a G1 cell cycle arrest resulting from DNA inhibition and G2/M cell cycle arrest through its activities on microtubules [23]. The latter mechanism of 2-ME (**28**) is evident through inhibition of dynamic changes in the tubulin-microtubule system by binding to the colchicine site [26]. The minimum inhibitory concentration reported so far was in the nanomolar range (10 – 80 nM) and was evident in several cancer cell lines such as breast, lung, ovarian and cervix cancers [25]. For most types of cancers, inhibition occurred at a threshold concentration of 0.1 – 0.3  $\mu$ M with maximum inhibitory concentration at 10 – 20  $\mu$ M [25].

#### **Apoptotic activity**

Apoptosis is a programmed process by which multiple intrinsic and extrinsic signalling pathways mediate the death of a cell [27]. 2-ME (**28**) induces apoptosis specifically in actively dividing cells such as tumour and activated endothelial cells [23]. On the contrary, it

does not induce apoptosis in normal epithelial cells or latent endothelial cells [23]. There are several mechanisms by which 2-ME (**28**) induces apoptosis, some of which include stimulated production of nitric oxide (NO) within the plasma membrane and inhibition of superoxide dismutase, an enzyme that regulates oxidative stress in the cells [23, 28]. However, not all forms of apoptotic pathways induced by 2-ME (**28**) are seen in every tumour type, meaning that 2-ME (**28**) adopts specific mechanisms for certain types of cancers. In leukaemia cells for instance, apoptosis is induced by inhibition of superoxide dismutase through a p53-independent pathway, consequently leading to oxidative stress, while in bovine endothelial cells, 2-ME (**28**) induces apoptosis by short activation of JNK (c-Jun N-terminal kinase) and overexpression of Fas and Bcl-2 ( $\beta$ -cell lymphoma 2) coupled with increased production of NO [25, 28, 29]. In prostate cancer cells, it was reported that 2-ME (**28**), induces apoptosis through p38<sup>MAPK</sup> (mitogen-activated protein kinase)-dependent pathway [23, 29]. The diverse mechanisms by which 2-ME (**28**) induces apoptosis and the degree of specificity in certain types of cancers makes it a unique anti-cancer agent.

### **Anti-angiogenic activity**

The anti-angiogenic activities of 2-ME (**28**) were first reported by Fotsis et al. in 1994 where it was established that 2-ME (**28**) inhibits tumour growth *in vivo* through inhibition of tumour-induced angiogenesis [30]. Furthermore, it has been proposed that disruption of tubulin dynamics by 2-ME (**28**) which inhibits the cellular build-up of hypoxia-induced factor-1 $\alpha$  (HIF-1 $\alpha$ ) and its translocation to the nucleus, consequently leading to inhibition of transcription and secretion of angiogenic factors like VEGF is a possible mode of action [31]. Additionally, induction of apoptosis in vascular endothelial cells is also a possible mechanism by which 2-ME (**28**) exerts its anti-angiogenic activities [31]. Unlike its apoptotic activities, 2-ME (**28**) inhibits angiogenesis also in non-tumour tissues [23]. This was however observed *in vitro* biologic assays (corneal micropocket vascularisation and chick chorioallantoic membrane assays) [23] and have not yet been confirmed *in vivo*. Anti-angiogenesis, principally introduced by Dr. Folkman (Folkman et. al) is very important to prevent metastatic spread of tumours [8] and therefore by this feature of 2-ME (**28**), it can be concluded that the endogenous metabolite of estradiol also possess anti-metastatic properties [8, 30, 31].

### 1.3.5 SAR studies of 2-methoxyestradiol for anti-cancer effect

Structure activity relationship studies conducted so far on 2-ME (**28**) have revealed that it is very potent and well tolerated in the body [32-34]. However, metabolism occurs rapidly as a result of oxidation and conjugation at C-17 on the D-ring and at C-2 and C-3 on the A-ring [33, 35] (see figure 10). Oxidation to 2-methoxyestrone (**31**) at C-17 is specifically known to account for its short half-life *in vivo* and poor bioavailability [34, 35] (see figure 10). Consequently, efforts have been made to synthesize and evaluate several analogs with structural modifications at C-2, C-3, C-16 and C-17 which are known to be important for activity and metabolism [32-34] (see figure 10). Of all the reported analogs with modifications at C-2, 2-ethoxyestradiol was found to be the most potent with IC<sub>50</sub> value at 0.90 μM, inhibiting both cancer cell growth and tubulin polymerization [34, 36].

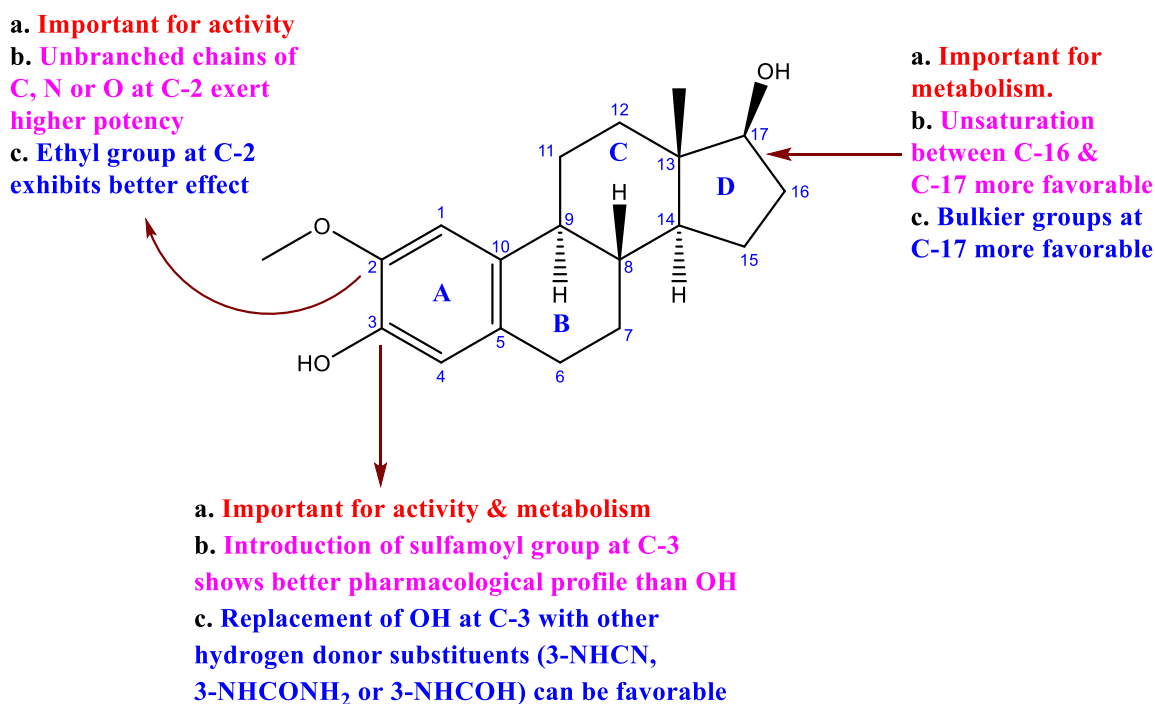


**Figure 10:** An overview of SAR studies of 2-methoxyestradiol (**28**) for anti-cancer effect. Created with ChemDraw 21.0.0 as inspired by; (Solum et al., 2014, al-Kazaale et al., 2017).

Cushman then concluded that, substituents (at C-2) containing unbranched chains of either carbon, nitrogen or oxygen from the second row of the periodic table exerted highest potency in terms of inhibition of tubulin polymerization and anti-proliferation [36] (see figure 10). Furthermore, it was observed that cytotoxicity decreased when the chain was lengthened or shortened [36]. Taking into consideration the hypothesis that C and D rings of 2-ME (**28**) functionally corresponds to A ring of colchicine (**5**) and that C ring of colchicine (**5**) is also

equivalent to A ring of 2-ME (**28**) [33, 37], Entremed, a pharmaceutical company developed the lead analog ENMD-1198 (**34**) (see figure 11) which was 5-6 times more potent than 2-ME (**28**) with respect to anti-proliferative activities on human umbilical vein endothelial cells (HUVECs) [38, 39]. ENMD-1198 (**34**) is currently in clinical trials. It was developed as a result of efforts to stabilise the metabolic and anti-tubulin properties of 2-ME (**28**) with structural modifications at C-3 and C-17 where metabolism occurs most [38] (see figure 10). Another interesting hypothesis that led to this discovery was that 2-ME (**28**) in addition to its structural similarities to colchicine (**5**) also inhibits tubulin polymerization by binding to the colchicine site [35, 36, 38]. Thus, the introduction of ketone functional group at C-3 in ENMD-1198 (**34**). Modification at C-17 of the alcohol to an alkene was primarily to diminish metabolism [38].

Another approach to decrease metabolism of 2-ME (**28**) was to add steric hindrance and electronic effects at C-16 [37, 40]. This approach seemed to be futile because as the rate of metabolism decreases as a result of increased steric hindrance, IC<sub>50</sub> values also increased, making the reported analogs similarly or less potent than 2-ME (**28**) with respect to anti-proliferative activities on MDA-MB-231 cell lines [40]. However, it was observed that introduction of sulfamoyl groups on the A and D rings provided significantly more potent analogs than 2-ME (**28**) [32, 41, 42]. In a special case with focus to synthesize possible steroid sulfatase inhibitors, two sulfamoyl groups were introduced in the same compound, one on the A ring at C-3 and one on the D-ring at C-17 producing a bis-sulfamoyl-2-ME analog (**38**) (see figure 11) which was 60 times more potent than 2-ME (**28**) when tested against HUVECs and up to 13 times higher potency against tubulin polymerization [41]. Consequently, a combined assessment of SAR-studies at C-2 and C-3 provided an analog which was 300 times more potent than 2-ME (**28**) apropos anti-proliferative activities against HUVECs, containing both ethyl- and sulfamoyl-groups at C-2 and C-3 respectively [41]. Subsequent modifications at C-3 with replacement of 3-OH group in 2-ME by hydrogen donor substituents such as 3-NHCN, 3-NHCONH<sub>2</sub> or 3-NHCOH provided analogs that exhibited promising anti-proliferative effects towards HUVECs and MDA-MB-231 cell lines [43]. Notwithstanding, replacement with 3-NH<sub>2</sub> and its derivatives showed lesser activity than 2-ME (**28**) [43] (see figure 10).

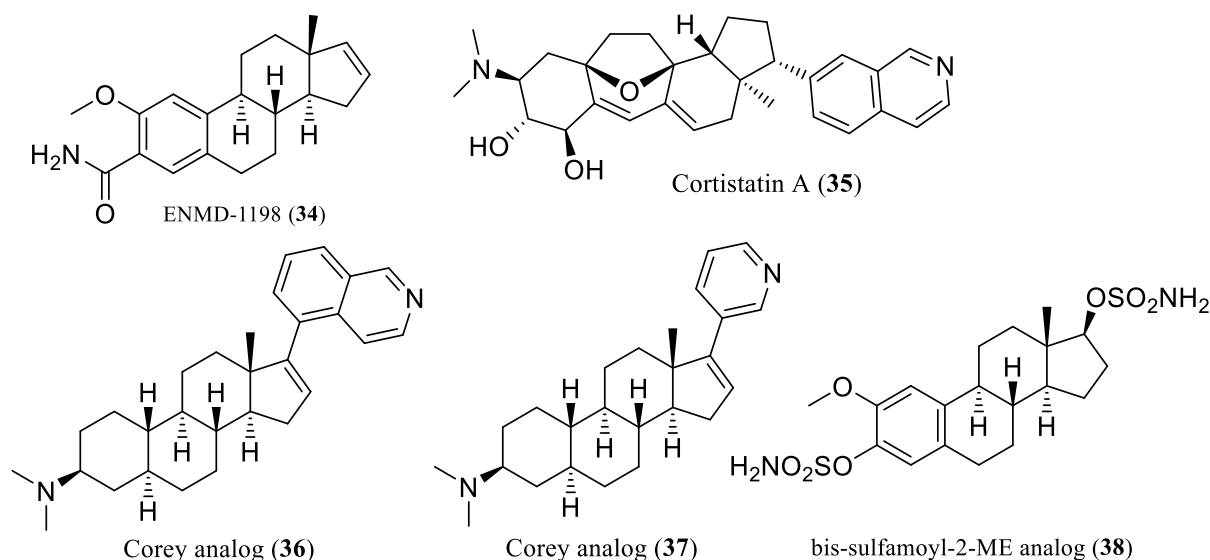


**Figure 11:** Structure of ENMD-1198 (**34**), cortistatin A (**35**), some Corey analogs (**36-37**) and a bis-sulfamoyl-2ME analog (**38**). Created with ChemDraw 21.0.0 as inspired by; (Solum et al., 2014, al-Kazaale et al., 2017).

Cortistatins (see **35** in figure 11 as example), a family of steroidal alkaloids originally isolated from the Indonesian marine sponge *Corticum simplex* by Kobayashi and co-workers is characterized by abeo-9(10-19)-androstane-type steroid core structures featuring a special C-5, C-8 connection and a C-3 dimethyl amino group [44]. Some cortistatins (J, K and L) have an isoquinoline groups at C-17 position, while others (cortistatins E, F, G and H) have N,3-dimethylpiperidine or 3-methylpyridine at the same position [45, 46]. Cortistatins exhibit cytotoxic effects towards several cancer cell lines but are most potent against HUVECs [44, 47]. SAR-studies of cortistatins have revealed that the dimethyl amino group at the C-3 position and the isoquinoline ring are important for activity while introduction of an oxygen function on the D-ring diminishes activity [44]. On the A-ring, the hydroxyl groups can be removed or replaced with other bioisosteres [44]. On account of this data coupled with the hypothesis that the distance between the dimethyl amino groups and the isoquinoline groups is essential for activity, Corey and co-workers prepared analogs (**36** and **37**) of cortistatin with a steroid core structure which exhibited better pharmacological profiles than cortistatins [48] (see figure 11). It was further observed that a double bond between C-16 and C-17 appeared more competitive than their saturated derivatives [48]. Based on conclusions from SAR studies of cortistatins and 2-ME (**28**), Hansen and co-workers subsequently prepared new analogs (**39-44**) of 2-ME (**28**) introducing pyridine, benzene and isoquinoline groups at C-17 as well as sulfamoyl groups at C-3 and ethyl-groups at C-2, consequently maintaining unsaturation between C-16 and C-17 [24, 32, 42] (see figure 12).

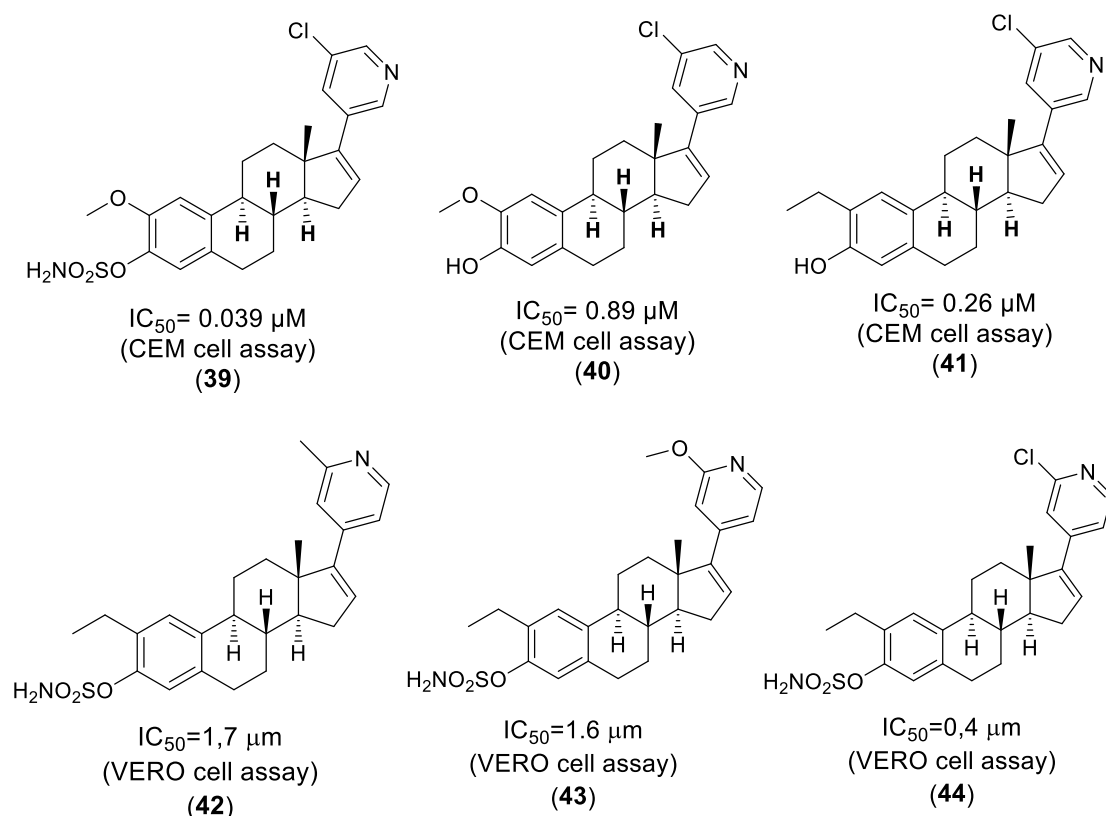


**Figure 12:** Examples of 2-ME analogs (39-44) recently prepared by Hansen and co-workers. Created with ChemDraw 21.0.0 as inspired by; (Solum et al., 2014, al-Kazaale et al., 2017).

Testing the analogs (39-44) against different cancer cell lines, tubulin polymerization and angiogenesis, a number of them showed promising results with the most potent analogs exhibiting as much as 5-6 times higher potency against cell proliferation and angiogenesis compared to 2-ME (28) [32, 42] (see figure 12). In terms of inhibition of tubulin polymerization, there were no significant differences in activity [32, 42].

In a nutshell, SAR-studies conducted on 2-ME (28) so far indicates that modifications at C-2, C-3, C-16 and C-17 are important to improve its potency and metabolism. At C-2, introduction of ethyl-group has shown to be best so far, while introduction of sulfamoyl group at C-3 and a double bond at C-16 and C-17 or bulkier groups such as pyridines and benzenes to provide steric hindrance and electronic effects have proven to be promising (see figure 10).

### 1.3.6 Clinical studies of 2-methoxyestradiol and its analogs

Based on promising results from preclinical trials, 2-ME (**28**) has been subjected to phase I and II clinical trials for the treatment of breast and prostate cancers where toxicity dose study was the focal point [23, 25, 39]. With oral doses of up to 1200 mg per day, no toxic effects were reported, concluding that 2-ME (**28**) was well tolerated in the body [23, 49]. Furthermore, it was reported that 2-ME (**28**) exhibited promising anti-cancer effects with no severe side effects [23, 49]. However, patients in the 1000 mg dose group were reported to have experienced hot flashes [23]. Other patients also experienced gastrointestinal side effects such as nausea, anorexia and fatigue, but none of the reported side effects were comparatively more severe than those from chemotherapy [25, 49].

A phase II randomized double-blind study conducted by Wisconsin University in collaboration with Indiana University featuring 33 patients with hormone-refractory prostate cancer receiving either 400 mg or 1200 mg of oral 2-ME (**28**) capsules daily in 4-week cycles demonstrated that prostate specific antigen as an endpoint in this study decreased between 21 to 40 % in 7 patients in the 1200 mg group and in 1 patient in the 400 mg group [50]. Despite this promising anti-cancer activity results, two cases of deep venous thrombosis were reported in two patients as well as grade 1 or 2 cases of liver transaminase elevation in three patients [50]. However, it was concluded that 2-ME (**28**) was well tolerated in the body with room for improvement in oral bioavailability [50]. Plasma concentration of 2-ME (**28**) was approximately 4 ng/ml in this study [50].

An attempt to determine maximum tolerated oral dosage proved futile in a phase I study where up to 6000 mg of 2-ME (**28**) was given daily without reaching therapeutic plasma concentration, generally because of poor solubility in water and poor bioavailability [23]. The latter is attributed to rapid hepatic first pass metabolism of 2-ME (**28**) as reported by Guo [51]. ENMD-1198 (**34**), an analog of 2-ME (**28**) has also been subjected to phase I and phase II clinical trials for the treatment of several different types of cancers such as breast and prostate cancers [49, 52]. Results from the trials show that ENMD-1198 (**34**) exhibits cytotoxic and anti-angiogenic properties with slightly better pharmacokinetic profiles than 2-ME (**28**), yet without any significant improvement in aqueous solubility and oral bioavailability [49].

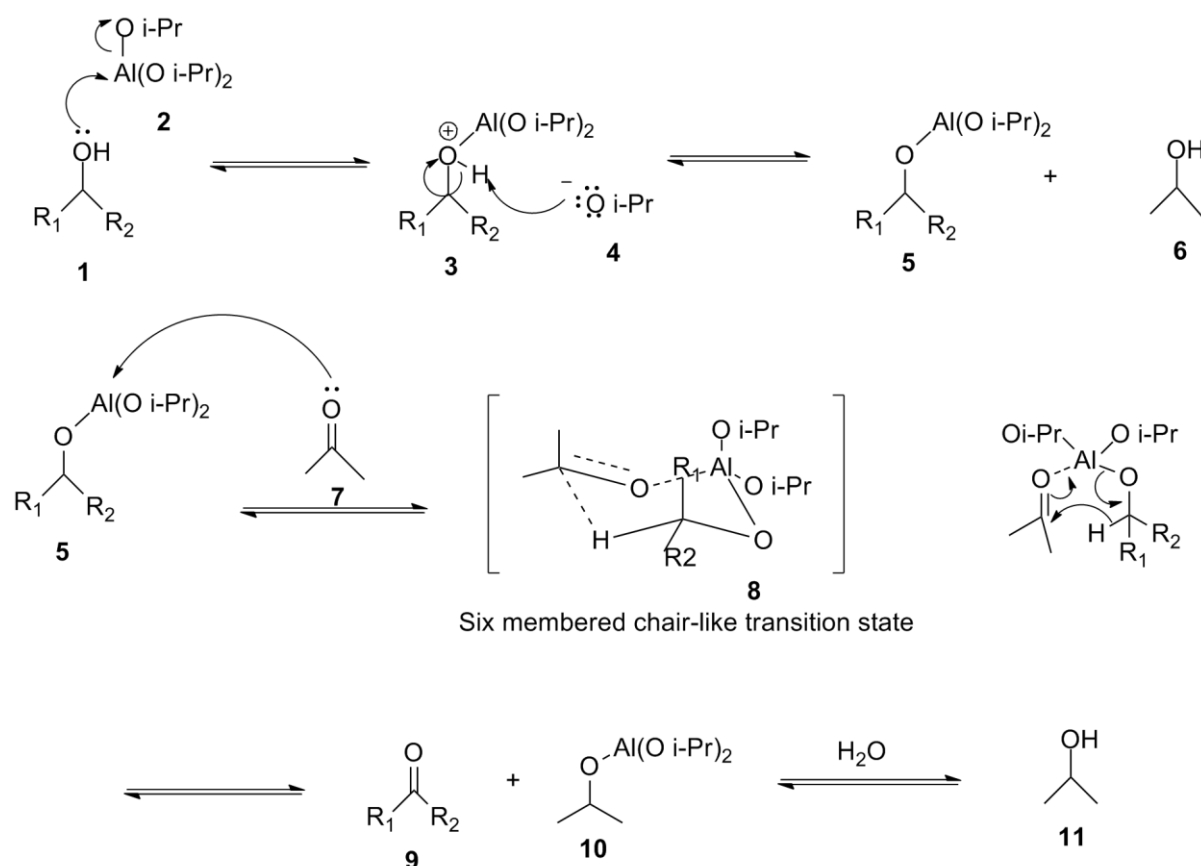
There was therefore the need to make a new formulation with better pharmacokinetic properties and as such Entremed developed a new formulation of ENMD-1198 (**34**) called

NanoCrystal dispersion 2-ME (Panzem®NCD) whose drug delivery approach is based on reduction of drug particle size into submicron particle sizes and formulated as nano crystals making it more soluble in water [53, 54]. A phase I study with this formulation demonstrated that it was generally well tolerated in the body with improved pharmacokinetic properties [53]. On the contrary, disease progression was observed in patients with highest plasma concentration [53]. The maximum tolerated oral dosage of Panzem®NCD was reported to be 1000 mg every 6 hours [53]. In a phase II study featuring patients with taxane-refractory metastatic castrate-resistant prostate cancer (CRPC), there was not observed any clinically significant activity of Panzem®NCD [54].

## 1.4 Synthetic methods

### 1.4.1 Oppenauer oxidation

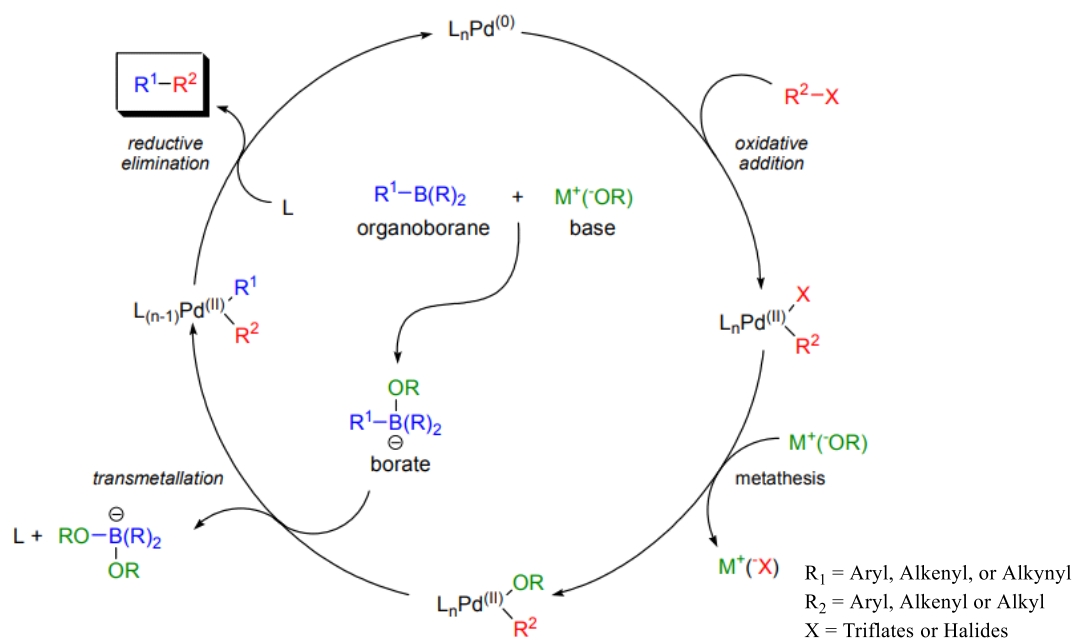
Oppenauer oxidation is a reversible reaction used to selectively oxidize secondary alcohols to ketones in the presence of aluminium alkoxide, and excess acetone or cyclohexanone which acts as the hydride acceptor to shift the equilibrium to the product side [55]. The opposite reaction of the equilibrium is called Meerwein-Ponndorf-Verley reduction [55]. In the synthesis of new analogs of 2-ME, Oppenauer oxidation was applied to convert 2-ME (**28**) to 2-ME-estrone (**31**), oxidizing the secondary alcohol on the D-ring at C-17 to a ketone. In the first step of the reaction, the alcohol binds to the aluminium to form a complex, after which it is deprotonated by an alkoxide ion to form an alkoxide intermediate [55]. This intermediate further binds to acetone / cyclohexanone to generate a six membered chair-like transition state where aluminium is bound to both the alkoxide and the acetone / cyclohexanone [55]. In this transition state, aluminium activates acetone / cyclohexanone for a hydride transfer from the alkoxide, thus forming the expected ketone [55] (see scheme 3).



**Scheme 3:** Mechanism of the Oppenauer oxidation reaction [56]. Accessed: April 27, 2023. from: [[https://en.wikipedia.org/wiki/Oppenauer\\_oxidation#/media/File:Oppenauer\\_oxidation\\_mechanism\\_layout.png](https://en.wikipedia.org/wiki/Oppenauer_oxidation#/media/File:Oppenauer_oxidation_mechanism_layout.png)]

## 1.4.2 Suzuki-Miyaura coupling reaction

Suzuki-Miyaura coupling reaction is a palladium catalysed cross-coupling reaction between organoboron compounds and organic halides or triflates to form carbon-carbon bonds [57]. It was first reported by Akira Suzuki and Norio Miyaura in 1979 in an attempt to synthesize stereoselective arylated alkenes from a reaction between 1-alkenylboranes and aryl halides in the presence of palladium catalyst [58]. The reaction occurs under mild conditions, is able to withstand water and inorganic biproducts formed can be easily removed, making it more suitable for industrial scale production [57]. In the synthesis of new analogs of 2-ME (**28**), Suzuki-Miyaura coupling reaction was employed to convert TBS-protected steroid triflate (**46**) (see scheme 4) to TBS-protected 2-ME steroid analogs by adding different boronic acids to the steroid triflate (**46**). In the mechanistic steps of the reaction, the organoboronic acid forms an alkyl-borate complex with the base, as the organic triflate is also activated by the palladium catalyst to form a complex which transforms into a suitable substrate by metathesis and then added to the alkyl-borate complex by transmetalation [57, 58]. The resulting complex formed is then transformed into a C-C sigma bond by reductive elimination as the palladium catalyst is regenerated [57] (see scheme 4).



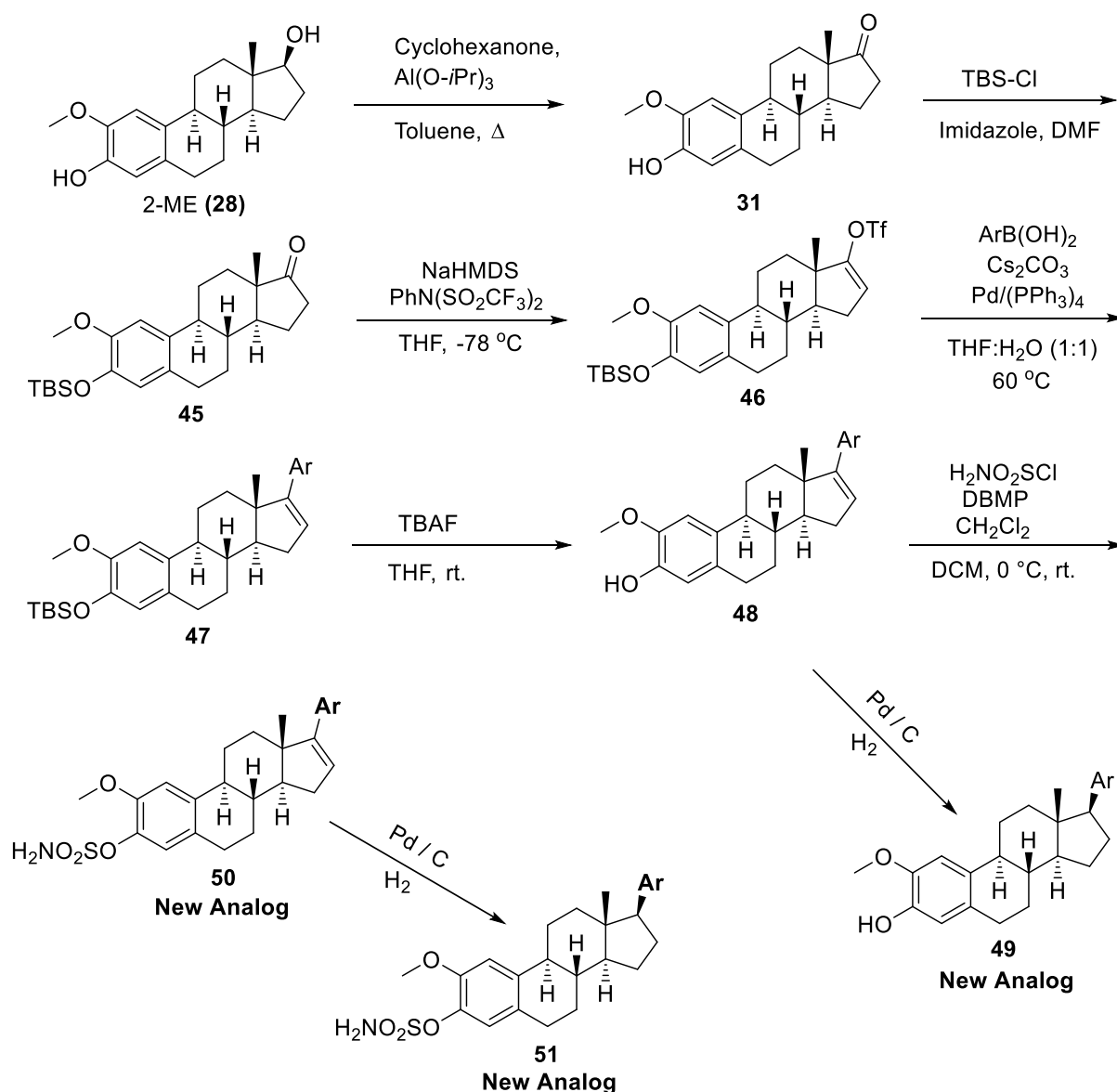
**Scheme 4:** Mechanism of the Suzuki coupling reaction. Taken from reference [57].

## 1.5 Aim of study

SAR-studies of 2-ME (**28**) have shown that C-2 and C-3 positions on the A-ring as well as C-16 and C-17 positions on the D-ring are important for anti-cancer activity and metabolism. Both 2-ME (**28**) and its analogs have demonstrated promising anti-cancer activities both in vitro and in vivo. Unfortunately, because of challenges with aqueous solubility and oral bioavailability, none of the analogs have made significant clinical breakthroughs. The purpose of this research is to synthesize new analogs of 2-ME (**28**) based on previous SAR-studies and clinical trials with the aim to improve cytotoxic activity and metabolism, as well as aqueous solubility and oral bioavailability. SAR studies at C-3, C-16 and C-17 have demonstrated that sulfonamide group at C-3 exhibits better cytotoxic effects than their corresponding OH derivatives, substituted pyridine ring with chlorine at C-17 showed promising anti-cancer activities and finally a double bond between C-16 and C-17 appeared more competitive than their saturated derivatives. Therefore, we synthesized four new analogs (**48-51**) of 2-ME (**28**) with modifications at C-3, C-16 and C-17, attaching a substituted pyridine ring with fluorine at C-17 and replacing OH with sulfonamide at C-3 while reducing the double bond between C-16 and C-17. All new analogs will be tested against different cancer cell lines in collaboration with Professor James Lorens, University of Bergen and Professor Cheng-Hong Chen, Taiwan University as well as the Norwegian Centre for Molecular Medicine, Oslo, Norway. Additionally, the analogs will be tested for estrogen agonism in collaboration with Professor Ragnhild Paulsen and her group at the Department of Pharmacy, University of Oslo.

## 2 Results and discussion

The synthesis of new analogs of 2-ME (**28**), precisely analogs **48-51** are shown in scheme 5. In the initial steps of the synthesis, Oppenauer oxidation was employed to convert 2-ME (**28**) to 2-methoxyestrone (**31**), oxidizing the secondary alcohol at C-17 to a ketone in the presence of aluminium isopropoxide and cyclohexanone, using toluene as organic solvent. The alcohol at C-3 in 2-methoxyestrone (**31**) was then protected with TBS to yield the steroid (**45**) which was further converted to enol triflate (**46**) (see scheme 5).



**Scheme 5:** Synthesis of new analogs (**48 – 51**) of 2-ME (**28**). Created with ChemDraw 21.0.0 as inspired by; (Solum et al., 2014, al-Kazaale et al., 2017).

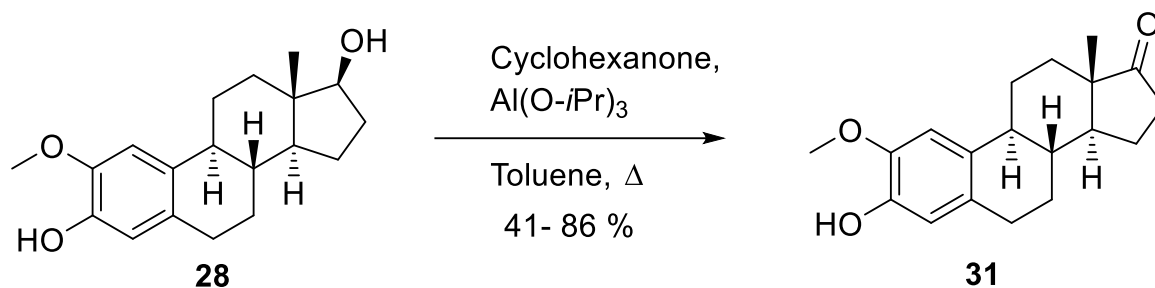
At this point the Suzuki coupling reaction was employed to attach the substituted organoboronic acid to the enol triflate (**46**) using palladium tetrakis as catalyst. This yielded the steroid molecule **47** which was then deprotected with TBAF to produce the first 2-ME analog (**48**) in the synthesis. Analog **48** was then treated with excess hydrogen in the presence of palladium on carbon to reduce the double bond between C-16 and C-17 yielding a new 2-ME analog (**49**). To attach sulfonamide at C-3, analog **48** was again treated with sulfamoyl chloride and DBMP (2,6-di-*tert*-butyl-4-methylphenol) using anhydrous dichloromethane as solvent to yield a new 2-ME analog (**50**). In similarity to analog **48**, analog **50** was also exposed to excess hydrogen in the presence of palladium on carbon to reduce the double bond between C-16 and C-17, yielding a new 2-ME analog (**51**) (see scheme 5).

## **2.1 Synthesis and characterization of new analogs of 2-methoxyestradiol**

This was an eight-step synthesis to produce four new analogs of 2-ME (**28**) in acceptable yields. All synthetic steps were previously reported by Solum et al. [24] with the key ones being Oppenauer Oxidation and Suzuki coupling reaction. The latter was employed to attach substituted organoboronic acids to steroid triflate (**46**), while the former, notably the first step in the synthesis apparently converted 2-ME (**28**) to 2-methoxyestrone (**31**).

### **2.1.1 Synthesis of 2-methoxyestrone (31)**

2-ME (**28**) was first dissolved in toluene in a round-bottomed flask attached to a Dean-Stark trap and a reflux condenser, after which excess cyclohexanone and five equivalents of aluminium isopropoxide were added. The reaction was then heated at reflux and allowed to stir for 24 hours. At this point, TLC was performed to detect the product, after which it was extracted with ethyl acetate, dried over magnesium sulfate and purified by flash chromatography to give the desired product. The reaction was performed thrice with variable yields between 41 and 86 % (see scheme 6).



**Scheme 6:** Synthesis of 2-methoxyestrone (**31**) by Oppenauer oxidation. Created with ChemDraw 21.0.0 as inspired by; (Solum et al., 2014, al-Kazaale et al., 2017).

### 2.1.2 NMR characterization of 2-methoxyestrone (**31**)

In the processed proton NMR spectrum (see figure 15 in appendix 7.1), two signals appeared in the aromatic region at 6.79 ppm and 6.66 ppm, representing the two aromatic protons in the molecule, both seen as singlets as expected. Two signals were expected to integrate for two methyl groups (three protons) in the molecule and are seen at 3.86 ppm and 0.92 ppm, both seen as singlets as expected. The signal at 3.86 ppm surely represents the methyl group attached to oxygen at C-2 because of deshielding effect while the other at 0.92 ppm represents the methyl group at C-13. A singlet with one proton appeared at 5.49 ppm and is most likely due to OH-group at C-3 as there is no other OH-group in the molecule. The rest of the signals appeared in the aliphatic region from 1-3 ppm as expected.

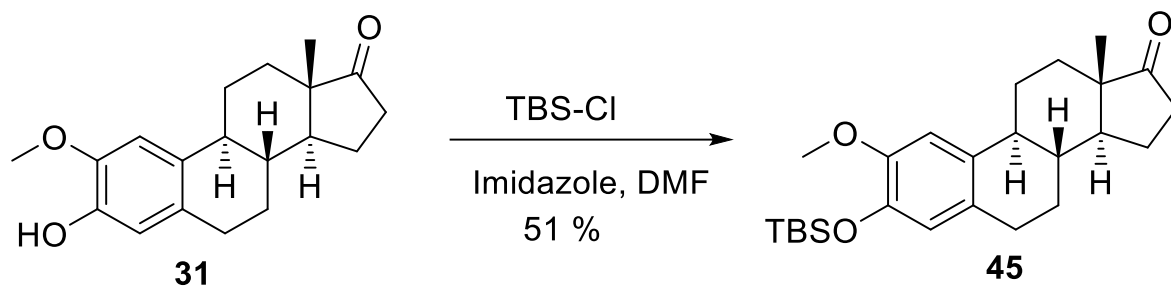
In the recorded <sup>13</sup>C NMR spectrum (see figure 16 in appendix 7.1), a characteristic signal for the only ketone in the molecule appeared at 221 ppm, confirming that the reaction has been successful. Furthermore, there was expected a total of 19 signals in the spectrum as there are 19 carbon atoms in the molecule and they all appeared as expected. Characteristically, six signals appeared in the aromatic region as expected, integrating for six carbon atoms in the A-ring. The signal at 14.35 ppm is likely to account for the methyl group at C-13 while the one at 22.04 ppm most likely represents the methyl group at C-2. The rest of the signals appeared between 25 and 60 ppm as expected.

The processed proton and carbon spectra for 2-methoxyestrone (**31**) were in accordance with what has earlier been reported in the literature. [24, 42].

### 2.1.3 Synthesis of 3-*tert*-butyldimethylsiloxy-2-methoxyestrone (**45**)

To protect the OH-group at C-2, 2-methoxyestrone (**31**) was dissolved in anhydrous DMF in a round-bottomed flask and treated with five equivalents of 3-*tert*-butyldimethylsilyloxychloride (TBSCl) and three equivalents of imidazole. The reaction was stirred under nitrogen gas and

at room temperature for 19 hours, after which TLC was performed to detect the product. Thereafter, the mixture was extracted with ethyl acetate alongside an aqueous workup with brine, dried over magnesium sulfate and finally purified by flash chromatography, yielding the desired product in 51 % output (see scheme 7).



**Scheme 7:** Synthesis of 3-tert-butyldimethylsiloxy-2-methoxyestrone (45). Created with ChemDraw 21.0.0 as inspired by; (Solum et al., 2014, al-Kazaale et al., 2017).

#### 2.1.4 NMR characterization of 3-tert-butyldimethylsiloxy-2-methoxyestrone (45)

In the processed proton NMR spectrum (see figure 17 in appendix 7.1), two signals were expected in the aromatic region as singlets integrating for one proton each in the A-ring and both were seen at 6.76 ppm and 6.56 ppm as projected. The singlet at 5.49 ppm which was due to the OH-group at C-3 in 2-methoxyestrone (31) has now disappeared, signifying that the proton in the OH-group at C-3 has been eliminated. To confirm that the OH-group has been protected with TBS, two characteristic singlets were expected in the aliphatic region between 0 – 1 ppm integrating for nine protons and six protons each and both were seen at 0.99 ppm and 0.15 ppm respectively. Thus, confirming the success of the reaction. The rest of the signals were similar to that reported for 2-methoxyestrone as expected.

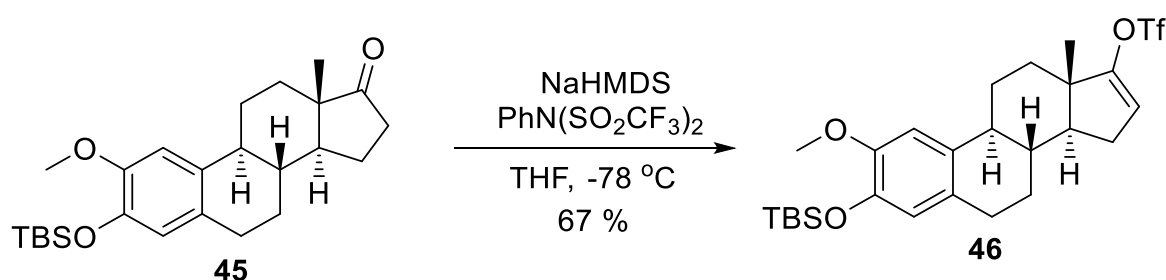
In the processed <sup>13</sup>Carbon NMR spectrum (see figure 18 in appendix 7.1), the characteristic signal for the only ketone in the molecule was still visible at 221 ppm, thus confirming that protection only occurred at C-3. Furthermore, six signals were expected to appear in the aromatic region as observed previously and all six were clearly visible from 110 ppm to 150 ppm, integrating for six carbon atoms in the A-ring. Obviously, the highest peaks in this region, namely 143 ppm and 149 ppm are likely to account for the carbon atoms at C-2 and C-3 as a result of deshielding effect from the oxygen atoms. The highest peak in the spectrum observed in the aliphatic region at 26.8 ppm is highly likely from the *tert*-butyl group whiles

the two negative signals at -4.4 ppm each account for the two methyl groups bound to silicon in the TBS-group, thus confirming the presence of TBS at C-3. Moreover, the methyl groups at C-2 and C-13 appeared at 18.6 ppm and 14.1 ppm respectively. The methyl at C-2 is higher in shift than C-13 because of deshielding effect from the oxygen atom. The rest of the signals were seen in the aliphatic region between 20 ppm and 60 ppm as expected.

The processed proton and carbon NMR spectra for 3-*tert*-butyldimethylsiloxy-2-methoxyestrone (**45**) were in accordance with what has earlier been reported in the literature. [24, 42].

### 2.1.5 Synthesis of 3-*tert*-butyldimethylsiloxy-2-methoxy-steroid-triflate (**46**)

To make the steroid molecule suitable for Suzuki coupling reaction, it had to be converted to enol triflate and therefore TBS-protected 2-methoxyestrone (**45**) was treated with one and a half equivalents of *N*-phenyl-bis (trifluoromethanesulfonamide) and three equivalents of sodium bis (trimethylsilyl) amide (NaHMDS, 1.0 M in toluene) in anhydrous THF in a round bottomed flask. The reaction was stirred at -78 °C for three hours after which TLC was performed to detect the product before being extracted with dichloromethane and brine, then dried over magnesium sulfate and purified by flash chromatography. The reaction yielded 67 % of the enol triflate seen as colourless oil (see scheme 8).



**Scheme 8:** Synthesis of TBS-protected-2-methoxy enol triflate (**46**). Created with ChemDraw 21.0.0 as inspired by; (Solum et al., 2014, al-Kazaale et al., 2017).

### 2.1.6 NMR characterization of 3-*tert*-butyldimethylsiloxy-2-methoxy-steroid-triflate (**46**)

The processed proton NMR spectrum (see figure 19 in appendix 7.1) showed two characteristic signals in the aromatic region, both seen as singlets as expected namely 6.73 ppm and 6.55 ppm. The proton at C-16 was visible as a doublet at 5.61 ppm signifying that a double has been formed between C-16 and C-17, hence confirming a successful reaction. The

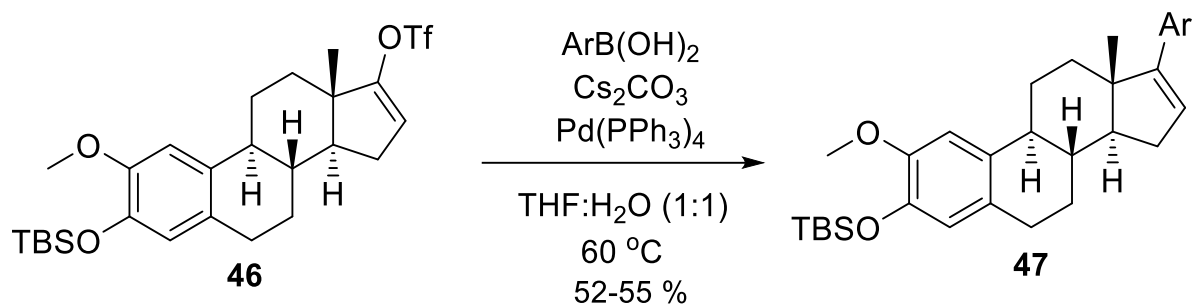
characteristic signals for the TBS-group were also present at 0.99 ppm and 0.15 ppm accounting for nine and six protons respectively. The methyl groups at C-2 and C-13 were seen at 3.77 ppm and 1.01 ppm respectively, with the protons at C-2 higher in shift due to deshielding effect from the oxygen atom. The rest of the signals appeared in the aliphatic region between 1 and 3 ppm as expected integrating for the remaining 13 protons.

In the processed  $^{13}\text{C}$  NMR spectrum (see figure 20 in appendix 7.1), the characteristic signal for the only ketone in the molecule which often appears at 221 ppm was not visible, confirming that the ketone has been transformed into the desired enol triflate. Moreover, there used to be six signals in the aromatic region, accounting for six carbon atoms in the A-ring, but this time the aromatic signals were eight in total, signifying the presence of a double bond between C-16 and C-17 which adds up to the six aromatic signals to make it eight in total. Moreover, the highest peak in the spectrum observed in the aliphatic region at 25.6 ppm is likely from the *tert*-butyl group while the two negative signals at -4.7 ppm each account for the two methyl groups bound to silicon in the TBS-group, thus confirming the presence of TBS at C-3. Moreover, the methyl groups at C-2 and C-13 were also visible at 18.3 ppm and 15.2 ppm respectively, with the methyl at C-2 showing higher shift than C-13 because of deshielding effect from the oxygen atom at C-2. The rest of the signals were seen in the aliphatic region between 20 ppm and 60 ppm as expected.

The processed proton and carbon spectra for the TBS-protected-2-methoxy-enol-triflate (**46**) were in accordance with what has earlier been reported in the literature. [24, 42].

### 2.1.7 Synthesis of 3-*tert*-butyldimethylsiloxy-2-methoxy-steroid-analog (**47**)

This was the most critical step in the synthesis of new analogs of 2-ME (**28**) in this project. Suzuki coupling reaction was employed to attach a substituted organoboronic acid to the enol triflate (**46**). In this reaction, the enol triflate (**46**) was dissolved in a 1:1 mixture of tetrahydrofuran and water together with two equivalents of cesium carbonate and 1.16 equivalents of the substituted organoboronic acid using 0.05 equivalent of palladium tetrakis as catalyst. The reaction was stirred at 60 °C under  $\text{N}_2$  atmosphere for 24 hours. At this point, TLC was performed to detect the product, after which it was extracted with ethyl acetate, dried over magnesium sulfate and purified by flash chromatography, yielding the desired product as white crystals. This reaction was performed twice with slightly variable yields between 52 and 55 % (see scheme 9).



**Scheme 9:** Synthesis of TBS-protected-2-ME-analog (**47**). Created with ChemDraw 21.0.0 as inspired by; (Solum et al., 2014, al-Kazaale et al., 2017).

### 2.1.8 NMR characterization of 3-*tert*-butyldimethylsiloxy-2-methoxy-steroid-analog (**47**)

In the processed proton NMR spectrum (see figure 21 in appendix 7.1), a total of five signals were observed in the aromatic region which corresponds to five aromatic protons in the molecule. The two highest shifts at 8.48 ppm and 8.34 ppm are very likely from the protons closest to nitrogen in the pyridine ring at C-21 and C-22 as a result of deshielding effect from nitrogen. The proton at C-21 in between fluorine and nitrogen must be the highest shift in the spectrum at 8.48 ppm due to deshielding effect from both nitrogen and fluorine. The signals at 6.76 ppm and 6.57 ppm represents the two aromatic protons at C-1 and C-4 in the A-ring, both integrating as singlets as expected. The remaining signal in the aromatic region at 7.40 ppm seen as doublet of triplets ( $J = 9.9, 2.3$  Hz) must be the proton at C-19 (farthest from the nitrogen atom in the pyridine ring). The olefinic proton at C-16 is observed at 6.09 ppm as a doublet of doublets ( $J = 3.4, 1.8$  Hz). The characteristic signals for the TBS-group were present at 0.99 ppm and 0.15 ppm, integrating for nine protons and six protons respectively as expected. The two methyl groups in the molecule at C-2 and C-13 were also observed at 3.78 ppm and 1.06 ppm respectively, with the one C-2 showing higher shift due to deshielding effect from the oxygen atom. The rest of the signals appeared in the aliphatic region between 1-3 ppm as expected. Moreover, a total of 40 protons were recorded in the spectra which corresponds to the number protons in the molecule. Thus, confirming that the reaction has been successful.

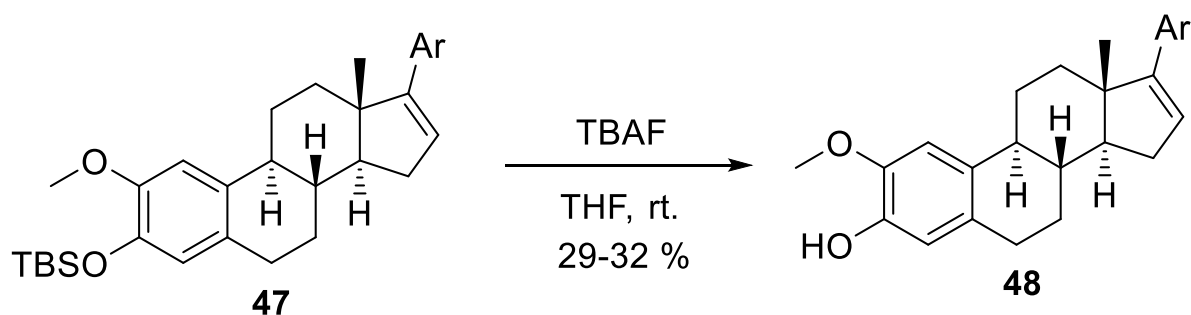
In the processed  $^{13}\text{C}$  NMR spectrum (see figure 22 in appendix 7.1), there were a total of 13 signals in the aromatic region representing six carbon atoms in the A-ring, five carbon atoms in the pyridine-ring and the two carbon atoms forming the double bond between C-16 and C-17. The characteristic signals for the TBS-group were present at 25.9 ppm and -4.4 ppm as

expected. The two methyl groups in the molecule were also seen at 18.9 ppm and 16.9 ppm representing attachment to C-2 and C-13 respectively, with the former higher in shift than the latter due to deshielding effect from the oxygen atom at C-2. The rest of the signals appeared in the aliphatic region between 20 and 60 ppm as expected. A total of 28 signals were recorded in the spectra representing 30 carbon atoms in the molecule and this is due to the fact the tert-butyl group shows only one signal (at 25.9 ppm) but contains three carbon atoms.

The recorded proton and carbon NMR spectra correspond to what was expected of the product and hence the reaction was deemed successful.

### 2.1.9 Synthesis of 2-methoxy-steroid-analog (48)

After successfully attaching the organoboronic acid to the steroid triflate (46), it was then necessary to remove the TBS-protecting group at C-3 in order to make the product molecule biologically active. The TBS-protected-2-ME-pyridine-analog (47) was dissolved in anhydrous THF and treated with 1.07 equivalents of tetra-n-butylammonium fluoride (TBAF) in a round bottomed flask. The reaction was stirred at room temperature under nitrogen atmosphere for 24 hours, after which TLC was performed to detect the product followed by extraction with ethyl acetate, drying over magnesium sulfate and purification by flash chromatography, yielding the desired product as white crystals. The reaction was performed twice with variable yields between 29-32 % (see scheme 10).



**Scheme 10:** Synthesis of 2-ME-pyridine-analog (48). Created with ChemDraw 21.0.0 as inspired by; (Solum et al., 2014, al-Kazaale et al., 2017).

### 2.1.10 NMR & HRMS characterization of 2-methoxy-steroid-analog (48)

In the processed proton NMR spectrum (see figure 23 in appendix 7.1), the characteristic signals for the TBS-group often seen as singlets between 0 – 1 ppm were not visible, signifying that the TBS-group has been removed. Moreover, the proton in the OH group at C-3 appeared clearly at 5.75 ppm as singlet as expected. In the aromatic region, five signals

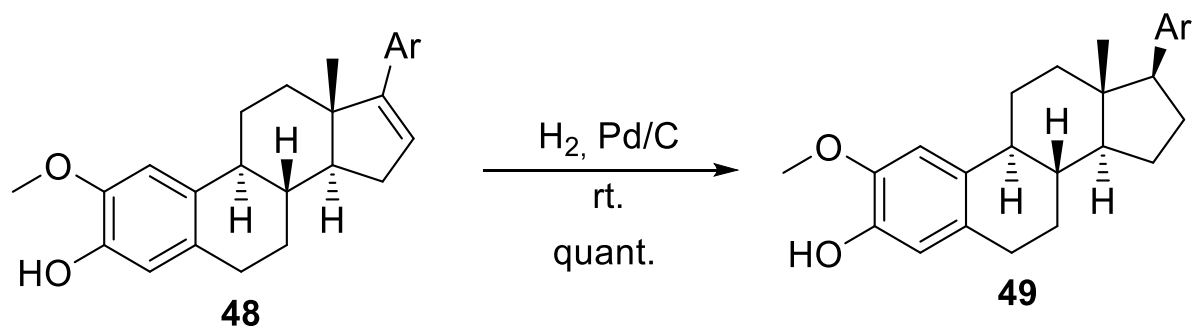
were projected to appear representing the five aromatic protons in the molecule and they were seen between 6.5 ppm and 8.5 ppm as projected, integrating for one proton each. The olefinic proton at C-16 was also visible at 6.10 ppm as doublet of doublets ( $J = 3.4, 1.8$  Hz). The two methyl groups in the molecule appeared at 1.06 ppm and 3.87 ppm as expected, with the one being higher in shift than the other due to deshielding effect from the oxygen atom at C-2. The rest of the signals were visible in the aliphatic region between 1 – 3 ppm as expected and thus confirming that the reaction has been successful.

In the processed  $^{13}\text{C}$  NMR spectrum (see figure 24 in appendix 7.1), the characteristic signals for the TBS-group often seen as one high peak and two negative shifts in the aliphatic region did not appear, signifying that the TBS group has been removed. Furthermore, 13 signals were projected to appear in the aromatic region representing six carbons in the A-ring, five carbons in the pyridine ring and two carbons forming a double bond between C-16 and C-17. They all appeared in the aromatic region as projected. The rest of the signals, 11 in total appeared in the aliphatic region between 20 ppm and 60 ppm as expected, representing the 11 remaining carbons.

In the HRMS elemental analysis report (see figure 31 in appendix 7.2), the total molecular mass found for the molecule  $\text{C}_{24}\text{H}_{26}\text{FNO}_2$   $[\text{M}-\text{H}]^-$  was 378.1874 and this corresponded almost exactly with the calculated molecular mass for the molecule  $\text{C}_{24}\text{H}_{26}\text{FNO}_2$   $[\text{M}-\text{H}]^-$  which is 378.1875, confirming that the product formed from the reaction is precisely the correct product. Meanwhile, a peak is observed at 379.1908 accounting for one-third of the peak at 378.1874 and this is most likely due to the presence of carbon 13 isotope in the molecule.

### 2.1.11 Synthesis of 2-methoxy-steroid-analog (49)

In order to make a new analog of 2-ME (**28**), 2-methoxy-pyridine steroid (**48**) was dissolved in ethyl acetate and treated with palladium on carbon (Pd/C 10 % w/w) under hydrogen gas. The reaction was allowed to stir at room temperature for 36 hours, after which TLC was performed to detect the product followed by filtration on celite to give the desired product as white crystals in 100 % yield (see scheme 11).



**Scheme 11:** Synthesis of 2-ME-pyridine-analog (**49**). Created with ChemDraw 21.0.0 as inspired by; (Solum et al., 2014, al-Kazaale et al., 2017).

### 2.1.12 NMR and HRMS characterization of 2-methoxy-steroid-analog (**49**)

In the processed proton NMR spectrum (see figure 25 in appendix 7.1), there were four signals in the aromatic region, integrating for five protons in total which corresponds to the number of aromatic protons in the molecule. The signal at 8.32 ppm shows a multiplet with two protons and most likely represents the two protons closest to nitrogen in the pyridine ring. The singlets at 6.78 ppm and 6.65 ppm most likely represents the two aromatic protons in the A-ring. The remaining signal in this region, namely at 7.30 ppm showing a doublet of triplets ( $J = 10.0, 2.3$  Hz) must be representing the other proton in the pyridine ring farthest from nitrogen. With a total of five signals in the aromatic region, it suggests that the signal which often integrates for the olefinic proton at C-16 is missing and this confirms the absence of a double bond between C-16 and C-17 meaning that the reaction has been successful. The two methyl groups in the molecule, specifically at C-2 and C-13 appeared at 3.85 ppm and 0.54 ppm respectively, with the former possessing higher shift than the latter due to deshielding effect from the oxygen atom at C-2. The singlet with one proton at 5.77 ppm represents the proton in the OH-group at C-3. The rest of the signals appeared in the aliphatic region between 1 – 3 ppm as expected, increasing with three more protons than usual which further confirms the presence of a saturated bond between C-16 and C-17. Moreover, the position of the pyridine-ring at C-17 is more or less stereoselective as a result of steric hindrance from the methyl group at C-13 which makes the hydrogen atom from  $H_2$  attach from the back side of C-17, thus forming the *S* configuration as seen in scheme 11.

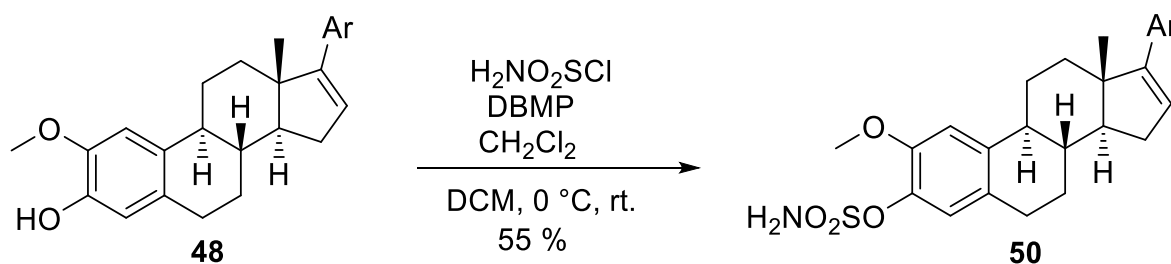
In the processed  $^{13}C$  NMR spectrum (see figure 26 in appendix 7.1), a total of 11 signals appeared in the aromatic region, representing five carbons in the pyridine ring and six carbons in the A-ring. The absence of two signals in the aromatic region suggests that the double bond between C-16 and C-17 has disappeared, thus confirming that the reaction has been

successful. The remaining signals appeared in the aliphatic region, integrating for the remaining 13 carbons as expected, increasing with two more signals than usual because of additional two aliphatic carbons, namely C-16 and C-17 as a result of hydrogenation.

In the recorded HRMS elemental analysis report (see figure 32 in appendix 7.2), the recorded molecular mass for  $C_{24}H_{28}FNO_2$   $[M-H]^-$  is 380.2031 and this corresponds to the calculated molecular mass projected for the compound, which is 380.2031, confirming that the product formed from the reaction is precisely in alignment with the actual product. Moreover, there is a peak at 381.2064 constituting about one-third of the highest peak in the spectrum as a result of carbon 13 isotope in the molecule.

### 2.1.13 Synthesis of 2-methoxy-steroid-analog (50)

With the aim to synthesize yet a new analog of 2-ME (**28**) by attaching a sulfonamide at C-3, the steroid molecule (**48**) was dissolved in anhydrous dichloromethane in a round bottomed flask at room temperature and cooled to 0 °C before being treated with three equivalents of 2,6-di-*tert*-butyl-4-methyl pyridine (DBMP) and three equivalents of sulfamoyl chloride under stirring for 30 minutes. The reaction was then heated to room temperature and allowed to stir for 24 hours under nitrogen atmosphere. At this point, TLC was performed to detect the product, before being extracted with ethyl acetate, dried over magnesium sulfate and purified by flash chromatography, yielding the desired product as white crystals in 55 % output (see scheme 12).



**Scheme 12:** Synthesis of 2-ME-pyridine-sulfonamide (**50**). Created with ChemDraw 21.0.0 as inspired by; (Solum et al., 2014, al-Kazaale et al., 2017).

### 2.1.14 NMR and HRMS characterization of 2-methoxy-steroid-analog (50)

In the processed proton NMR spectrum (see figure 27 in appendix 7.1), a total of five signals appeared in the aromatic region, integrating for one proton each and representing the five aromatic protons in the molecule as expected. The olefinic proton at C-16 is seen as quintet at 6.11 ppm, confirming the presence of a double bond between C-16 and C-17. The signal at

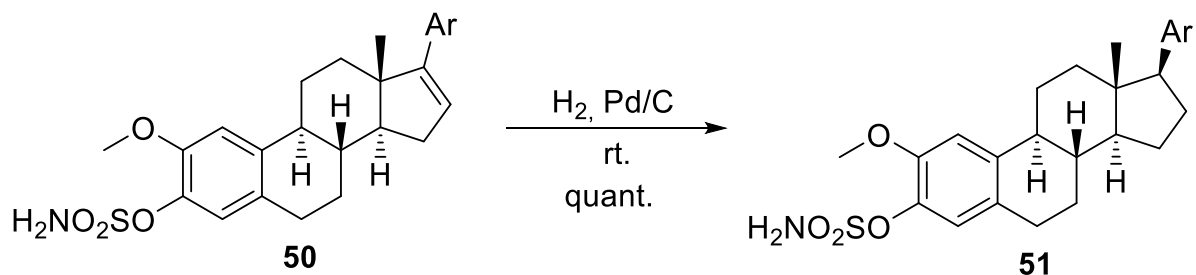
5.02 ppm integrating for two protons must be the protons from the sulfonamide group at C-3. The two methyl groups in the molecule at C-2 and C-13 appeared at 3.89 ppm and 1.06 ppm respectively as expected. The signal at 3.89 ppm is higher in shift because of deshielding effect from the oxygen atom at C-2. Furthermore, the signal for the OH-group at C-3 which often appears at approximately 5.7 ppm as singlet was not visible, confirming the attachment of a sulfonamide group at C-3. The rest of the signals appeared in the aliphatic region between 1 – 3 ppm as expected.

In the processed  $^{13}\text{C}$  Carbon NMR spectrum (see figure 28 in appendix 7.1), a total of 13 signals appeared in the aromatic region, representing five aromatic carbons in the pyridine ring, six carbons in the A-ring and the two carbons forming the double bond between C-16 and C-17. The signal at 17.2 ppm represents the methyl group at C-13. The rest of the signals appeared in the aliphatic region between 20 and 60 ppm as expected. Moreover, there are 24 signals in the spectrum, which corresponds to the total number of carbons in the molecule.

In the recorded HRMS elemental analysis report (see figure 33 in appendix 7.2), it was found that the molecular mass of the compound  $\text{C}_{24}\text{H}_{27}\text{FN}_2\text{O}_4\text{S}$   $[\text{M}+\text{Na}]^+$  is 481.1567 which corresponds almost exactly with the calculated molecular mass, 481.1568. Meanwhile, there is a peak at 482.1599, about one-third of the highest peak in the spectrum and this is due to carbon 13 isotope in the molecule.

### 2.1.15 Synthesis of 2-methoxy-steroid-analog (51)

To synthesize the final analog of 2-ME (28) in this project, 2-ME-pyridine sulfonamide (50) was dissolved in ethyl acetate in a round bottomed flask and exposed to palladium on carbon (Pd/C 10 % w/w) under hydrogen gas. The reaction was stirred at room temperature for 36 hours, after which TLC was performed to detect the product followed by filtration on celite to give the desired product as white crystals in 100 % yield (see scheme 13).



**Scheme 13:** Synthesis of 2-ME-steroid-analog (51). Created with ChemDraw 21.0.0 as inspired by; (Solum et al., 2014, al-Kazaale et al., 2017).

### 2.1.16 NMR and HRMS characterization of 2-methoxy-steroid-analog (51)

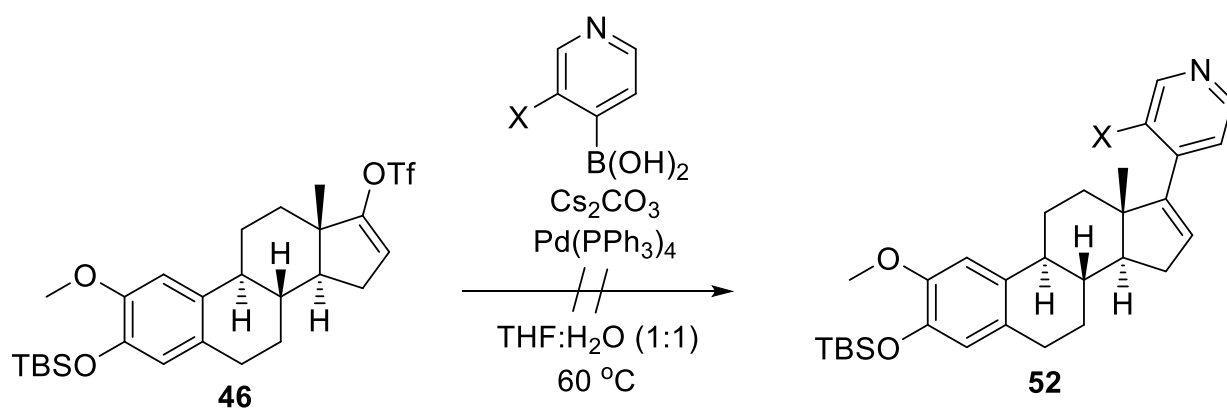
In the processed proton NMR spectrum (see figure 29 in appendix 7.1), there were four signals in the aromatic region, integrating for five protons which corresponds to the expected number of aromatic protons in the molecule. The signal at 8.28 ppm seen as multiplet and integrating for two protons is likely to be representing the two protons in the pyridine ring closest to the nitrogen atom as a result of deshielding effect from the nitrogen atom. The protons in the sulfonamide group at C-3 were seen at 5.24 ppm as singlet, integrating for two protons as expected. The absence of the characteristic signal for the olefinic proton at C-16 in the aromatic region signifies that the double bond between C-16 and C-17 has disappeared, thus confirming the success of the reaction. Moreover, there are additional three protons than usual in the aliphatic region between 1 – 3 ppm which further confirms hydrogenation of C-16 and C-17. The characteristic signals for the two methyl groups in the molecule appeared at 3.86 ppm and 0.54 ppm as expected. The rest of the signals appeared in the aliphatic region between 1 – 3 ppm as expected. Moreover, the position of the pyridine-ring at C-17 is more or less stereoselective as a result of steric hindrance from the methyl group at C-13 which makes the hydrogen atom from H<sub>2</sub> attach from the back side of C-17, thus forming the S configuration as seen in scheme 13.

In the processed <sup>13</sup>C NMR spectrum (see figure 30 in appendix 7.1), there are 11 signals in the aromatic region which corresponds to the number of aromatic carbons in the molecule, namely five carbons in the pyridine ring and six carbons in the A-ring. Meanwhile, the characteristic signals for the double bond between C-16 and C-17 which often appear in the aromatic region were missing, confirming that the reaction has been successful. The signal at 12.6 ppm represents the methyl group at C-13. The remaining 12 carbons appeared in the aliphatic region between 20 and 60 ppm as expected, making it a total of 24 signals in the spectrum as projected, since there are 24 carbons in the molecule.

In the recorded HRMS elemental analysis report (see figure 34 in appendix 7.2), the molecular mass found for C<sub>24</sub>H<sub>29</sub>FN<sub>2</sub>O<sub>4</sub>S [M+Na]<sup>+</sup> was 483.1724 which corresponds to the calculated molecular mass of the compound C<sub>24</sub>H<sub>29</sub>FN<sub>2</sub>O<sub>4</sub>S [M+Na]<sup>+</sup> been 483.1724. Meanwhile, there is a peak at 484.1757 accounting for one-third of the highest peak in the spectrum which most likely represents carbon 13 isotope in the molecule.

### 2.1.17 Attempted synthesis of 3-*tert*-butyldimethylsilyloxy-2-methoxysteroid-analog (52)

As part of the aim of study for this project, an attempt was made to synthesize other alternative analogs of the newly prepared analogs of 2-ME (**28**). In this attempt, a different organoboronic acid, alternative to the first one was to be attached to the steroid triflate (**46**) by the Suzuki coupling reaction in order to form a new TBS-protected steroid analog (**52**), but this proved futile. The reaction conditions were similar to the previous Suzuki reaction, where 1.16 equivalents of the boronic acid and two equivalents of cesium carbonate were added to the steroid triflate (**46**) in addition to 0.05 equivalent of palladium tetrakis under stirring under nitrogen atmosphere at 60 °C for 24 hours. The reaction was performed twice, but no products were formed in both cases (see scheme 14). Later, it was found out that, the conditions for the reaction can be optimized using xxx catalyst to form the desired product in 5 minutes. Unfortunately, there was not much time to test these conditions.



**Scheme 14:** Attempted synthesis of TBS-protected-2-ME-steroid-analog (**52**). Created with ChemDraw 21.0.0 as inspired by; (Solum et al., 2014, al-Kazaale et al., 2017).

## 2.2 Biological testing of new analogs of 2-methoxyestradiol

All new analogs (**48-51**) are currently under biological testing in collaboration with the Norwegian Centre for Molecular Medicine, Oslo, Norway. Unfortunately, testing results were not available at the time of submission of this master project and therefore much cannot be said about the potency of these analogs. However, results from SAR studies of previous analogs in the LIPCHEMA group [32, 42] suggest that analog **50** is likely to be the most potent of all the four newly prepared analogs (**48-51**) of 2-ME (**28**) and possibly the most potent analog prepared in the LIPCHEMA group by far. It is also expected that all new analogs will exert higher potency than 2-ME (**28**) [32, 42]. The analogs (**48-51**) will primarily be tested for anti-proliferative, anti-angiogenic and apoptotic activities on different cancer lines. In addition, estrogen agonism will be tested in collaboration with professor Ragnhild Paulsen and her group at the Department of Pharmacy, University of Oslo. It is not expected that the new analogs (**48-51**) will exhibit any significant estrogenic activities based on results from previous SAR studies [32, 42]. Moreover, we will not be surprised if the new analogs (**48-51**) exhibit other biological activities of 2-ME (**28**) such as cardioprotection, but this will not be the main focus of the biological testing.

### 3 Future prospective

As discussed previously, an attempt was made to synthesize alternative analogs of the already prepared analogs of 2-ME (**28**) in this project, but this attempt was unsuccessful. An optimization of the Suzuki coupling reaction to attach an alternative organoboronic acid to the 2-ME steroid triflate (**46**) can be an interesting hypothesis to explore. Consequently, the triflate group in **46** can be replaced with a halide such as iodide since halides are more reactive than triflates and iodide is the most reactive halide or leaving group in this series in terms of Suzuki coupling reactions between organoboron compounds and organic halides or triflates to form carbon-carbon bonds using palladium tetrakis as catalyst [59]. Given that this reaction is successful, further synthesis can be made to produce corresponding analogs (**53-56**) of 2-ME (**28**) as performed in this project (see figure 13).

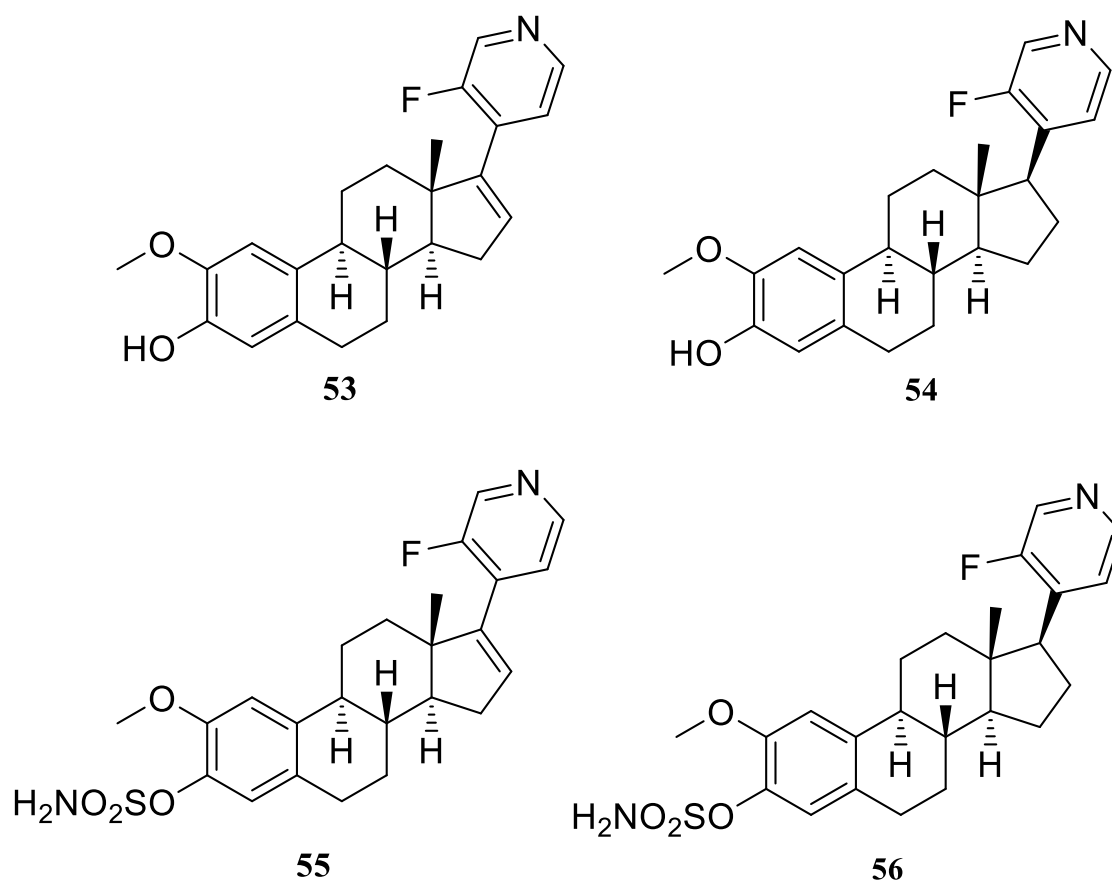


**Figure 13:** Examples of future analogs (**53-56**) of 2-ME (**28**). Created with ChemDraw 21.0.0 as inspired by; (Solum et al., 2014, al-Kazaale et al., 2017).

Furthermore, the most challenging issues with 2-ME (**28**) and its analogs which have been poor aqueous solubility and poor oral bioavailability can be explored further with the

introduction of spiro morpholinone and hydroxychloroacetamide derivatives [60]. Montiel-Smith and co-workers recently prepared two analogs of estrone in a six-step synthesis, giving rise to a hydroxychloroacetamide derivative (**57**) and a morpholinone derivative (**58**) (see figure 14). Upon exposure to six different cancer cell lines, both compounds showed promising anti-proliferative activities, with the morpholinone derivative (**58**) exhibiting lower potency ( $GI_{50} = 2.0\text{--}11\ \mu\text{M}$ ) than the hydroxychloroacetamide derivative (**57**). ( $GI_{50} = 0.25\text{--}2.4\ \mu\text{M}$ ) [60]. However, both compounds showed higher anti-cancer activity than the famous anti-cancer agents abiraterone and galeterone [60]. In view of this, several analogs (**59-62**) of 2-ME (**28**) can be prepared in light of the recently prepared analogs of 2-ME (**28**) (see figure 14).

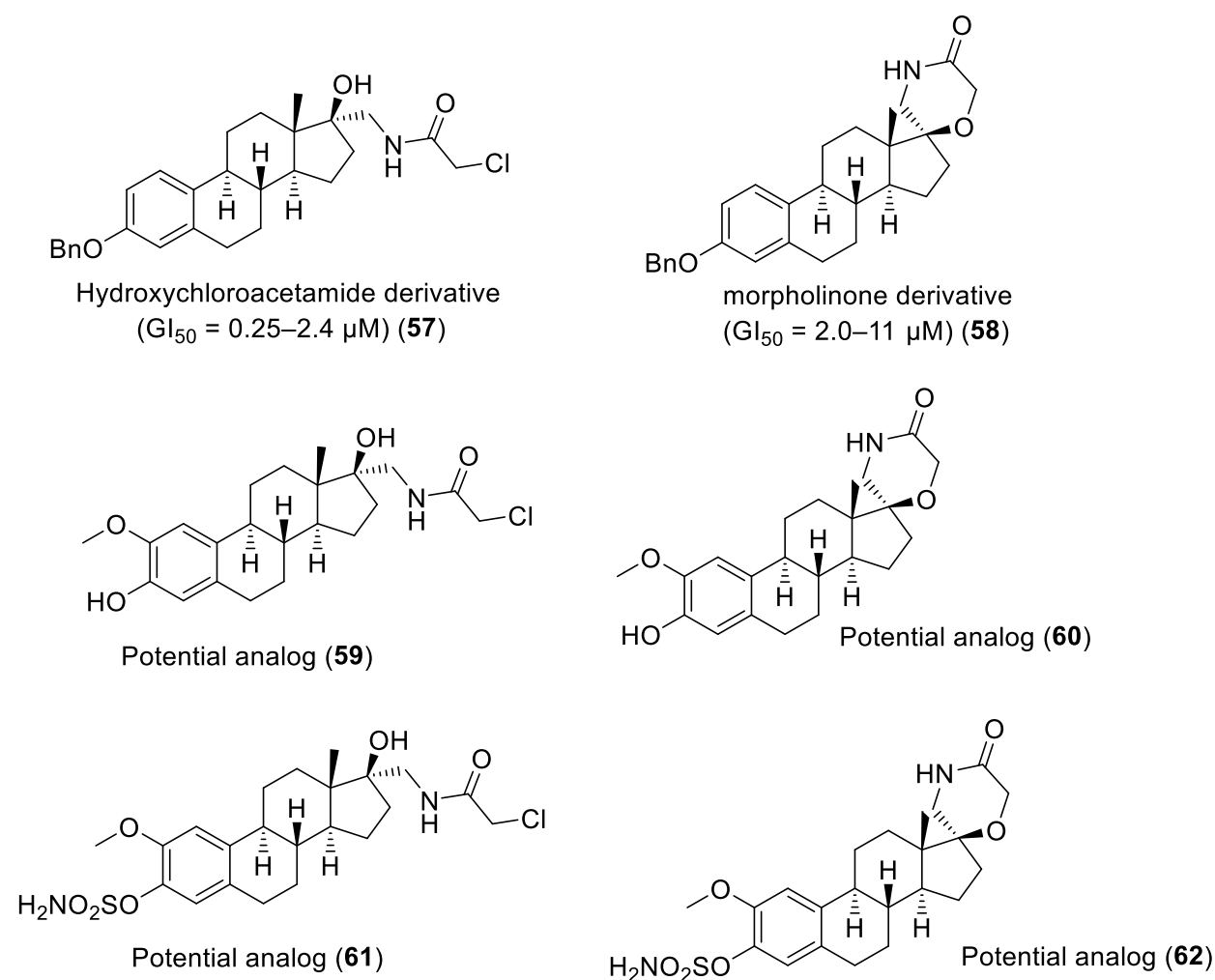


**Figure 14:** Structures of new analogs (**57-58**) of estrone (see scheme 1) and future analogs (**59-62**) of 2-ME (**28**). Created with ChemDraw 21.0.0 as inspired by; (Solum et al., 2014, al-Kazaale et al., 2017, Cobos-Ontiveros et al., 2023).

## 4 Conclusion

Synthesis of new analogs of 2-ME (**28**) remains a promising research arena for the discovery and development of new anti-cancer agents. In this project, effort was made to synthesize eight new analogs of 2-ME (**28**) with modifications at C-3, C-16 and C-17 via two main mechanisms, namely the Oppenauer oxidation and the Suzuki coupling reaction. However, it ended with four new analogs of 2-ME (analogs **48-51**) as a result of a failed attempt to attach an alternative organoboronic acid to the steroid triflate (**46**). All four new analogs (**48-51**) are currently under biological testing in collaboration with the Norwegian Centre for Molecular Medicine, Oslo, Norway. The analogs will be primarily tested for anti-proliferative, anti-angiogenic and apoptotic activities on different cancer cell lines, but also for estrogenic activities. Of all the four new analogs (**48-51**), analog **50** is expected to exert the highest potency based on previous results from the LIPCHEM group. It is also expected that all analogs will exert higher potency than 2-ME (**28**). Other activities of 2-ME (**28**) such as cardioprotection may be exhibited by the new analogs. Notwithstanding, there is no doubt that results from this project have and will pave way for further exploration into synthesis and pharmacology of new analogs of 2-ME (**28**) as well as discovery and development of new anti-cancer agents.

# 5 Methods and Procedures

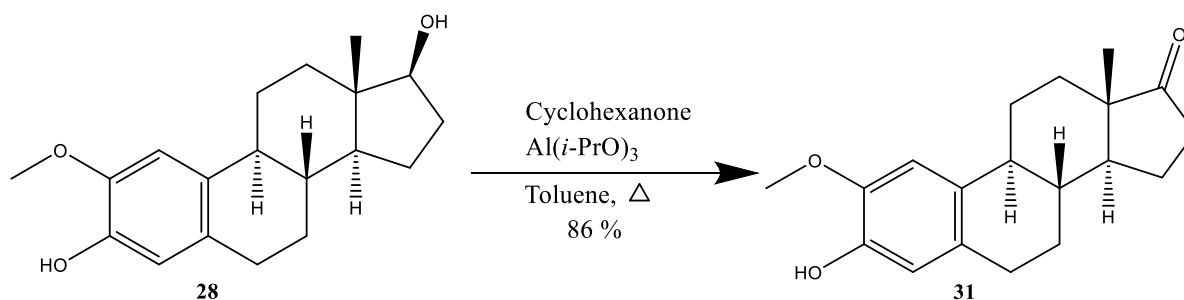
## 5.1 General Methods

All chemical materials and reagents were purchased and used without any further purification except specified otherwise. With respect to thin layer chromatography (TLC), aluminium plates with silica gel 60 (F<sub>254</sub>) purchased from Merck were used for testing. Potassium permanganate solution was used as stain for identification of spots on the silica plates. Flash chromatography was performed with silica gel 60 purchased from Merck.

The NMR instruments Bruker AVIII 400 MHz and Bruker AVNEO 400 MHz were employed for measuring the prepared samples and recording NMR spectra of the compounds while the app Mestre Nova 64 was used for spectra characterization. The peak initials were interpreted as follows; s for singlet, d for doublet, dd for doublet of doublets, ddd for doublet of doublet of doublets, t for triplet, dt for doublet of triplets, td for triplet of doublets, q for quintet and m for multiplet. The coupling constant ( $J$ ) was measured in hertz (Hz) whereas the chemical shifts were recorded in part per million (ppm). Every sample was dissolved in deuterated chloroform (CDCl<sub>3</sub>) with reference signals at 7.26 ppm (<sup>1</sup>H NMR) and 77.16 ppm (<sup>13</sup>C NMR). MS and HRMS were recorded at 70 electron volts (eV) using ESI as the ionization method. Optical rotation values were recorded with Modular Compact Polarimeter, MCP 100 made by Anton Paar with cell-length of 1.0 dm and maximum volume of 1.0 ml at 25 °C where each sample was dissolved in methanol. Melting point ranges were determined using Stuart SMP3 Melting Point Apparatus. All reactions and analysis were performed at the Department of Pharmaceutical Chemistry, University of Oslo.

## 5.2 Synthetic and Experimental procedures

### 5.2.1 Synthesis of 2-Methoxyestrone (31)

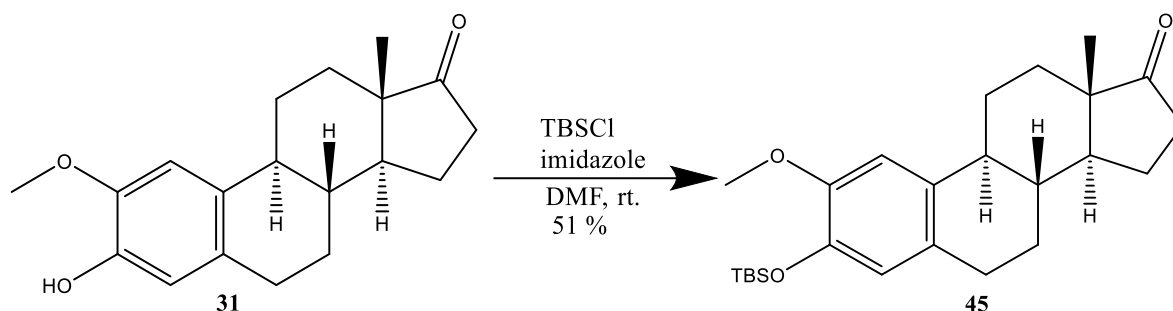


**Scheme 15:** Synthesis of 2-methoxyestrone (31). Created with ChemDraw 21.0.0 as inspired by; (Solum et al., 2014, al-Kazaale et al., 2017).

2-Methoxyestrone (31) was prepared according to Solum et al [24].

2-Methoxyestradiol **28** (1.19 g, 4.00 mmol, 1.00 equiv.) was transferred to a 100 ml round-bottomed flask with two neck and attached with a 5 ml Dean-Stark trap as well as a reflux condenser. All equipment were flame-dried. Toluene (40 ml) was then added in order to dissolve the starting material. Aluminium isopropoxide (4.07 g, 20.0 mmol, 5.00 equiv.) and cyclohexanone (17.00 ml, 160.0 mmol, 40.00 equiv.) were also added and the reaction mixture was allowed to heat until reflux and then placed under stirring for 24 hours. The mixture was cooled to room temperature, after which water (50 ml) and 1 M HCl (22 ml) were added. It was then extracted with ethyl acetate (3 × 75 ml). Thereafter, 1 M HCl (25 ml) was added to the aqueous phase until there was separation and then extracted once more with ethyl acetate (50 ml). The combined organic phases were dried over MgSO<sub>4</sub>, filtered and evaporated in vacuo. The residue was purified by flash chromatography (silica gel, 30 % ethyl acetate in heptane, R<sub>f</sub> = 0.42) to give the desired product in 86 % yield (1.03 g). Melting point range: 188-190 °C; <sup>1</sup>H NMR (400 MHz, CDCl<sub>3</sub>) δ 6.79 (s, 1H), 6.66 (s, 1H), 5.49 (s, 1H), 3.86 (s, 3H), 2.90 – 2.74 (m, 2H), 2.51 (dd, *J* = 18.9, 8.6 Hz, 1H), 2.41 – 2.33 (m, 1H), 2.19 – 2.08 (m, 1H), 2.00 – 1.90 (m, 4H), 1.71 – 1.31 (m, 6H), 0.92 (s, 1H). <sup>13</sup>C NMR (101 MHz, CDCl<sub>3</sub>) δ 221.5, 145.1, 144.1, 131.6, 129.8, 115.1, 108.5, 56.5, 50.9, 48.5, 44.7, 38.8, 36.4, 32.1, 29.3, 27.1, 26.7, 22.0, 14.4. The spectroscopic data agreed with that reported by Solum et al [24].

## 5.2.2 Synthesis of 3-*tert*-butyldimethylsiloxy-2-methoxyestrone (45)



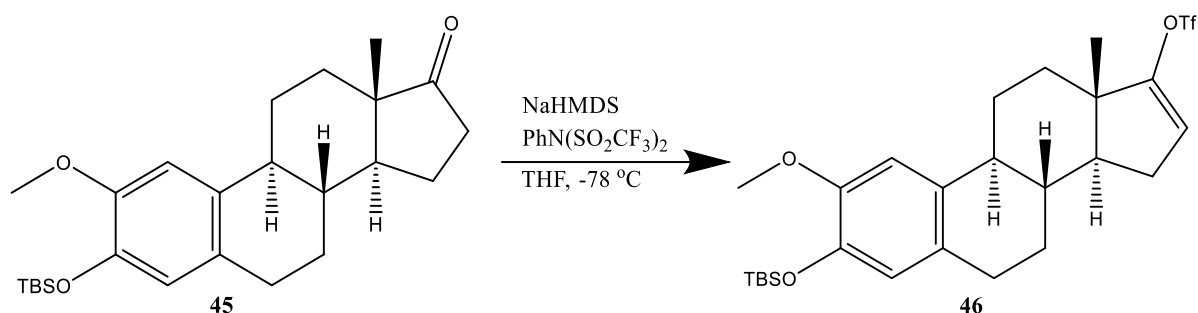
**Scheme 16:** Synthesis of 3-*tert*-butyldimethylsiloxy-2-methoxyestrone (45). Created with ChemDraw 21.0.0 as inspired by; (Solum et al., 2014, al-Kazaale et al., 2017).

3-*tert*-butyldimethylsiloxy-2-methoxyestrone (45) was prepared according to Solum et al [24].

2-Methoxyestrone **31** (1.01 g, 3.40 mmol, 1.00 equiv.) was dissolved in dry DMF (17 ml) in a 100 ml round-bottomed flask and then imidazole (1.14 g, 16.7 mmol, 4.91 equiv.) and TBSCl (1.44 g, 10.0 mmol, 2.94 equiv.) were added under stirring, after which the mixture was allowed to stir at room temperature under Nitrogen atmosphere for 19 hours. Then saturated aqueous NaCl (10 ml) was added, and the mixture was extracted with ethyl acetate (3 × 15 ml). The combined organic phases were washed with NaCl (10 ml), aqueous AcOH (10 %, 10 ml) and aqueous NaHCO<sub>3</sub> (10 ml) respectively, dried over MgSO<sub>4</sub>, filtered and evaporated in vacuo. The resulting product was purified by flash chromatography (silica gel, 20 % ethyl acetate in heptane, R<sub>f</sub> = 0.35) to give the desired product in 51 % yield (0.52 g). Melting point range: 163 – 166 °C. <sup>1</sup>H NMR (400 MHz, CDCl<sub>3</sub>) δ 6.76 (s, 1H), 6.56 (s, 1H), 3.77 (s, 3H), 2.83 – 2.74 (m, 2H), 2.50 (dd, *J* = 19.0, 8.4 Hz, 1H), 2.40 – 1.89 (m, 5H), 1.70 – 1.34 (m, 6H), 0.99 (s, 9H), 0.92 (s, 3H), 0.15 (s, 6H). <sup>13</sup>C NMR (101 MHz, CDCl<sub>3</sub>) δ 221.2, 149.0, 143.2, 132.7, 128.9, 121.2, 110.0, 56.0, 50.6, 48.2, 44.5, 38.4, 36.1, 31.8, 28.9, 26.8, 26.2, 25.9, 21.7, 18.6, 14.1, -4.4, -4.4. The spectroscopic data agreed with that reported by Solum et al [24].

### 5.2.3 Synthesis of 3-*tert*-butyldimethylsilyloxy-2-methoxy-steroid-triflate

(46)

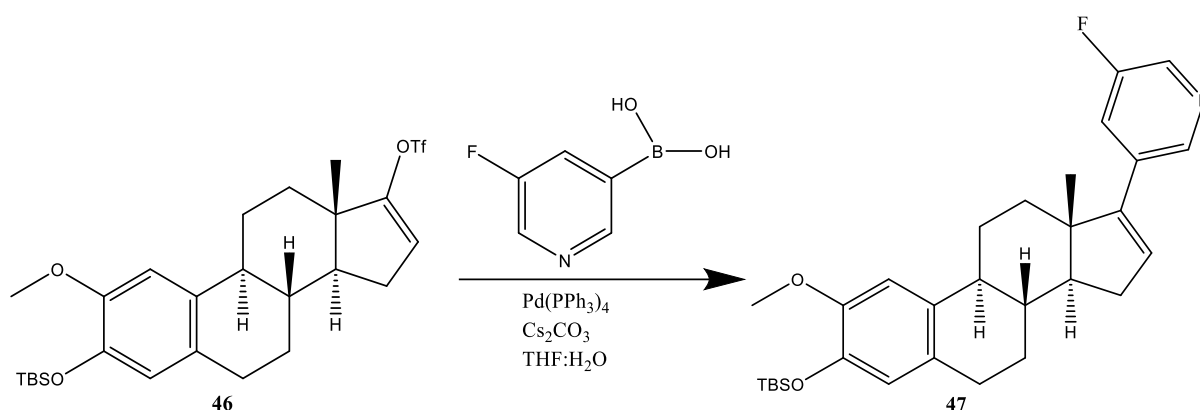


**Scheme 17:** Synthesis of 2-methoxy-steroid triflate (**46**). Created with ChemDraw 21.0.0 as inspired by; (Solum et al., 2014, al-Kazaale et al., 2017).

The steroid compound **46** was prepared as previously reported by Solum et al [24].

TBS protected 2-methoxyestrone **45** (0.440 g, 1.06 mmol, 1.00 equiv.) and N-phenyl-bis (trifluoromethanesulfonamide) (0.580 g, 1.60 mmol, 1.51 equiv.) were placed in a flame dried 100 ml round-bottomed flask and dissolved in dry THF (27 ml). The reaction mixture was cooled to -78 °C, after which NaHMDS (1.0 M in toluene) (3.20 ml, 3.20 mmol, 3.02 equiv.) was added dropwise and the reaction mixture was placed under stirring at -78 °C for 3 hours. The reaction mixture was then brought to room temperature and quenched with saturated NH<sub>4</sub>Cl (15 ml), after which it was extracted with CH<sub>2</sub>Cl<sub>2</sub> (2 × 15 ml). The combined organic extracts were washed with water (10 ml) and brine (10 ml), dried over MgSO<sub>4</sub>, filtered and evaporated in vacuo. The residue was purified by flash chromatography (silica gel, 2.5 % ethyl acetate in heptane, R<sub>f</sub> = 0.30) to give the desired product as colourless oil in 67 % yield (0.29 g). <sup>1</sup>H NMR (400 MHz, CDCl<sub>3</sub>) δ 6.73 (s, 1H), 6.55 (s, 1H), 5.61 (d, *J* = 1.8 Hz, 1H), 3.77 (s, 3H), 2.79 (d, *J* = 11.1 Hz, 2H), 2.34 – 2.29 (m, 2H), 2.09 (ddd, *J* = 14.9, 11.1, 1.8 Hz, 1H), 1.88 (d, 2H), 1.78 (td, *J* = 11.3, 6.3 Hz, 1H), 1.71 – 1.54 (m, 4H), 1.47 – 1.31 (m, 1H), 1.01 (s, 3H), 0.99 (s, 9H), 0.15 (s, 6H). <sup>13</sup>C NMR (101 MHz, CDCl<sub>3</sub>) δ 159.2, 148.6, 143.0, 132.5, 128.5, 120.9, 114.3, 109.4, 55.7, 53.5, 44.9, 44.4, 36.4, 32.6, 28.3, 28.2, 26.7, 25.8, 25.6, 18.3, 15.2, -4.7, -4.8. The spectroscopic data agreed with that reported by Solum et al [24].

## 5.2.4 Synthesis of 3-*tert*-butyldimethylsilyloxy-2-methoxy-steroid-analog (47)

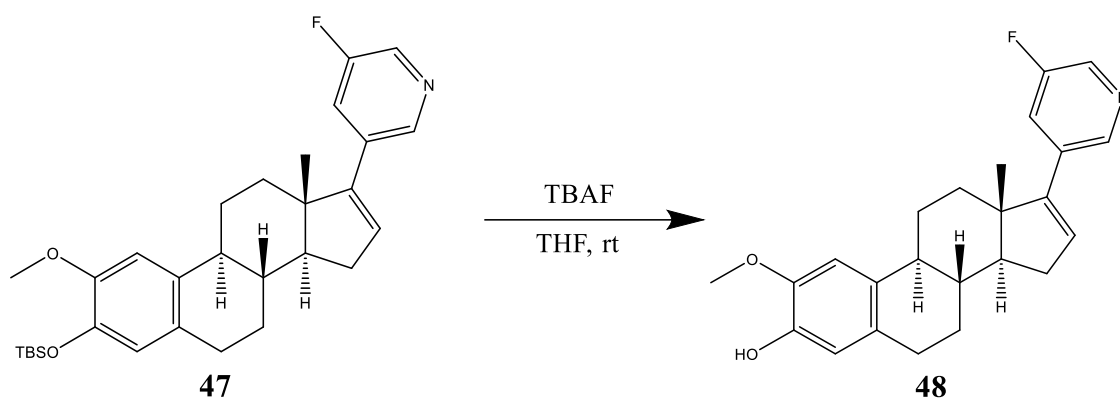


**Scheme 18:** Synthesis of the steroid compound **47**. Created with ChemDraw 21.0.0 as inspired by; (Solum et al., 2014, al-Kazaale et al., 2017).

The steroid compound **47** was prepared using a protocol reported for a similar steroid compound by Solum et al [24].

TBS-protected-2-methoxy triflate **46** (0.280 g, 0.510 mmol, 1.00 equiv.), cesium carbonate (0.330 g, 1.01 mmol, 2.00 equiv.) and 5-fluoropyridine-3-boronic acid (0.0800 g, 0.590 mmol, 1.16 equiv.) were placed in a flame dried 25 ml round-bottomed flask and dissolved in a 1:1 mixture of THF and water (10 ml). Then Pd(PPh<sub>3</sub>)<sub>4</sub> (0.03 g, 0.03 mmol, 0.05 equiv.) was added and the reaction mixture was stirred at 60 °C under N<sub>2</sub> atmosphere overnight. The reaction mixture was then allowed to cool to room temperature, after which saturated NaCl (15 ml) was added. The mixture was extracted with ethyl acetate (4 × 10 ml) and the combined organic extracts were dried over MgSO<sub>4</sub>, filtered and evaporated in vacuo. The residue was purified by flash chromatography (silica gel, 10 % ethyl acetate in heptane, R<sub>f</sub> = 0.07) to give the desired product as white crystals in 54 % yield (0.15 g). <sup>1</sup>H NMR (400 MHz, CDCl<sub>3</sub>) δ 8.48 (s, 1H), 8.34 (d, *J* = 2.7 Hz, 1H), 7.40 (dt, *J* = 9.9, 2.3 Hz, 1H), 6.76 (s, 1H), 6.57 (s, 1H), 6.09 (dd, *J* = 3.4, 1.8 Hz, 1H), 3.78 (s, 3H), 2.90 – 2.72 (m, 2H), 2.42 – 2.26 (m, 3H), 2.22 – 2.10 (m, 2H), 1.81 (td, *J* = 11.4, 6.5 Hz, 1H), 1.72 – 1.57 (m, 4H), 1.45 (qd, *J* = 11.9, 6.7 Hz, 1H), 1.06 (s, 3H), 0.99 (s, 9H), 0.15 (s, 6H). <sup>13</sup>C NMR (101 MHz, CDCl<sub>3</sub>) δ 150.8, 148.9, 143.9, 143.2, 136.3, 136.0, 133.2, 130.9, 129.1, 121.2, 120.5, 120.3, 109.8, 56.9, 56.1, 47.9, 44.5, 37.3, 35.5, 31.7, 28.9, 28.0, 26.7, 25.9, 18.6, 16.9, -4.4, -4.4.

## 5.2.5 Synthesis of 2-methoxy-steroid-analog (48)

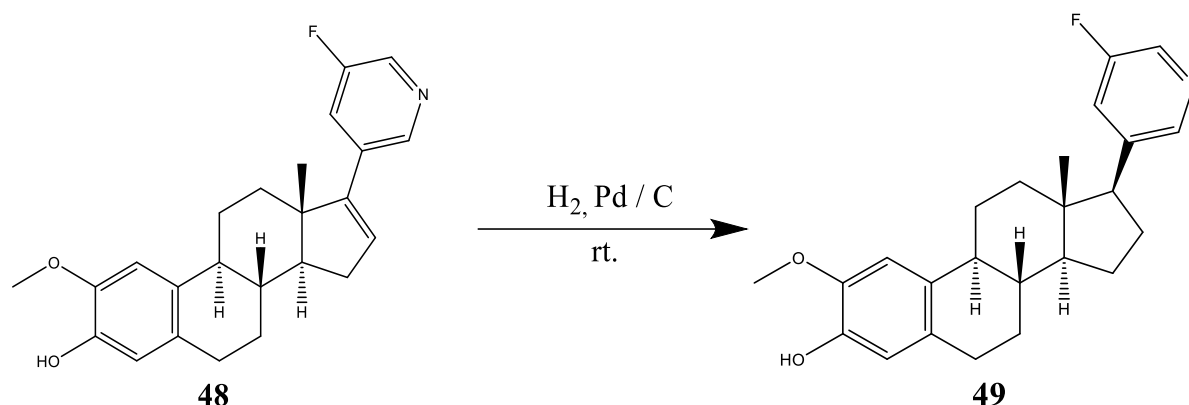


**Scheme 19:** Synthesis of the steroid compound **48**. Created with ChemDraw 21.0.0 as inspired by; (Solum et al., 2014, al-Kazaale et al., 2017).

The steroid compound **48** was prepared using a protocol reported for a similar steroid compound by Solum et al [24].

TBS-protected-2-methoxy steroid **47** (0.230 g, 0.466 mmol, 1.00 equiv.) was placed in a flame dried 10 ml round-bottomed flask. Anhydrous THF (2 ml) was added to dissolve the starting material. TBAF (0.497 ml, 0.497 mmol, 1.07 equiv.) was added dropwise and the reaction mixture was allowed to stir under N<sub>2</sub> atmosphere at room temperature overnight. It was then poured into saturated NaHCO<sub>3</sub> (10 ml) and extracted with ethyl acetate (4 × 7 ml). The combined organic extracts were dried over MgSO<sub>4</sub>, filtered and evaporated in vacuo. The product was purified by flash chromatography (silica gel, 20 % ethyl acetate in heptane, R<sub>f</sub> = 0.09) to give the desired product as white crystals in 31 % yield (0.07 g).  $[\alpha]_D^{25} = +51$  (c = 0.9 mg/ml, MeOH). Melting point range: 214 – 217 °C. <sup>1</sup>H NMR (400 MHz, CDCl<sub>3</sub>) δ 8.49 (s, 1H), 8.35 (d, J = 2.7 Hz, 1H), 7.41 (dt, J = 9.9, 2.3 Hz, 1H), 6.79 (s, 1H), 6.67 (s, 1H), 6.10 (dd, J = 3.4, 1.8 Hz, 1H), 5.75 (s, 1H), 3.87 (s, 3H), 2.93 – 2.74 (m, 2H), 2.43 – 2.27 (m, 3H), 2.22 – 2.10 (m, 2H), 2.00 – 1.90 (m, 1H), 1.87 – 1.76 (m, 1H), 1.73 – 1.62 (m, 3H), 1.52 – 1.21 (m, 1H), 1.06 (s, 3H). <sup>13</sup>C NMR (101 MHz, CDCl<sub>3</sub>) δ 160.4, 157.9, 150.4, 144.5, 143.4, 135.9, 135.6, 134.3, 131.4, 130.6, 129.2, 114.6, 107.7, 56.5, 55.9, 47.5, 44.1, 37.0, 35.1, 31.4, 28.7, 27.6, 26.6, 16.6. HRMS calculated for C<sub>24</sub>H<sub>26</sub>FNO<sub>2</sub> [M-H]<sup>-</sup> is 378.1875. Found: 378.1874.

## 5.2.6 Synthesis of 2-methoxy-steroid-analog (49)

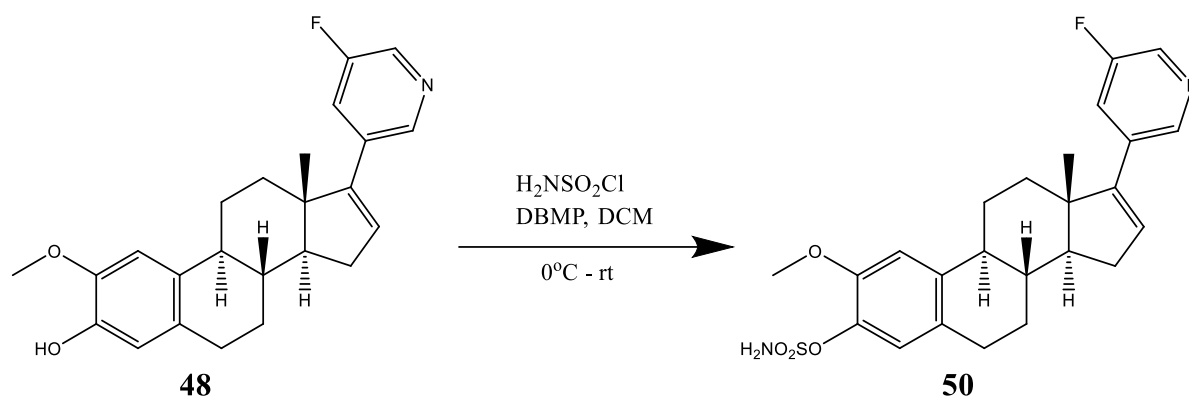


**Scheme 20:** Synthesis of the steroid compound **49**. Created with ChemDraw 21.0.0 as inspired by; (Solum et al., 2014, al-Kazaale et al., 2017).

The steroid compound **49** was prepared using a hydrogenation protocol reported for a similar steroid compound by Solum et al [24].

2-Methoxy-pyridine steroid **48** (0.039 g, 0.103 mmol, 1.00 equiv.) was dissolved in ethyl acetate (5 ml) at room temperature. A stirred solution of Pd/C (10 % w/w) in ethyl acetate was added to the mixture. The resulting mixture was stirred under H<sub>2</sub> gas for 36 hours, after which it was filtered on celite with ethyl acetate as eluent to give the desired product as white crystals in 100 % yield (0.039 g).  $[\alpha]_D^{25} = +31$  (c = 1.2 mg/ml, MeOH). Melting point range: 225 – 230 °C. <sup>1</sup>H NMR (400 MHz, CDCl<sub>3</sub>) δ 8.34 – 8.30 (m, 2H), 7.30 (dt, *J* = 10.0, 2.3 Hz, 1H), 6.78 (s, 1H), 6.65 (s, 1H), 5.77 (s, 1H), 3.85 (s, 3H), 2.89 – 2.72 (m, 3H), 2.33 – 2.20 (m, 2H), 2.13 – 2.02 (m, 2H), 1.97 – 1.88 (m, 1H), 1.70 (dd, *J* = 8.5, 2.5 Hz, 1H), 1.57 – 1.32 (m, 6H), 1.30 – 1.23 (m, 1H), 0.54 (s, 3H). <sup>13</sup>C NMR (101 MHz, CDCl<sub>3</sub>) δ 161.1, 158.6, 146.6, 145.1, 144.0, 136.1, 135.9, 132.0, 129.9, 115.2, 108.5, 56.5, 55.7, 54.5, 45.4, 44.6, 39.6, 38.0, 29.5, 28.3, 27.0, 26.6, 24.5, 13.3. HRMS calculated for C<sub>24</sub>H<sub>28</sub>FNO<sub>2</sub> [M-H]<sup>-</sup> is 380.2031. Found: 380.2031.

## 5.2.7 Synthesis of 2-methoxy-steroid-analog (50)

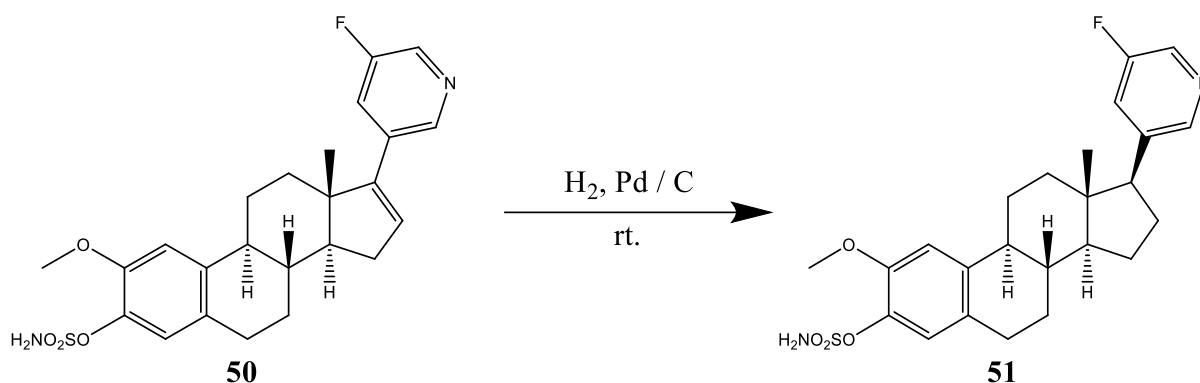


**Scheme 21:** Synthesis of the steroid compound **50**. Created with ChemDraw 21.0.0 as inspired by; (Solum et al., 2014, al-Kazaale et al., 2017).

The steroid compound **50** was prepared using a protocol reported for a similar steroid compound by Solum et al [24].

2-Methoxy-pyridine steroid **48** (0.273 g, 0.719 mmol, 1.00 equiv.) was dissolved in anhydrous dichloromethane (15.0 ml) in a flame-dried 25 ml round bottomed flask. The mixture was cooled to  $0^\circ\text{C}$  and 2,6-di-*tert*-butyl-4-methyl pyridine (DBMP) (0.443 g, 2.16 mmol, 3.00 equiv.) was added under stirring. Sulfamoyl chloride ( $\text{H}_2\text{NSO}_2\text{Cl}$ ) (0.249 g, 2.16 mmol, 3.00 equiv.) was then added, after which the mixture was allowed to stir for 30 minutes. The resulting mixture was cooled to room temperature and allowed to stir under nitrogen atmosphere for 24 hours.  $\text{NaHCO}_3$  (15.0 ml) was then added to quench the mixture, after which it was extracted with ethyl acetate ( $4 \times 15.0$  ml). The combined organic phases were dried over  $\text{MgSO}_4$ , filtered and evaporated in vacuo. The resulting product was purified by flash chromatography (silica gel, 50 % ethyl acetate in heptane,  $R_f = 0.2$ ) to give the desired product as white crystals in 55 % yield (0.15 g).  $[\alpha]_D^{25} = +49$  ( $c = 1.2$  mg/ml, MeOH). Melting point range:  $189 - 194^\circ\text{C}$ .  $^1\text{H}$  NMR (400 MHz,  $\text{CDCl}_3$ )  $\delta$  8.47 (t,  $J = 1.8$  Hz, 1H), 8.34 (d,  $J = 2.7$  Hz, 1H), 7.40 (dt,  $J = 9.9, 1.7$  Hz, 1H), 7.07 (s, 1H), 6.92 (s, 1H), 6.11 (q, 1H), 5.02 (s, 2H), 3.89 (s, 3H), 2.91 – 2.83 (m, 2H), 2.44 – 2.29 (m, 3H), 2.23 – 2.12 (m, 2H), 2.03 – 1.93 (m, 1H), 1.82 (td,  $J = 11.4, 6.5$  Hz, 1H), 1.72 – 1.60 (m, 3H), 1.55 – 1.39 (m, 1H), 1.06 (s, 3H).  $^{13}\text{C}$  NMR (101 MHz,  $\text{CDCl}_3$ )  $\delta$  161.1, 158.5, 150.9, 149.5, 144.1, 140.8, 137.4, 136.6, 136.4, 131.3, 130.7, 124.7, 110.7, 57.1, 56.9, 48.1, 45.0, 37.2, 35.7, 32.0, 28.9, 27.9, 27.0, 17.2. HRMS calculated for  $\text{C}_{24}\text{H}_{27}\text{FN}_2\text{O}_4\text{S}$   $[\text{M}+\text{Na}]^+$  is 481.1568. Found: 481.1567.

## 5.2.8 Synthesis of 2-methoxy-steroid-analog (51)



**Scheme 22:** Synthesis of the steroid compound **51**. Created with ChemDraw 21.0.0 as inspired by; (Solum et al., 2014, al-Kazaale et al., 2017).

The steroid compound **51** was prepared using a hydrogenation protocol reported for a similar steroid compound by Solum et al [24].

2-Methoxy-pyridine steroid **50** (0.056 g, 0.122 mmol, 1.00 equiv.) was dissolved in ethyl acetate (7.0 ml) at room temperature. A stirred solution of Pd-C (10 % w/w) in ethyl acetate was added to the mixture. The resulting mixture was stirred under H<sub>2</sub> gas for 36 hours, after which it was filtered on celite with ethyl acetate as eluent to give the desired product as white crystals in 100 % yield (0.056 g).  $[\alpha]_D^{25} = +30$  (c = 1.0 mg/ml, MeOH). Melting point range: 196 – 199 °C. <sup>1</sup>H NMR (400 MHz, CDCl<sub>3</sub>) δ 8.31 – 8.24 (m, 2H), 7.29 (dt, *J* = 9.8, 2.3 Hz, 1H), 7.04 (s, 1H), 6.90 (s, 1H), 5.24 (s, 2H), 3.86 (s, 3H), 2.86 – 2.77 (m, 3H), 2.35 – 2.22 (m, 2H), 2.13 – 2.03 (m, 2H), 2.00 – 1.90 (m, 1H), 1.75 – 1.68 (m, 1H), 1.51 – 1.35 (m, 6H), 1.34 – 1.24 (m, 1H), 0.54 (s, 3H). <sup>13</sup>C NMR (101 MHz, CDCl<sub>3</sub>) δ 160.5, 158.0, 148.8, 145.9, 140.0, 136.7, 135.6, 135.3, 130.0, 124.0, 110.3, 56.2, 55.1, 53.8, 44.6, 44.2, 38.5, 37.2, 28.5, 27.3, 26.1, 25.9, 23.9, 12.6. HRMS calculated for C<sub>24</sub>H<sub>29</sub>FN<sub>2</sub>O<sub>4</sub>S [M+Na]<sup>+</sup> is 483.1724. Found: 483.1724.

## 6 References

1. WHO. *Cancer*. 2023 [cited 2023 January 27, 2023]; Available from: <https://www.who.int/news-room/fact-sheets/detail/cancer>.
2. Ruddon, R.W., *Cancer biology*. 2007, Oxford University Press: New York. p. 3-36.
3. WHO. *Cancer factsheet*. 2023 [cited 2023 January 30, 2023]; Available from: <https://www.who.int/news-room/fact-sheets/detail/cancer>.
4. Allison, S.J., *Novel Anti-Cancer Agents and Cellular Targets and Their Mechanism(s) of Action*. *Biomedicines*, 2022. **10**(8): p. 1767-1767.
5. Tilsed, C.M., et al., *Cancer chemotherapy: insights into cellular and tumor microenvironmental mechanisms of action*. *Frontiers in oncology*, 2022. **12**: p. 960317-960317.
6. Marmé, D., *Tumor Angiogenesis : A Key Target for Cancer Therapy*. 2019, Springer International Publishing : Imprint: Springer: Cham. p. 4-26.
7. *Tumour angiogenesis*. 2020. March 18, 2022 [cited 2023 April 27]; Available from: [https://commons.wikimedia.org/wiki/File:Tumor\\_angiogenesis.svg](https://commons.wikimedia.org/wiki/File:Tumor_angiogenesis.svg).
8. Folkman, J., *Tumor Angiogenesis: Therapeutic Implications*. *New England Journal of Medicine*, 1971. **285**(21): p. 1182-1186.
9. *Angiogenesis inhibitors*. 2021. March 9, 2021 [cited 2023 March 8]; Available from: <https://www.lungevity.org/for-patients-caregivers/navigating-your-diagnosis/treatment-options/angiogenesis-inhibitors>.
10. FDA. *Avastin (bevacizumab) information*. 2011. [cited 2023 February 1]; Available from: <https://www.fda.gov/drugs/postmarket-drug-safety-information-patients-and-providers/avastin-bevacizumab-information>.
11. Board, R. and G.C. Jayson, *Platelet-derived growth factor receptor (PDGFR): A target for anticancer therapeutics*. *Drug Resistance Updates*, 2005. **8**(1): p. 75-83.
12. Naito, H., T. Iba, and N. Takakura, *Mechanisms of new blood-vessel formation and proliferative heterogeneity of endothelial cells*. *International Immunology*, 2020. **32**(5): p. 295-305.
13. Cragg, G.M., P.G. Grothaus, and D.J. Newman, *Impact of Natural Products on Developing New Anti-Cancer Agents*. *Chemical Reviews*, 2009. **109**(7): p. 3012-3043.
14. Cragg, G.M.L., D.G.I. Kingston, and D.J. Newman, *Anticancer agents from natural products*. 2012, CRC Press: Boca Raton. p. 27-193.

15. Teicher, B.A. and A.T. Fojo, *Microtubule targets in cancer therapy*. 2009, Springer-Verlag: New York. p. 1-41.
16. Cole, T.J., K.L. Short, and S.B. Hooper, *The science of steroids*. Seminars in Fetal and Neonatal Medicine, 2019. **24**(3): p. 170-175.
17. Abduljabbar, H. and H. Abduljabbar, *Steroids : Basic Science*, in *Steroids*. 2012, IntechOpen: Croatia. p. 3-5.
18. Luo, J., H. Yang, and B.-L. Song, *Mechanisms and regulation of cholesterol homeostasis*. Nature Reviews. Molecular Cell Biology, 2020. **21**(4): p. 225-245.
19. Richfield, D. and M. Häggström, *Diagram of the pathways of human steroidogenesis*. Wiki Journal of Medicine, 2014. **1**(1): p. 1-5.
20. Gupta, A., B. Sathish Kumar, and A.S. Negi, *Current status on development of steroids as anticancer agents*. The Journal of Steroid Biochemistry and Molecular Biology, 2013. **137**: p. 242-270.
21. Anbar, H.S., et al., *Steroid sulfatase inhibitors: the current landscape*. Expert Opinion on Therapeutic Patents, 2021. **31**(6): p. 453-472.
22. Patel, H.K. and T. Bihani, *Selective estrogen receptor modulators (SERMs) and selective estrogen receptor degraders (SERDs) in cancer treatment*. Pharmacology and Therapeutics (Oxford), 2018. **186**: p. 1-24.
23. Sutherland, T.E., et al., *2-Methoxyestradiol – a unique blend of activities generating a new class of anti-tumour/anti-inflammatory agents*. Drug Discovery Today, 2007. **12**(13): p. 577-584.
24. Solum, E.J., et al., *Synthesis and biological evaluations of new analogs of 2-methoxyestradiol: Inhibitors of tubulin and angiogenesis*. European Journal of Medicinal Chemistry, 2014. **85**: p. 391-398.
25. Kumar, B.S., et al., *Recent Advances in chemistry and pharmacology of 2-methoxyestradiol: An anticancer investigational drug*. Steroids, 2016. **110**: p. 9-34.
26. D'Amato, R.J., et al., *2-Methoxyestradiol, an Endogenous Mammalian Metabolite, Inhibits Tubulin Polymerization by Interacting at the Colchicine Site*. Proceedings of the National Academy of Sciences - PNAS, 1994. **91**(9): p. 3964-3968.
27. Carneiro, B.A. and W.S. El-Deiry, *Targeting apoptosis in cancer therapy*. Nature Reviews Clinical Oncology, 2020. **17**(7): p. 395-417.
28. Younus, H., *Therapeutic potentials of superoxide dismutase*. International Journal of Health Sciences, 2018. **12**(3): p. 88-93.

29. Yue, J. and J.M. López, *Understanding MAPK signaling pathways in apoptosis*. International Journal of Molecular Sciences, 2020. **21**(7): p. 2346.
30. Fotsis, T., et al., *The endogenous oestrogen metabolite 2-methoxyoestradiol inhibits angiogenesis and suppresses tumour growth*. Nature, 1994. **368**(6468): p. 237-239.
31. Dubey, R.K. and E.K. Jackson, *Potential vascular actions of 2-methoxyestradiol*. Trends in Endocrinology and Metabolism, 2009. **20**(8): p. 374-379.
32. Solum, E.J., et al., *Synthesis, biological evaluation and molecular modeling of new analogs of the anti-cancer agent 2-methoxyestradiol: Potent inhibitors of angiogenesis*. The Royal Society of Chemistry (RSC) Advances, 2015. **5**(41): p. 32497-32504.
33. Miller, T.A., et al., *Synthesis and Structure–Activity Profiles of A-Homoestrans, the Estratropones*. Journal of Medicinal Chemistry, 1997. **40**(23): p. 3836-3841.
34. Peyrat, J.-F., J.-D. Brion, and M. Alami, *Synthetic 2-methoxyestradiol derivatives: structure-activity relationships*. Current Medicinal Chemistry, 2012: p. 4142-4156(15).
35. Shah, J.H., et al., *Synthesis of 2- and 17-substituted estrone analogs and their antiproliferative structure–activity relationships compared to 2-methoxyestradiol*. Bioorganic and Medicinal Chemistry, 2009. **17**(20): p. 7344-7352.
36. Cushman, M., et al., *Synthesis, Antitubulin and Antimitotic Activity, and Cytotoxicity of Analogs of 2-Methoxyestradiol, an Endogenous Mammalian Metabolite of Estradiol That Inhibits Tubulin Polymerization by Binding to the Colchicine Binding Site*. Journal of Medicinal Chemistry, 1995. **38**(12): p. 2041-2049.
37. Edsall, A.B., et al., *Effects of Altering the Electronics of 2-Methoxyestradiol on Cell Proliferation, on Cytotoxicity in Human Cancer Cell Cultures, and on Tubulin Polymerization*. Journal of Medicinal Chemistry, 2004. **47**(21): p. 5126-5139.
38. Agoston, G.E., et al., *Synthesis, antiproliferative, and pharmacokinetic properties of 3- and 17-double-modified analogs of 2-methoxyestradiol*. Bioorganic and Medicinal Chemistry Letters, 2009. **19**(21): p. 6241-6244.
39. LaVallee, T.M., et al., *Significant antitumor activity in vivo following treatment with the microtubule agent ENMD-1198*. Molecular Cancer Therapeutics, 2008. **7**(6): p. 1472-1482.
40. Agoston, G.E., et al., *Synthesis and structure–activity relationships of 16-modified analogs of 2-methoxyestradiol*. Bioorganic and Medicinal Chemistry, 2007. **15**(24): p. 7524-7537.

41. Newman, S.P., et al., *Inhibition of in vitro angiogenesis by 2-methoxy- and 2-ethyl-estrogen sulfamates*. International Journal of Cancer, 2004. **109**(4): p. 533-540.
42. al-Kazaale, N., et al., *Synthesis, molecular modeling and biological evaluation of potent analogs of 2-methoxyestradiol*. Steroids, 2018. **136**: p. 47-55.
43. Suwandi, L.S., et al., *Synthesis and antitumor activities of 3-modified 2-methoxyestradiol analogs*. Bioorganic and Medicinal Chemistry Letters, 2009. **19**(22): p. 6459-6462.
44. Aoki, S., et al., *Structure–activity relationship and biological property of cortistatins, anti-angiogenic spongean steroidal alkaloids*. Bioorganic and Medicinal Chemistry, 2007. **15**(21): p. 6758-6762.
45. *Cortistatins J, K, L, novel abeo-9(10-19)-androstane-type steroidal alkaloids with isoquinoline unit, from marine sponge Corticium simplex*. 2007: [Oxford] ; [New York] :. p. 4485-4488.
46. *Cortistatins E, F, G, and H, four novel steroidal alkaloids from marine sponge Corticium simplex*. 2007: [Oxford] ; [New York] :. p. 4074-4079.
47. Aoki, S., et al., *Cortistatins A, B, C, and D, Anti-angiogenic Steroidal Alkaloids, from the Marine Sponge Corticium simplex*. Journal of the American Chemical Society, 2006. **128**(10): p. 3148-3149.
48. Czakó, B., et al., *Discovery of Potent and Practical Antiangiogenic Agents Inspired by Cortistatin A*. Journal of the American Chemical Society, 2009. **131**(25): p. 9014-9019.
49. Zhou, Q., et al., *A phase I dose-escalation, safety and pharmacokinetic study of the 2-methoxyestradiol analog ENMD-1198 administered orally to patients with advanced cancer*. Investigational New Drugs, 2011. **29**(2): p. 340-346.
50. Sweeney, C., et al., *A Phase II Multicenter, Randomized, Double-Blind, Safety Trial Assessing the Pharmacokinetics, Pharmacodynamics, and Efficacy of Oral 2-Methoxyestradiol Capsules in Hormone-Refractory Prostate Cancer*. Clinical Cancer Research, 2005. **11**(18): p. 6625-6633.
51. Guo, X.-H., et al., *An investigation on intestinal absorption of a new anticancer drug, 2-methoxyestradiol*. Pharmazie, 2009. **64**(11): p. 748-751.
52. Kulke, M.H., et al., *A prospective phase II study of 2-methoxyestradiol administered in combination with bevacizumab in patients with metastatic carcinoid tumors*. Cancer Chemotherapy and Pharmacology, 2011. **68**(2): p. 293-300.

53. Tevaarwerk, A.J., et al., *Phase I Trial of 2-Methoxyestradiol NanoCrystal Dispersion in Advanced Solid Malignancies*. *Clinical Cancer Research*, 2009. **15**(4): p. 1460-1465.
54. Harrison, M.R., et al., *A phase II study of 2-methoxyestradiol (2ME2) NanoCrystal® dispersion (NCD) in patients with taxane-refractory, metastatic castrate-resistant prostate cancer (CRPC)*. *Investigational New Drugs*, 2011. **29**(6): p. 1465-1474.
55. Kürti, L. and B. Czakó, *Strategic applications of named reactions in organic synthesis : background and detailed mechanisms : 250 named reactions*. 2005, Amsterdam: Elsevier Academic Press. p. 320-321.
56. *Oppenauer oxidation mechanism*. 2010. May 13, 2022 [cited 2023 April 27]; Available from:  
[https://en.wikipedia.org/wiki/Oppenauer\\_oxidation#/media/File:Oppenauer\\_oxidation\\_mechanism\\_layout.png](https://en.wikipedia.org/wiki/Oppenauer_oxidation#/media/File:Oppenauer_oxidation_mechanism_layout.png).
57. Kürti, L. and B. Czakó, *Strategic applications of named reactions in organic synthesis : background and detailed mechanisms : 250 named reactions*. 2005, Amsterdam: Elsevier Academic Press. p. 448-449.
58. Miyaura, N. and A. Suzuki, *Palladium-Catalyzed Cross-Coupling Reactions of Organoboron Compounds*. *Chemical Reviews*, 1995. **95**(7): p. 2457-2483.
59. Ohe, T., N. Miyaura, and A. Suzuki, *Palladium-catalyzed cross-coupling reaction of organoboron compounds with organic triflates*. *Journal of organic chemistry*, 1993. **58**(8): p. 2201-2208.
60. Cobos-Ontiveros, L.A., et al., *Synthesis, antiproliferative evaluation and in silico studies of a novel steroidal spiro morpholinone*. *Steroids*, 2023. **192**: p. 109173-109173.

## **7 Appendix**

### **7.1 $^1\text{H}$ NMR and $^{13}\text{C}$ NMR of the synthesized compounds**

# <sup>1</sup>H NMR of 2-methoxyestrone (31)

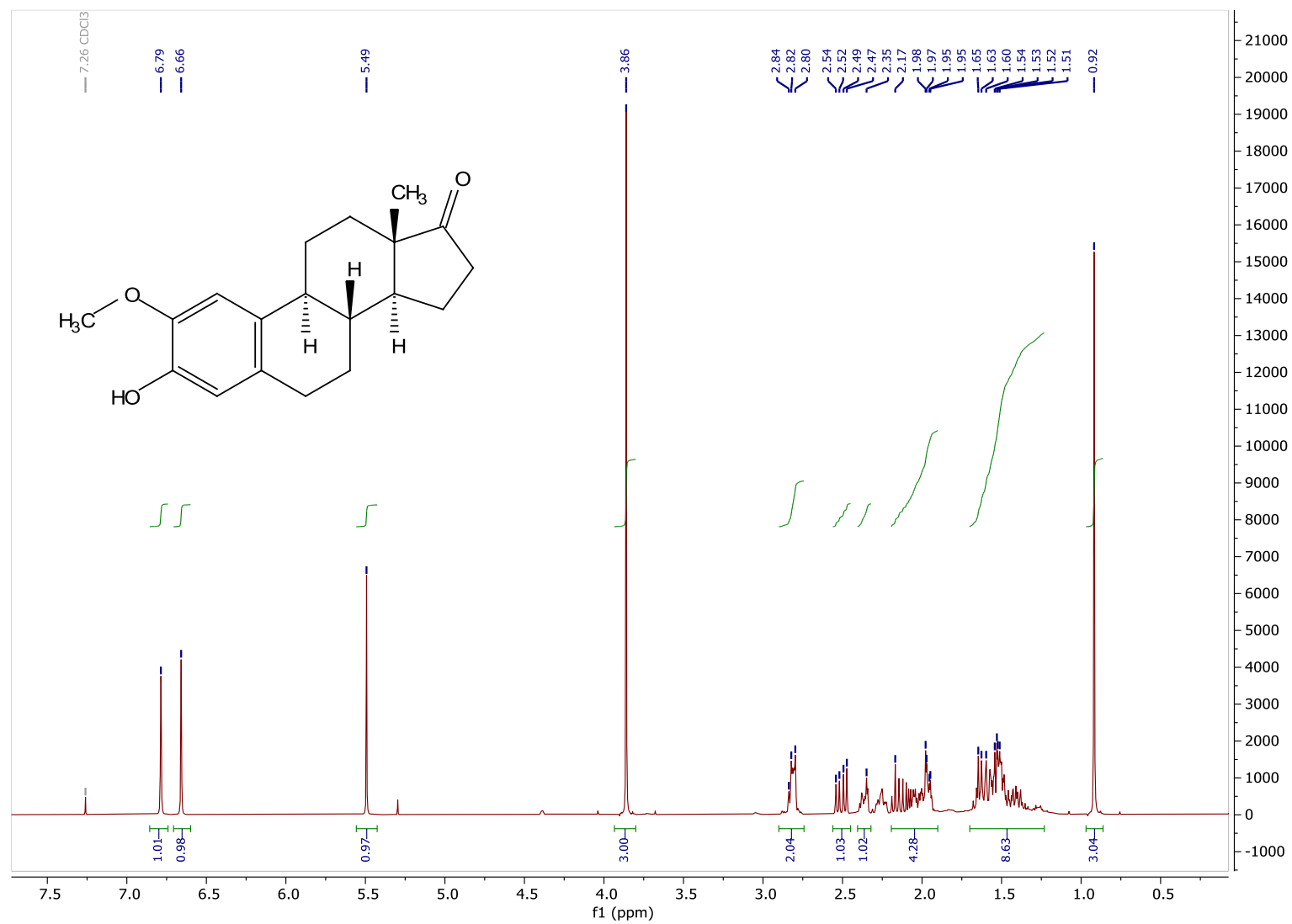


Figure 15: <sup>1</sup>H NMR of 2-methoxyestrone (31).

### <sup>13</sup>C NMR of 2-methoxyestrone (31)

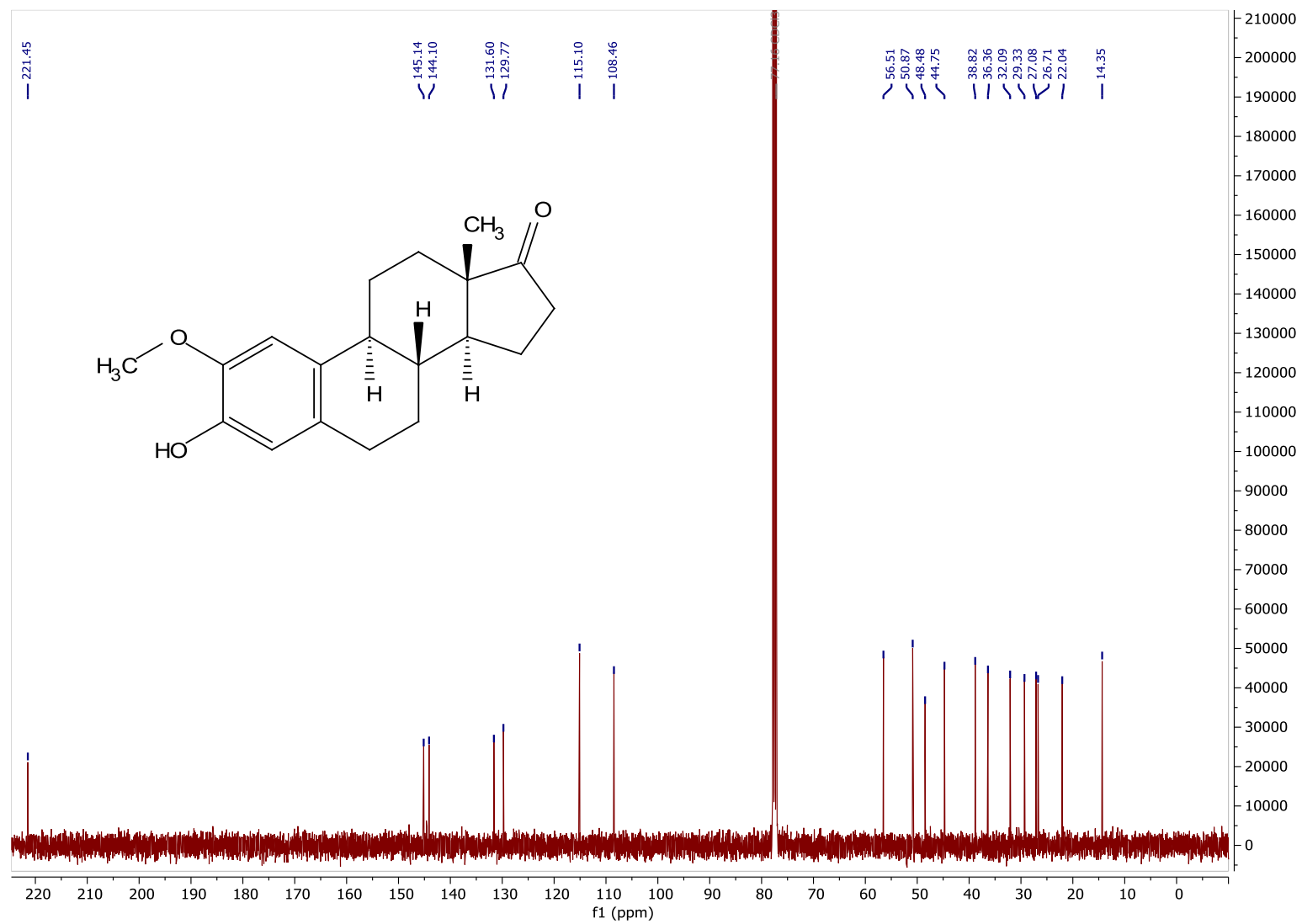
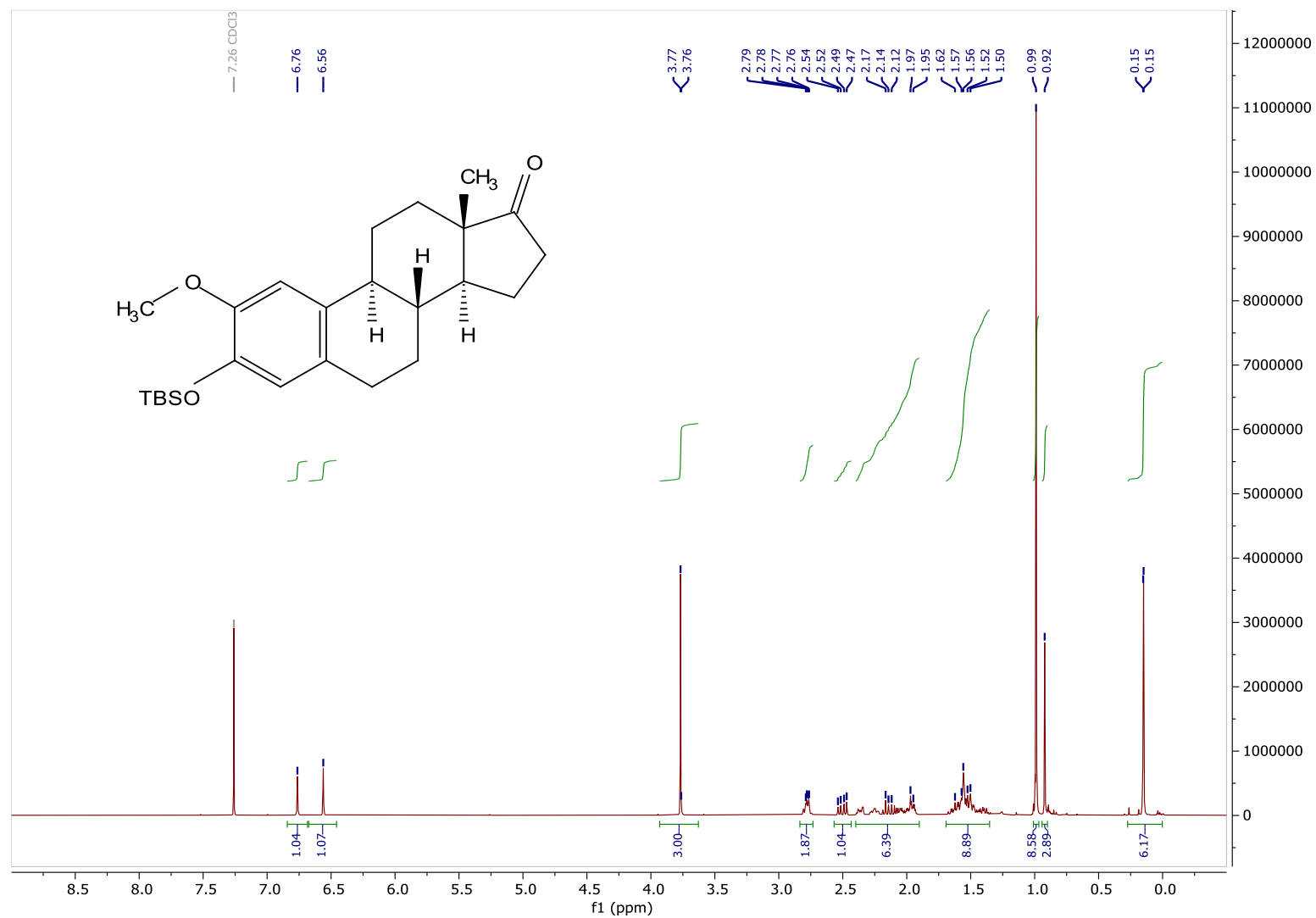


Figure 16: <sup>13</sup>C NMR of 2-methoxyestrone (31).

**<sup>1</sup>H NMR of 3-*tert*-butyldimethylsiloxy-2-methoxyestrone (45)**



**Figure 17:** <sup>1</sup>H NMR of 3-*tert*-butyldimethylsiloxy-2-methoxyestrone (45).

**$^{13}\text{C}$  NMR of 3-*tert*-butyldimethylsiloxy-2-methoxyestrone (45)**

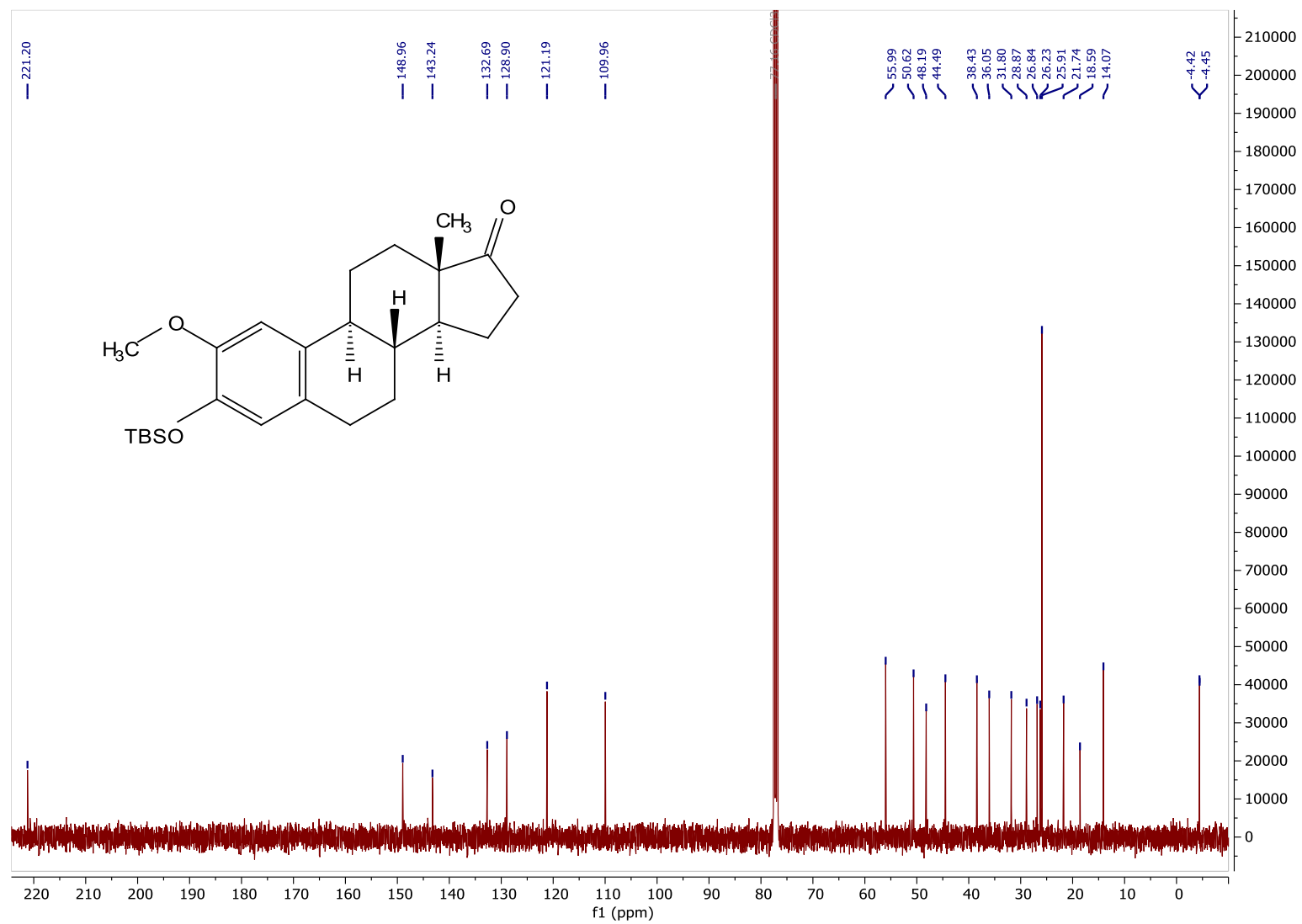


**Figure 18:**  $^{13}\text{C}$  NMR of 3-*tert*-butyldimethylsiloxy-2-methoxyestrone (45).

**$^1\text{H}$  NMR of (8*R*,9*S*,13*S*,14*S*)-3-((*tert*-butyldimethylsilyl)oxy)-2-methoxy-13-methyl-7,8,9,11,12,13,14,15-octahydro-6*H*-cyclopenta[*a*]phenanthren-17-yl trifluoromethanesulfonate (46)**

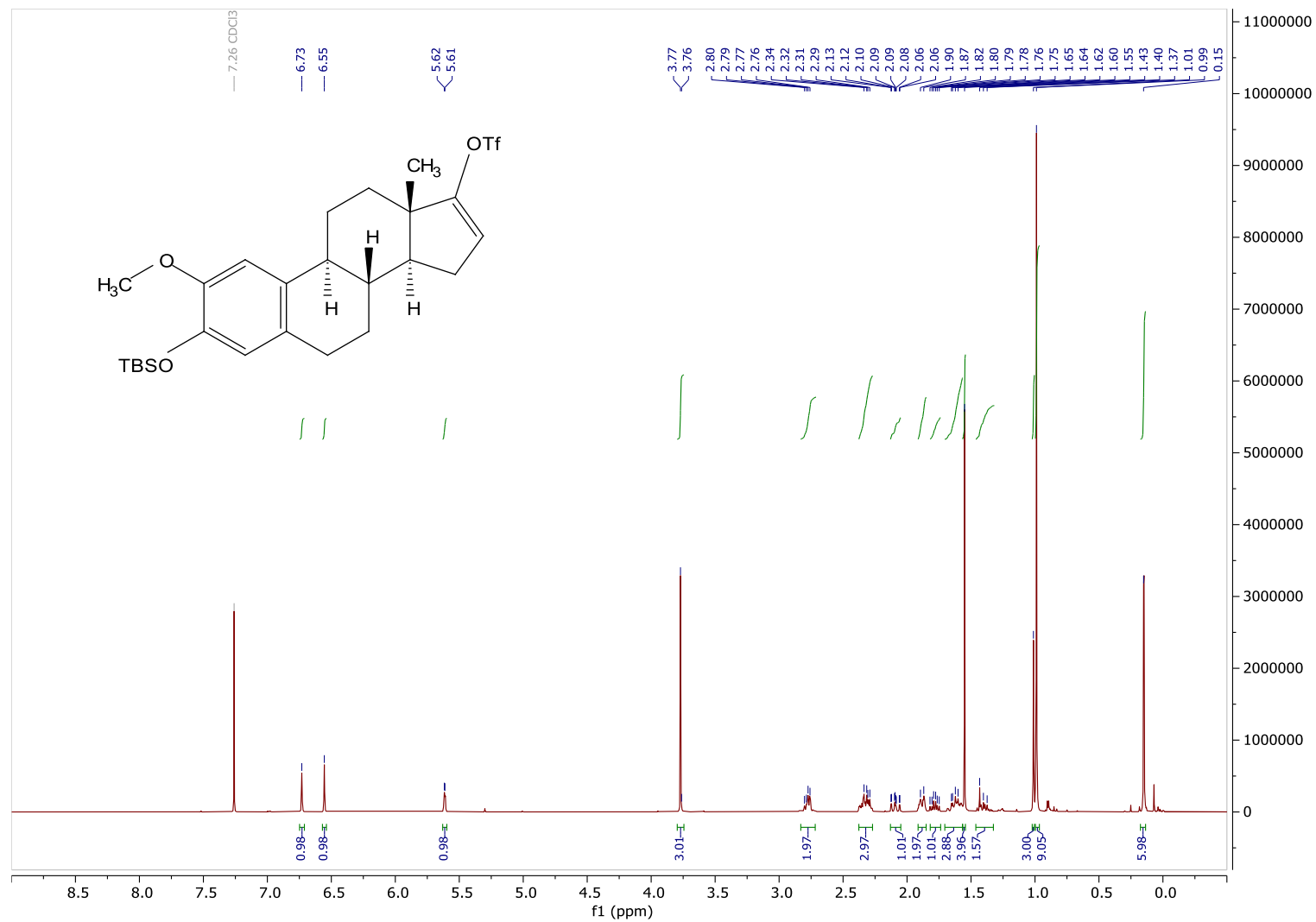


**Figure 19:**  $^1\text{H}$  NMR of 2-methoxy-steroid triflate (46).

**$^{13}\text{C}$  NMR of (8*R*,9*S*,13*S*,14*S*)-3-((*tert*-butyldimethylsilyl)oxy)-2-methoxy-13-methyl-7,8,9,11,12,13,14,15-octahydro-6*H*-cyclopenta[*a*]phenanthren-17-yl trifluoromethanesulfonate (46)**

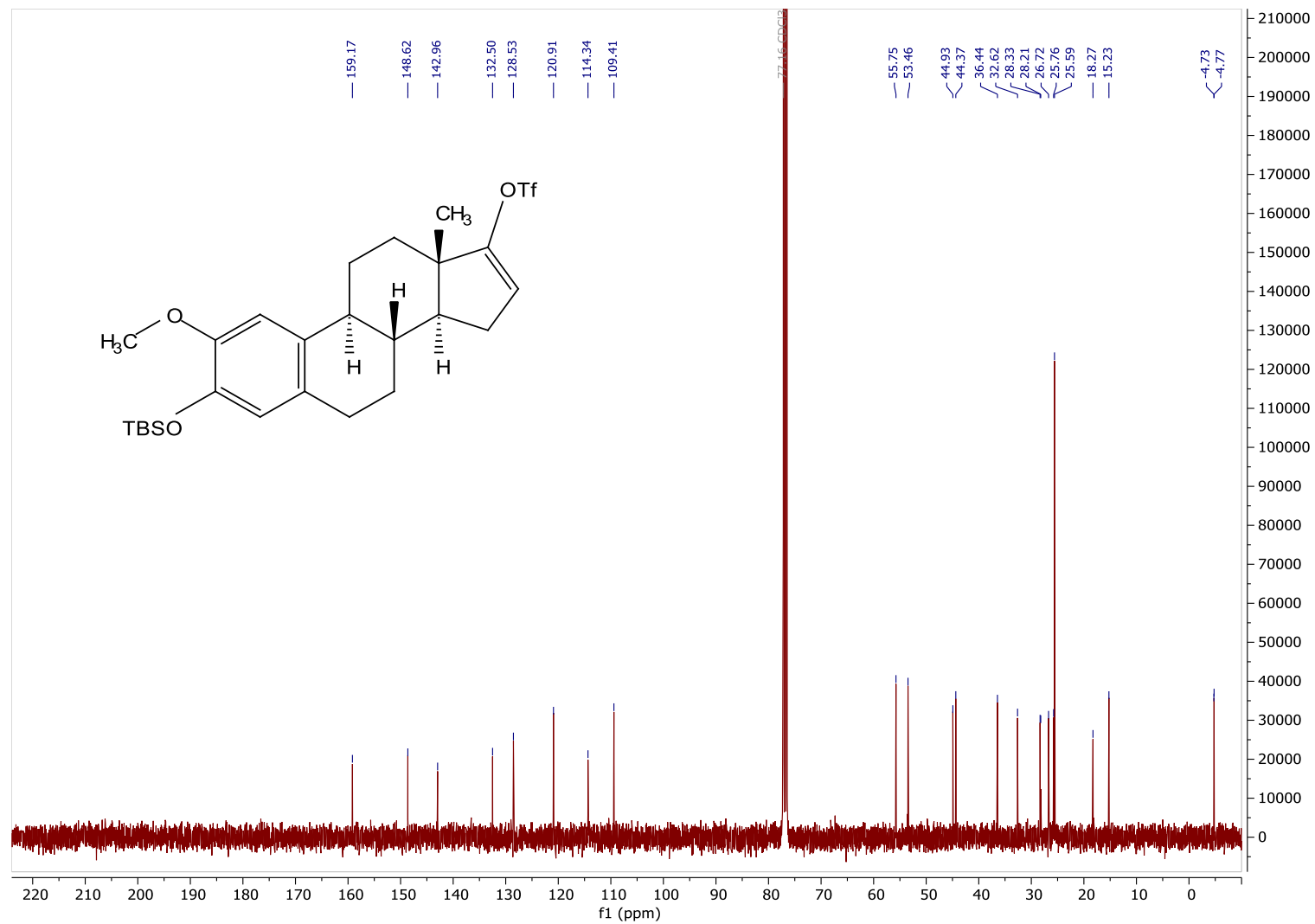


**Figure 20:**  $^{13}\text{C}$  NMR of 2-methoxy-steroid triflate (46).

**$^1\text{H}$  NMR of 3-((8*S*,9*S*,13*S*,14*S*)-3-((*tert*-butyldimethylsilyl)oxy)-2-methoxy-13-methyl-7,8,9,11,12,13,14,15-octahydro-6*H*-cyclopenta[*a*]phenanthren-17-yl)-5-fluoropyridine (47)**

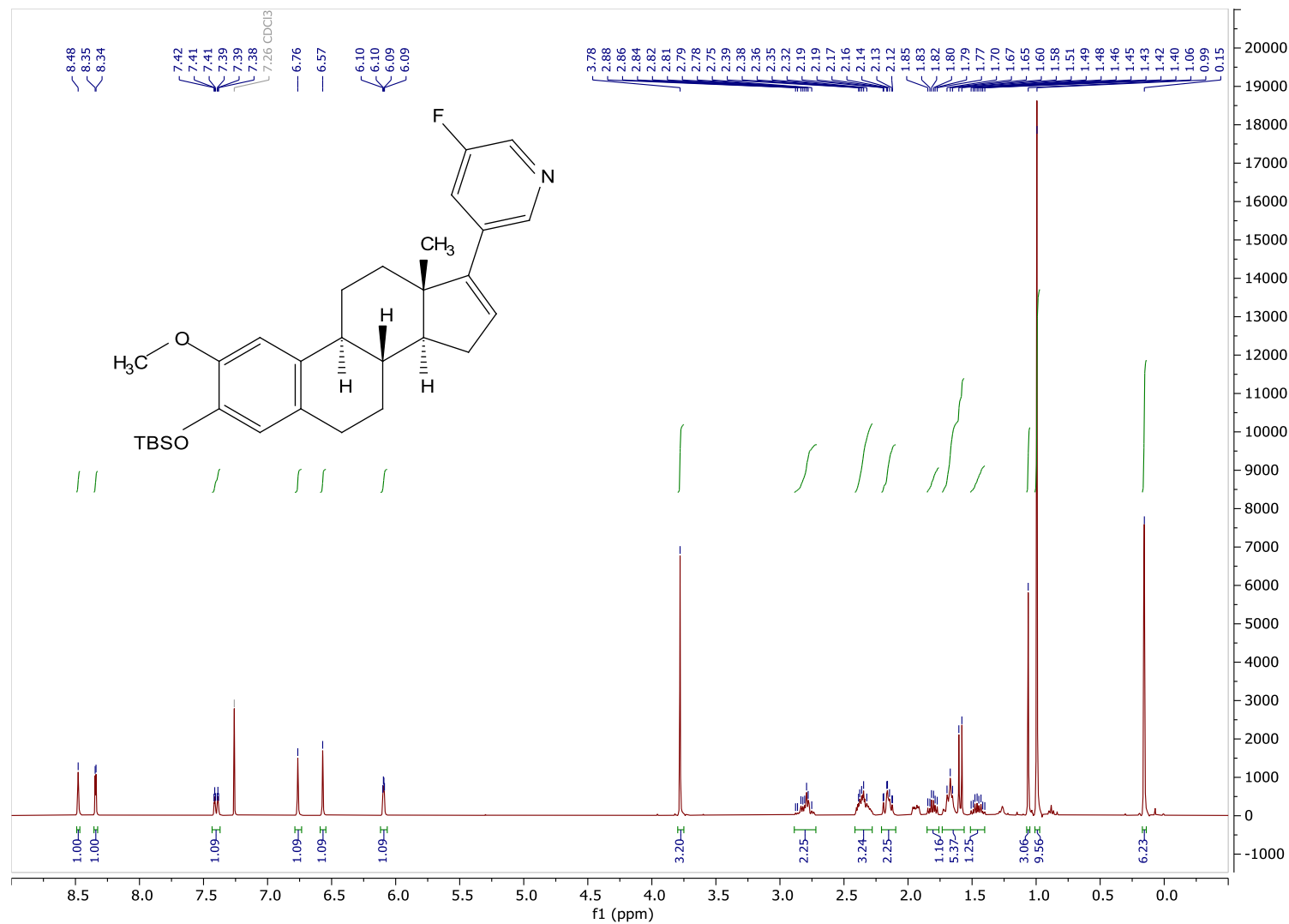


**Figure 21:**  $^1\text{H}$  NMR of the steroid compound 47.

**$^{13}\text{C}$  NMR of 3-((8*S*,9*S*,13*S*,14*S*)-3-((*tert*-butyldimethylsilyl)oxy)-2-methoxy-13-methyl-7,8,9,11,12,13,14,15-octahydro-6*H*-cyclopenta[*a*]phenanthren-17-yl)-5-fluoropyridine (47)**

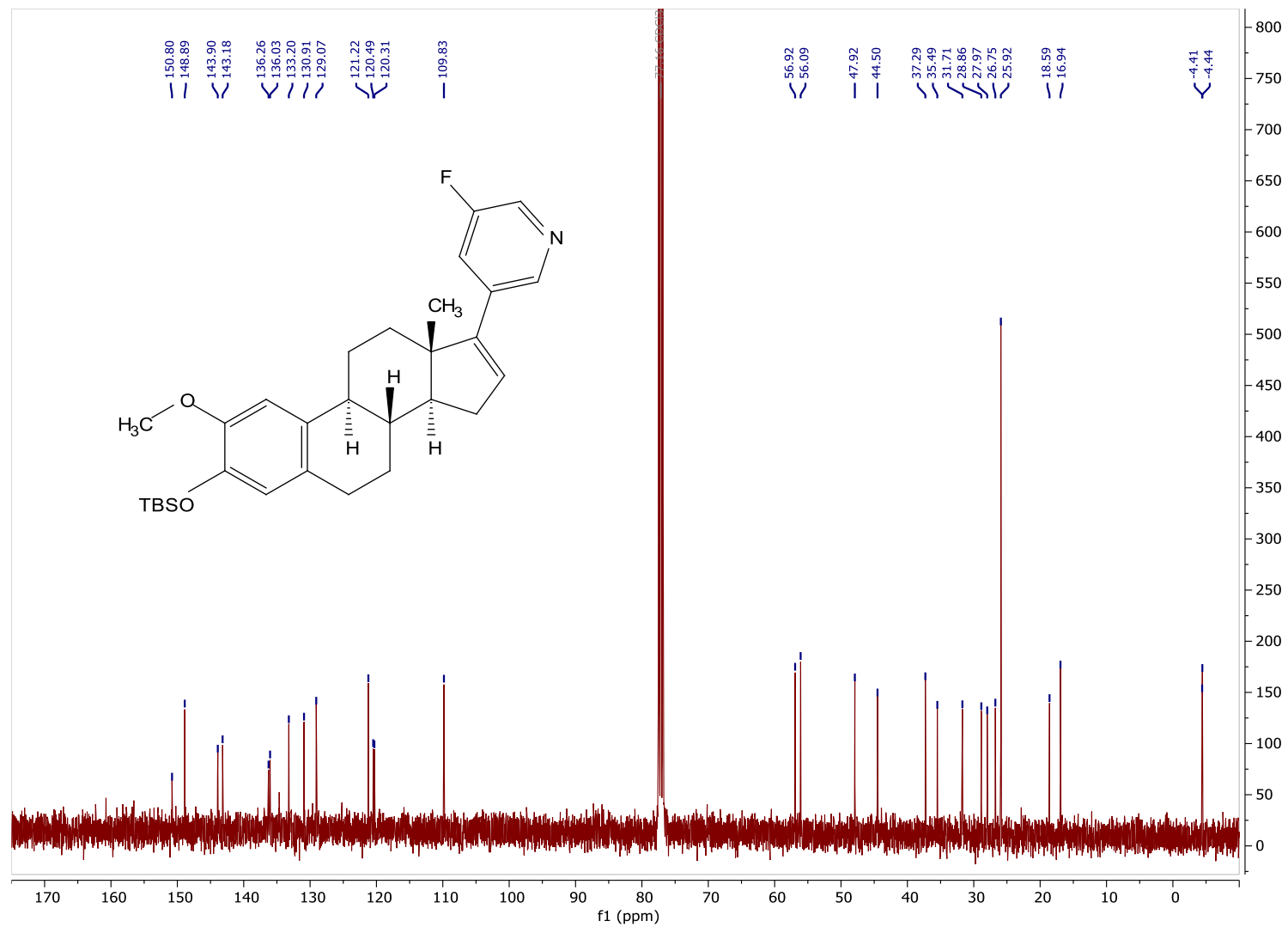


**Figure 22:**  $^{13}\text{C}$  NMR of the steroid compound 47.

**<sup>1</sup>H NMR of (8*S*,9*S*,13*S*,14*S*)-17-(5-fluoropyridin-3-yl)-2-methoxy-13-methyl-7,8,9,11,12,13,14,15-octahydro-6*H*-cyclopenta[*a*]phenanthren-3-ol (48)**

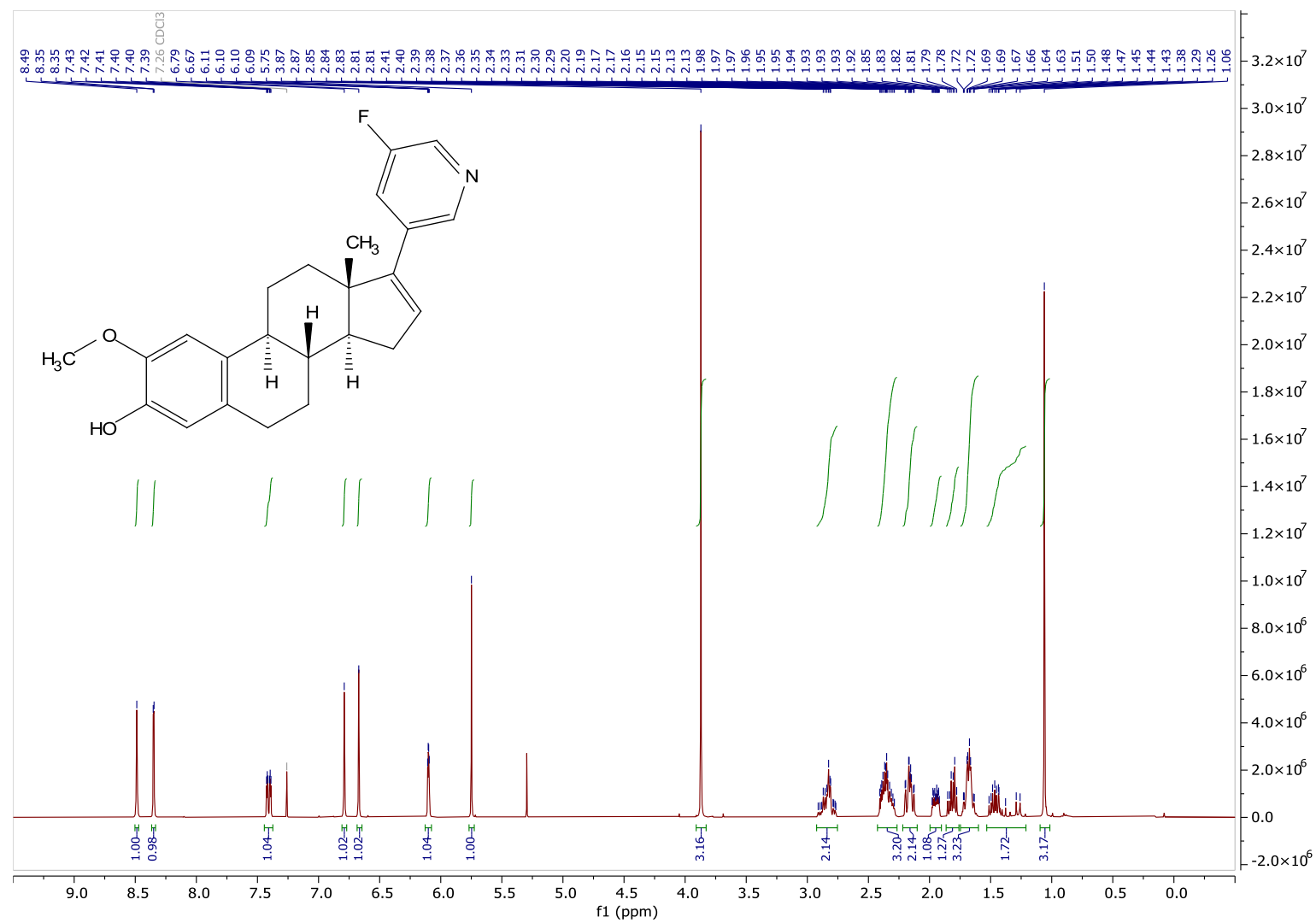


**Figure 23:** <sup>1</sup>H NMR of the steroid compound 48.

**<sup>13</sup>C NMR of (8*S*,9*S*,13*S*,14*S*)-17-(5-fluoropyridin-3-yl)-2-methoxy-13-methyl-7,8,9,11,12,13,14,15-octahydro-6*H*-cyclopenta[*a*]phenanthren-3-ol (48)**

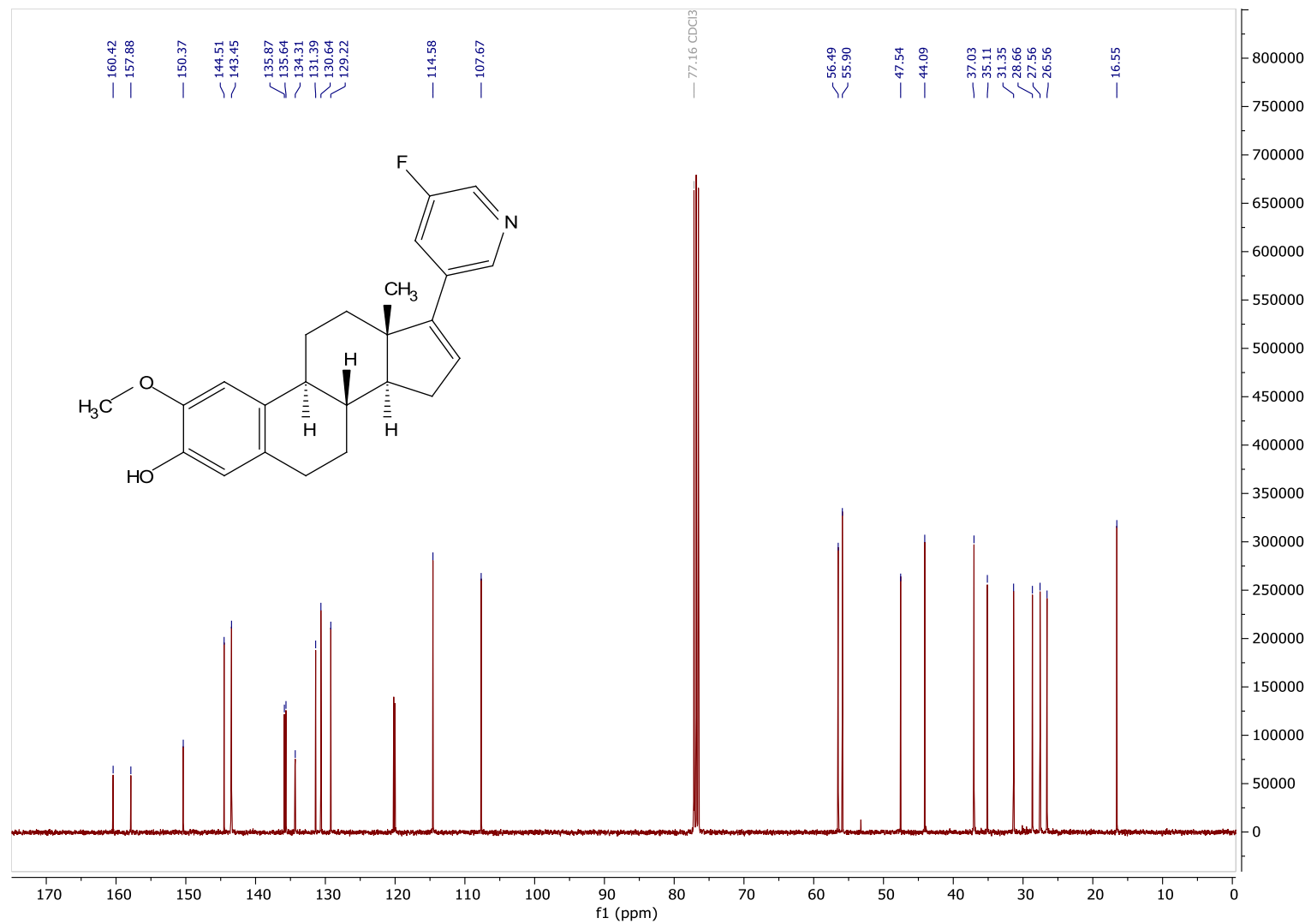


**Figure 24:** <sup>13</sup>C NMR of the steroid compound 48.

**$^1\text{H}$  NMR of rac-(8*S*,9*S*,13*R*,14*S*)-17-(5-fluoropyridin-3-yl)-2-methoxy-13-methyl-7,8,9,11,12,13,14,15,16,17-decahydro-6*H*-cyclopenta[*a*]phenanthren-3-ol (49)**

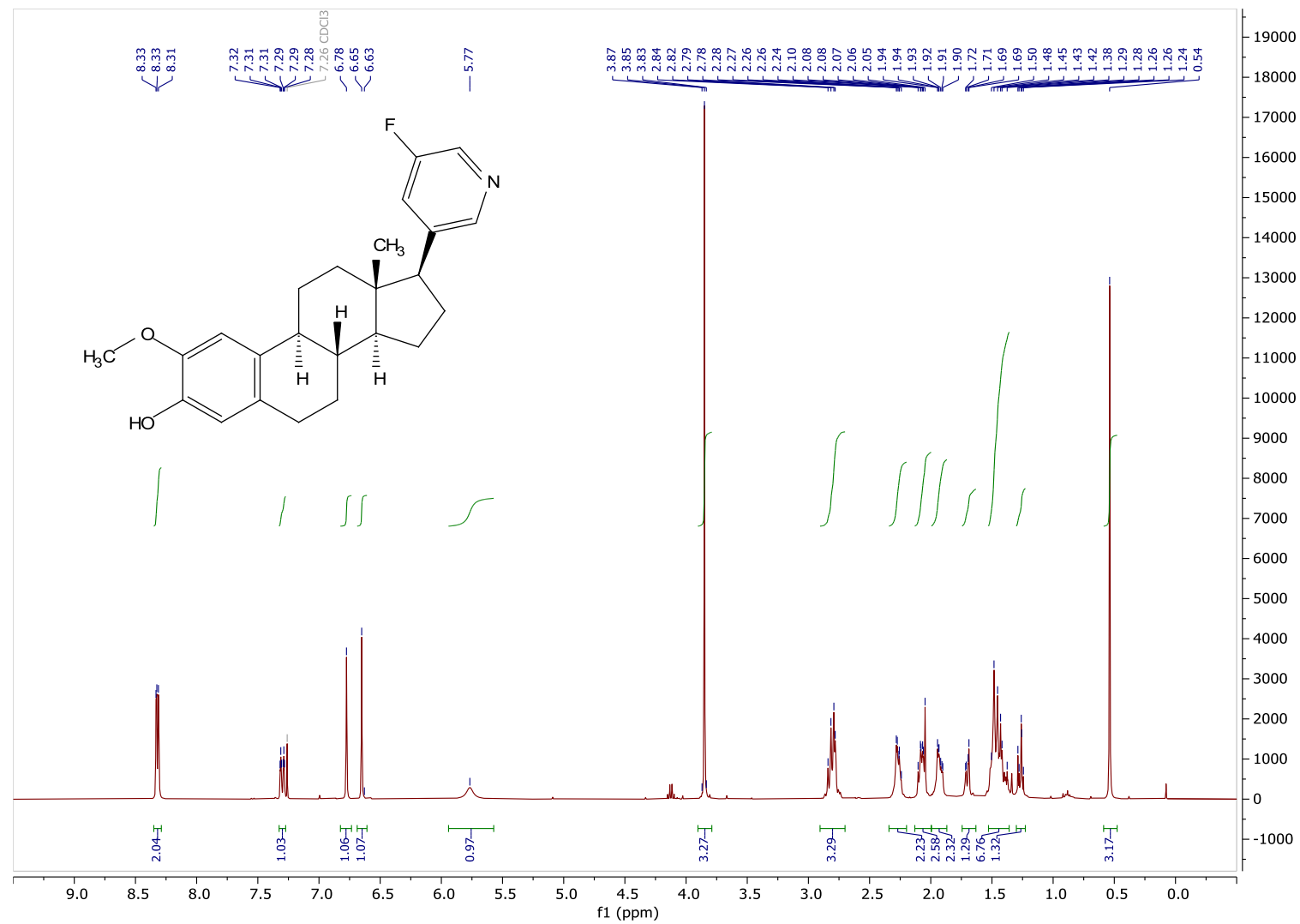


**Figure 25:**  $^1\text{H}$  NMR of the steroid compound 49.

**<sup>13</sup>C NMR of rac-(8*S*,9*S*,13*R*,14*S*)-17-(5-fluoropyridin-3-yl)-2-methoxy-13-methyl-7,8,9,11,12,13,14,15,16,17-decahydro-6*H*-cyclopenta[*a*]phenanthren-3-ol (49)**

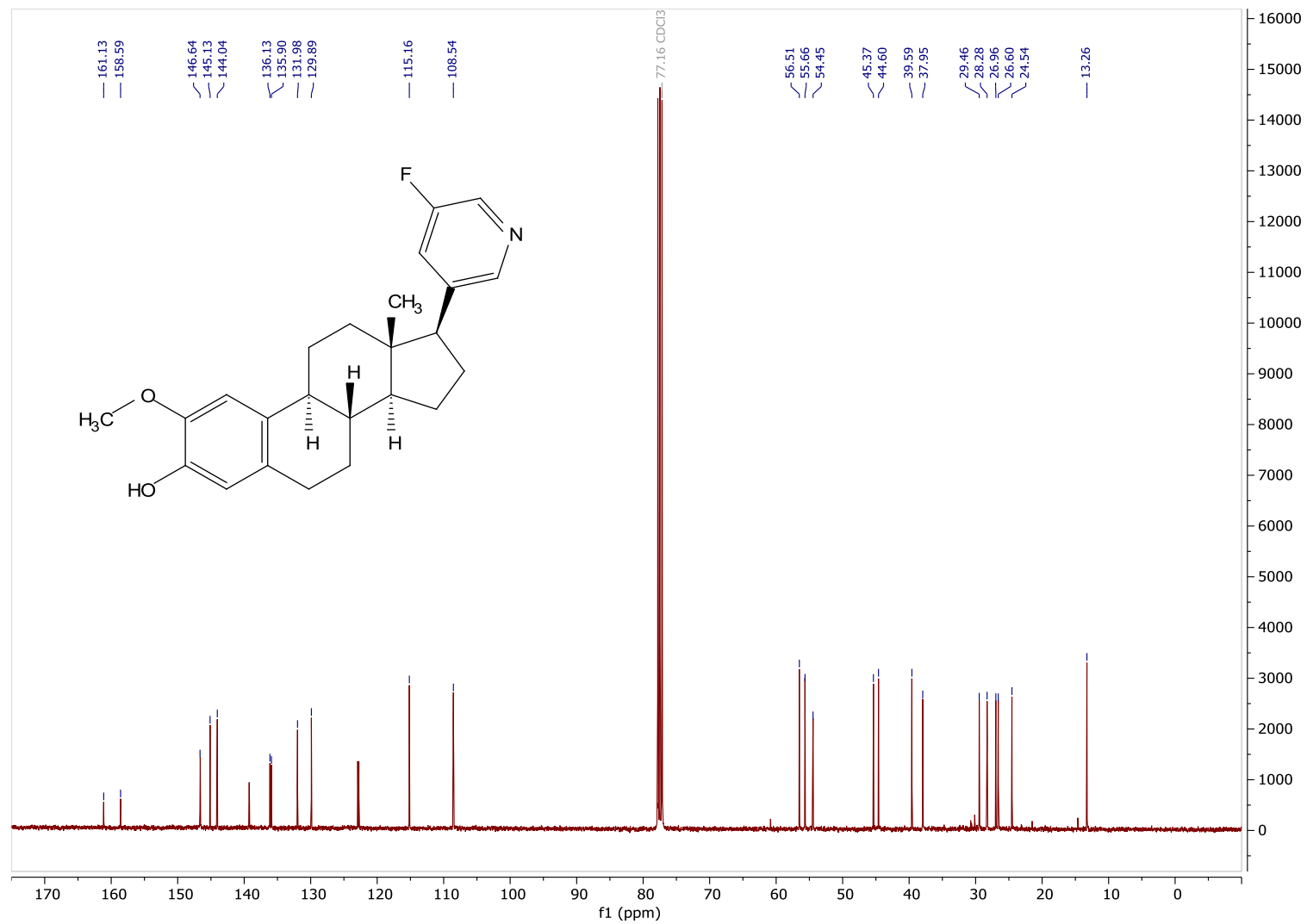


**Figure 26:** <sup>13</sup>C NMR of the steroid compound 49.

**<sup>1</sup>H NMR of (8*S*,9*S*,13*S*,14*S*)-17-(5-fluoropyridin-3-yl)-2-methoxy-13-methyl-7,8,9,11,12,13,14,15-octahydro-6*H*-cyclopenta[*a*]phenanthren-3-yl sulfamate (50)**

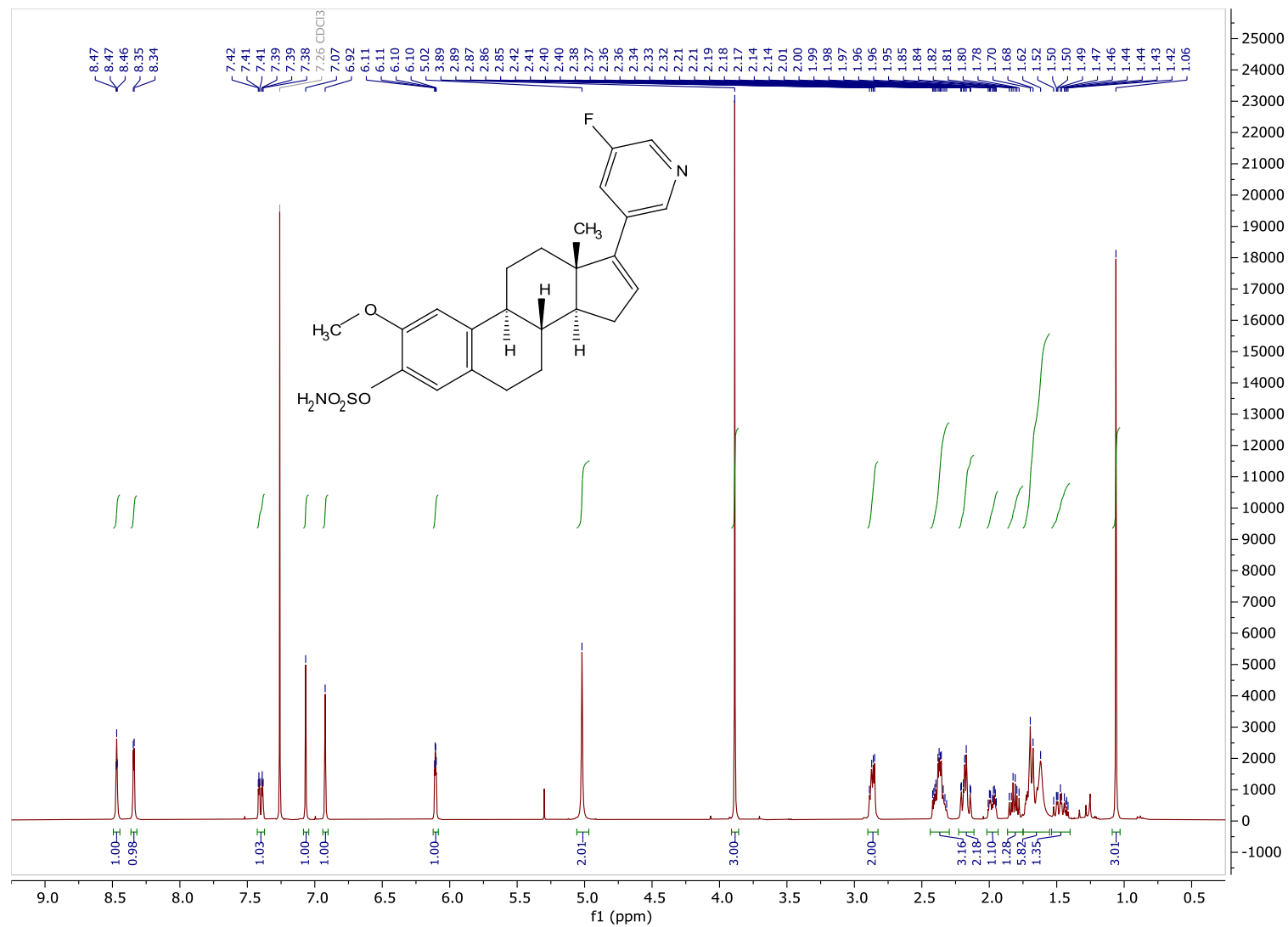


**Figure 27:** <sup>1</sup>H NMR of the steroid compound 50.

**<sup>13</sup>C NMR of (8*S*,9*S*,13*S*,14*S*)-17-(5-fluoropyridin-3-yl)-2-methoxy-13-methyl-7,8,9,11,12,13,14,15-octahydro-6*H*-cyclopenta[*a*]phenanthren-3-yl sulfamate (50)**

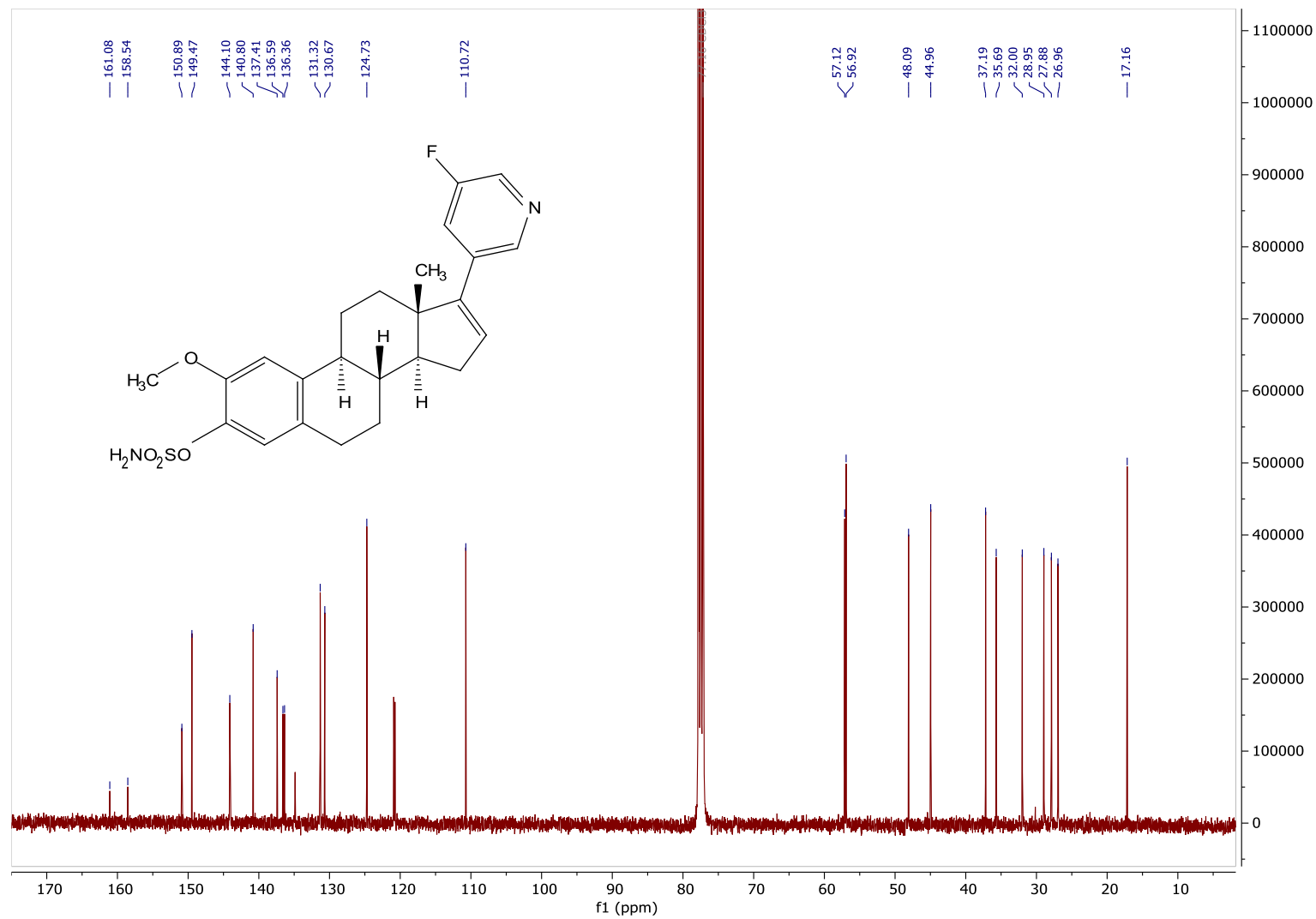


**Figure 28:** <sup>13</sup>C NMR of the steroid compound 50.

**<sup>1</sup>H NMR of (8*S*,9*S*,13*S*,14*S*)-17-(5-fluoropyridin-3-yl)-2-methoxy-13-methyl-7,8,9,11,12,13,14,15-octahydro-6*H*-cyclopenta[*a*]phenanthren-3-yl sulfamate (51)**

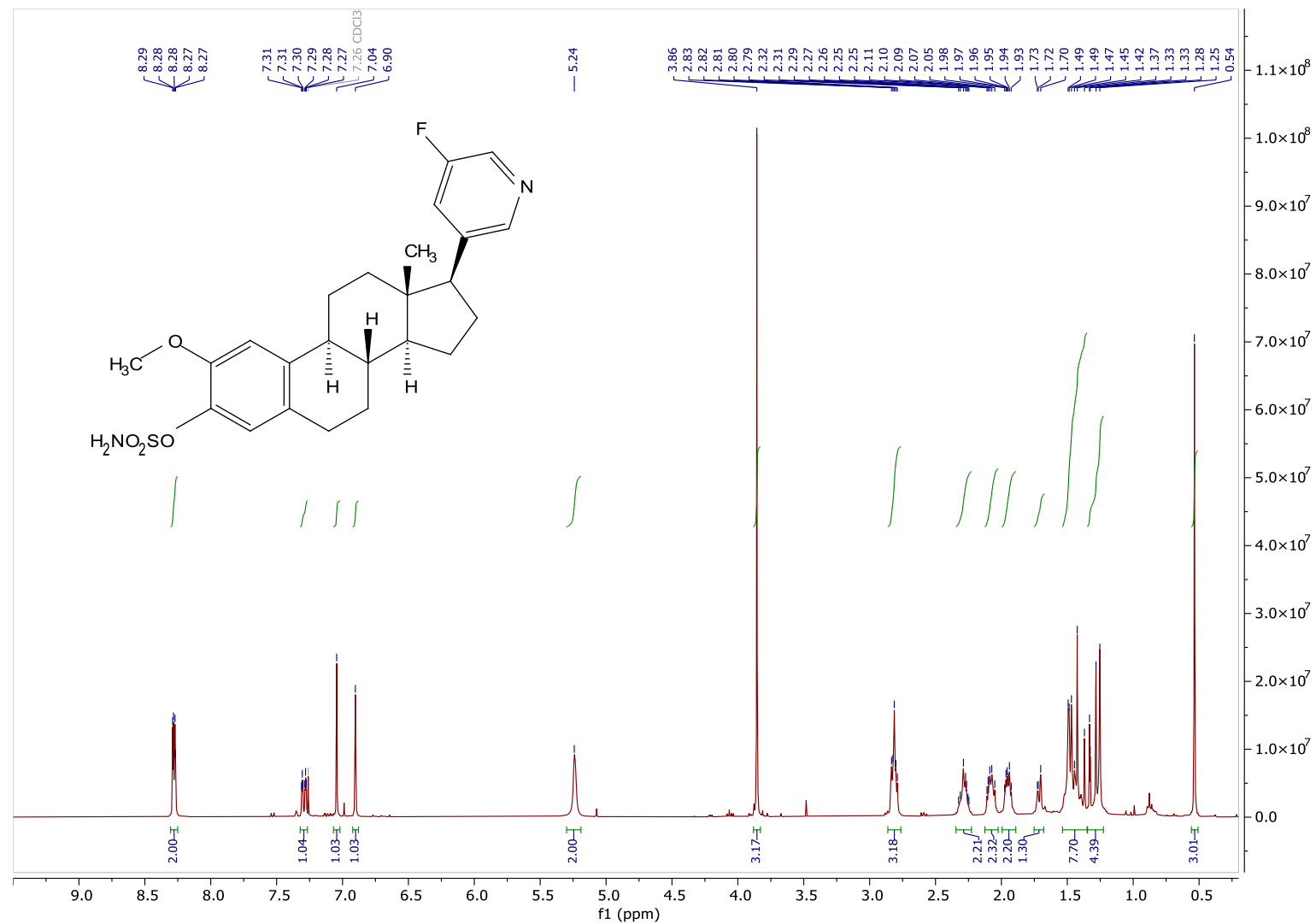


**Figure 29:** <sup>1</sup>H NMR of the steroid compound 51.

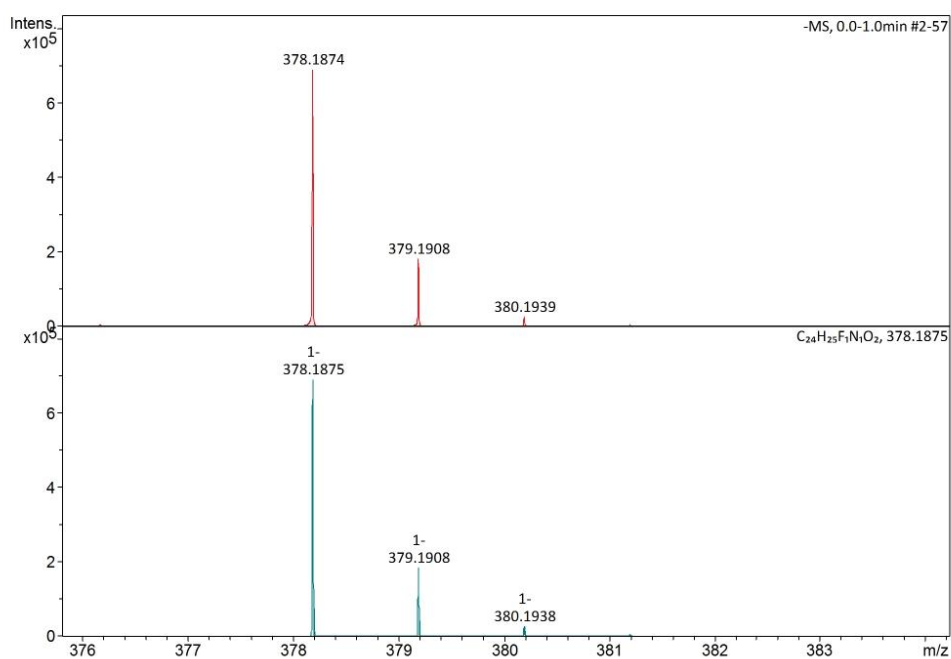


## **7.2 HRMS of the synthesized compounds**

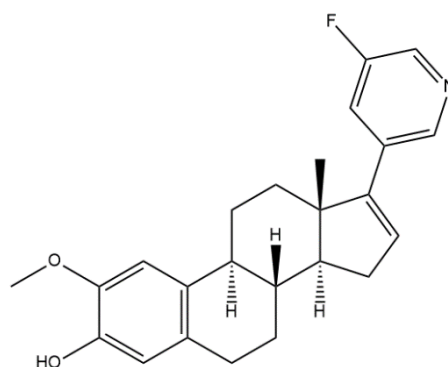
**(8*S*,9*S*,13*S*,14*S*)-17-(5-fluoropyridin-3-yl)-2-methoxy-13-methyl-7,8,9,11,12,13,14,15-octahydro-6*H*-cyclopenta[*a*]phenanthren-3-ol (48)**

### Elemental Analysis Report

Analysis Info		Acquisition Date		30-Jan-23 3:09:34 PM	
Sample Name	sk025	Analysis Name	D:\Data\maxis2023\19257.d		
Method	ESI_neg_50_1500_os.m				
Acquisition Parameter					
Source Type	ESI	Set Capillary	3500 V	Set Nebulizer	1.0 Bar
Focus	Not active	Set End Plate Offset	-500 V	Set Dry Heater	200 °C
Scan Begin	50 m/z	Set Charging Voltage	0 V	Set Dry Gas	4.0 l/min
Scan End	1500 m/z	Set Corona	0 nA	Set Divert Valve	Source
				Set APCI Heater	0 °C



Meas. m/z	Ion Formula	m/z	err [ppm]
378.1874	C <sub>24</sub> H <sub>25</sub> FN <sub>1</sub> O <sub>2</sub>	378.1875	0.2



19257.d

Bruker Compass DataAnalysis 4.3

printed: 30-Jan-23 3:14:58 PM

Page 1 of 1

**Figure 31:** Elemental analysis report of steroid compound 48.

**rac-(8S,9S,13R,14S)-17-(5-fluoropyridin-3-yl)-2-methoxy-13-methyl-7,8,9,11,12,13,14,15,16,17-decahydro-6H-cyclopenta[*a*]phenanthren-3-ol (49)**

### Elemental Analysis Report

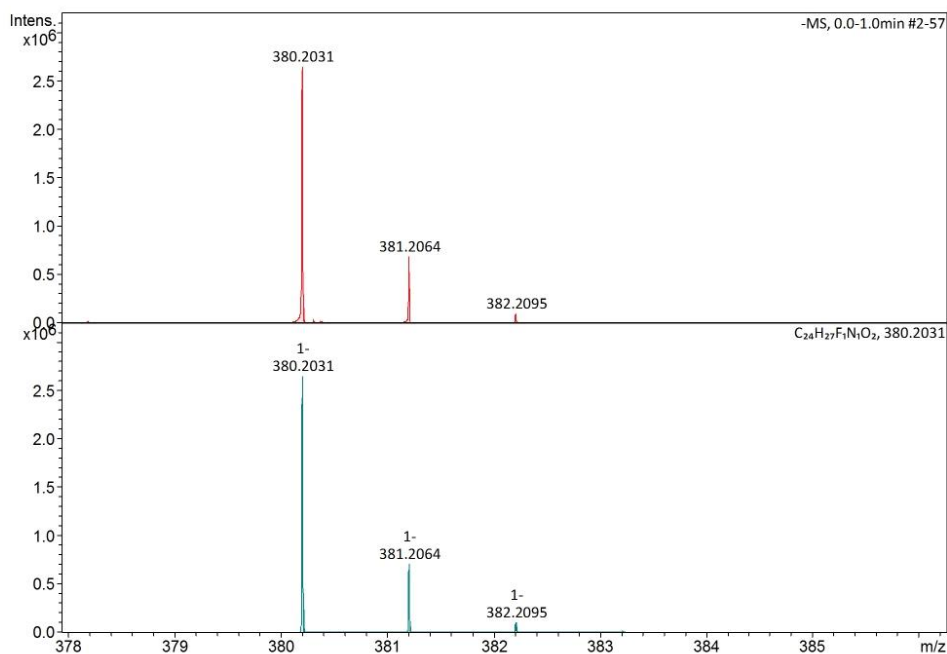
**Analysis Info**

Sample Name sk026  
Method ESI\_neg\_50\_1500\_os.m

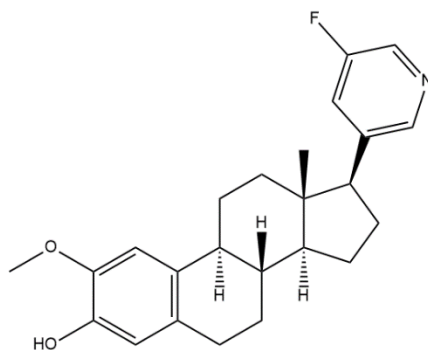
Acquisition Date 30-Jan-23 3:30:48 PM  
Analysis Name D:\Data\maxis2023\19258.d

**Acquisition Parameter**

Source Type	ESI	Set Capillary	3500 V	Set Nebulizer	0.5 Bar
Focus	Not active	Set End Plate Offset	-500 V	Set Dry Heater	200 °C
Scan Begin	50 m/z	Set Charging Voltage	0 V	Set Dry Gas	4.0 l/min
Scan End	1500 m/z	Set Corona	0 nA	Set Divert Valve	Source
				Set APCI Heater	0 °C



Meas. m/z	Ion Formula	m/z	err [ppm]
380.2031	C <sub>24</sub> H <sub>27</sub> FN <sub>1</sub> O <sub>2</sub>	380.2031	0.2



19258.d

Bruker Compass DataAnalysis 4.3

printed: 30-Jan-23 3:37:47 PM

Page 1 of 1

**Figure 32:** Elemental analysis report of steroid compound **49**.

**(8*S*,9*S*,13*S*,14*S*)-17-(5-fluoropyridin-3-yl)-2-methoxy-13-methyl-7,8,9,11,12,13,14,15-octahydro-6*H*-cyclopenta[*a*]phenanthren-3-yl sulfamate (50)**

**Elemental Analysis Report**

Analysis Info		Acquisition Date		24-Mar-23 4:01:32 PM	
Sample Name	sk027	Analysis Name	D:\Data\maxis2023\19430.d		
Method	ESI_pos_50_1500_os.m				
Acquisition Parameter					
Source Type	ESI	Set Capillary	3500 V	Set Nebulizer	0.5 Bar
Focus	Not active	Set End Plate Offset	-500 V	Set Dry Heater	200 °C
Scan Begin	50 m/z	Set Charging Voltage	2000 V	Set Dry Gas	4.0 l/min
Scan End	1500 m/z	Set Corona	0 nA	Set Divert Valve	Waste
				Set APCI Heater	0 °C

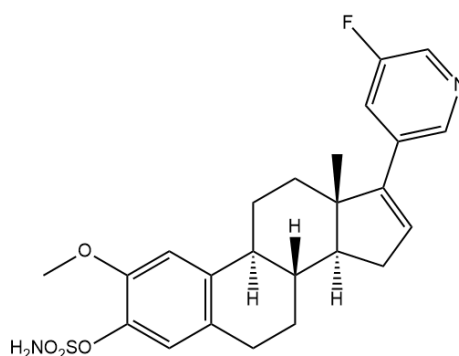
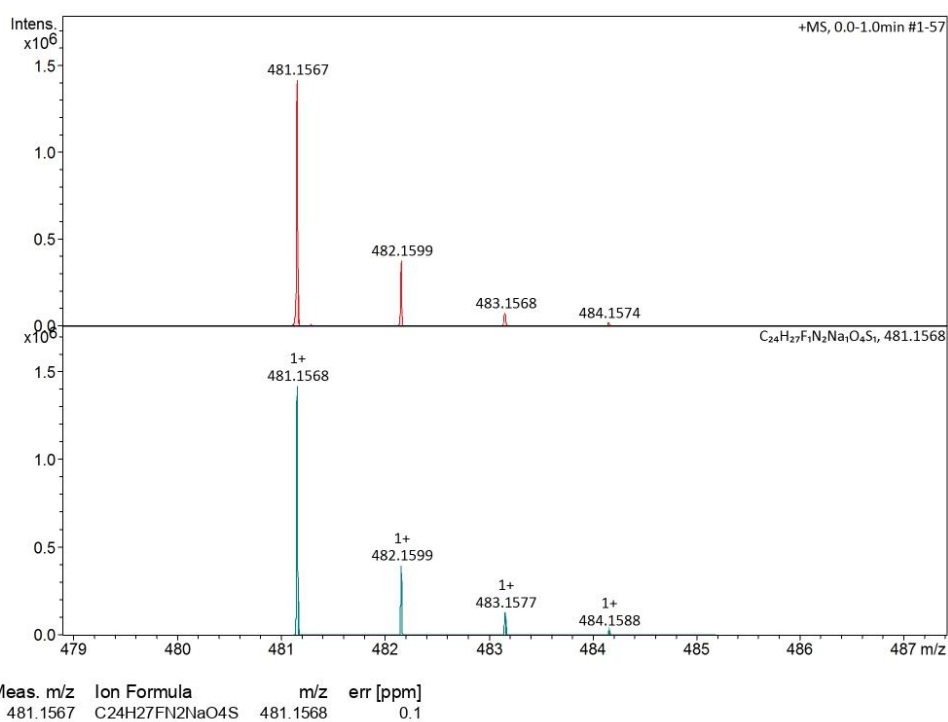
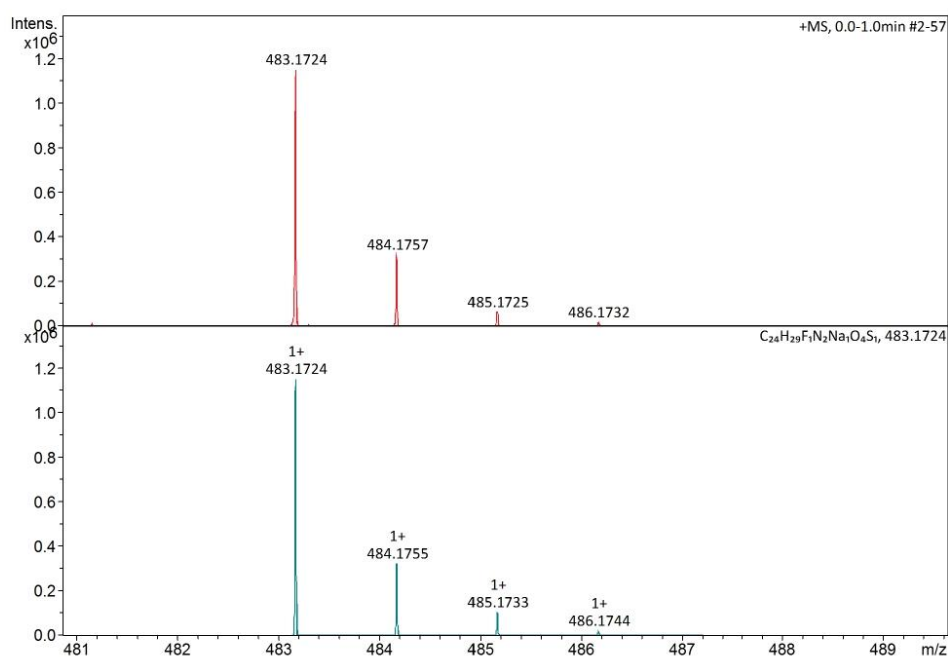


**Figure 33: Elemental analysis report of the steroid compound 50.**

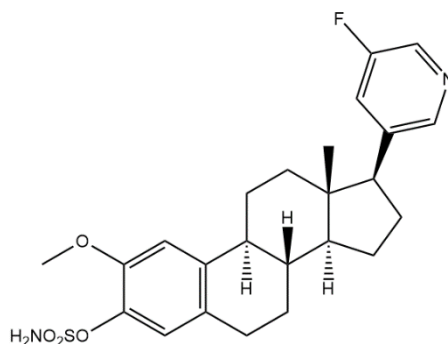
**(8*S*,9*S*,13*S*,14*S*)-17-(5-fluoropyridin-3-yl)-2-methoxy-13-methyl-7,8,9,11,12,13,14,15-octahydro-6*H*-cyclopenta[*a*]phenanthren-3-yl sulfamate (51)**

**Elemental Analysis Report**

Analysis Info		Acquisition Date		31-Mar-23 2:05:17 PM	
Sample Name	SK028	Analysis Name	D:\Data\maxis2023\19457.d		
Method	ESI_pos_50_1500_os.m				
Acquisition Parameter					
Source Type	ESI	Set Capillary	3500 V	Set Nebulizer	0.5 Bar
Focus	Not active	Set End Plate Offset	-500 V	Set Dry Heater	200 °C
Scan Begin	50 m/z	Set Charging Voltage	2000 V	Set Dry Gas	4.0 l/min
Scan End	1500 m/z	Set Corona	0 nA	Set Divert Valve	Waste
				Set APCI Heater	0 °C



Meas. m/z	Ion Formula	m/z	err [ppm]
483.1724	C <sub>22</sub> H <sub>24</sub> FN <sub>2</sub> O <sub>2</sub> S	483.1721	-0.6
	C <sub>24</sub> H <sub>29</sub> FN <sub>2</sub> NaO <sub>4</sub> S	483.1724	-0.0



19457.d

Bruker Compass DataAnalysis 4.3

printed: 31-Mar-23 2:10:08 PM

Page 1 of 1

**Figure 34:** Elemental analysis report of the steroid compound 51.